Analysis and Design of Long Haul Fiber-Optic Communication Systems

Analysis and Design of Long Haul Fiber-Optic Communication Systems

By

Dong Yang

ECE Dept, McMaster University

A Thesis
Submitted to the School of Graduate Studies
in Partial Fulfilment of the Requirements
for the Degree
Doctor of Philosophy

McMaster University
by Dong Yang, August, 2010

DOCTOR OF PHILOSOPHY (2010) McMaster University
Electrical and Computer Engineering Hamilton, Ontario

TITLE: Analysis and Design of Long Haul Fiber-Optic Communication Systems

AUTHOR: Dong Yang, M. A. Sc. (McMaster University)

SUPERVISOR: Dr. Shiva Kumar

NUMBER OF PAGES: 12, 147

Abstract

This thesis deals with the limiting factors in the design of a long-haul fiber-optic communication system, and the techniques used to suppress their resulting impairments. These limiting factors include both linear and nonlinear effects, such as fiber chromatic dispersion and the Kerr nonlinearity, and the modulator-induced nonlinearity.

In Chapter 3, the conditional probability density function (PDF) of the received electrical signal given transmitted bit '1'/'0' for a coherent fiber-optic transmission system based on binary phase shift keying (BPSK) is mathematically derived. Both amplified spontaneous emission (ASE) noise and fiber nonlinearity are taken into account. The results show that the conditional PDF of given bit '1' or '0' is asymmetric when intra-channel four-wave mixing (IFWM) is dominant, while it becomes nearly symmetric when the variance of ASE is much larger than that due to IFWM. The standard deviation of the received signal is calculated analytically. The system parameters, including optimum dispersion map and pre-compensation ratio, are optimized by analytically calculating variance of IFWM. Significant computation efforts can be saved using this approach as compared to full numerical simulations of the nonlinear Schrödinger equation, without losing much accuracy.

In Chapter 4, an improved 4-f time-lens configuration is proposed. Fourier transform (FT) and inverse Fourier transform (IFT) can be realized using time lenses such that there is no need for time reversal at the end. A typical 4-f configuration consists of two 2-f systems and a temporal filter. The first 2-f system consisting of a time lens and two dispersive elements produces the Fourier transform (FT) of the input signal. The temporal

filter modifies the spectrum. The next 2-f system produces the inverse Fourier transform (IFT). A wavelength division demultiplexer and a higher-order dispersion compensator based on 4-f configuration are numerical implemented. One of the advantages of the time-lens–based temporal filtering technique is that the transfer function of the temporal filter can be dynamically altered by changing the input voltage to the temporal filter (amplitude/phase modulator) and therefore, this technique could be used for dynamic switching and multiplexing in optical networks.

In chapter 5, a direct-detection optical orthogonal frequency division multiplexing (DD-O-OFDM) is realized using time lenses. Typically, in OFDM systems, discrete Fourier transform (DFT) is used at the transmitter and inverse discrete Fourier transform (IDFT) is used at the receiver. In this chapter, it is proposed to use continuous Fourier transform (FT) and inverse Fourier transform (IFT) using time lenses that replace DFT and IDFT in the electrical domain. The third- and higher-order dispersive effects can be considerably reduced using the proposed DD-O-OFDM scheme.

In Chapter 6, a coherent optical orthogonal frequency division multiplexing (OFDM) (CO-O-OFDM) scheme using time lenses is analyzed. The comparison of performance between the proposed scheme and the conventional optical OFDM scheme using fast Fourier transform (FFT) and inverse FFT in the electrical domain is made. Both the Mach-Zehnder modulator (MZM) induced and fiber induced nonlinearities are investigated. Results show that the time-lens-based CO-O-OFDM performs almost the same as the FFT-based CO-O-OFDM when the message signal launched to MZM is low so that MZM operates in the linear region. The nonlinearity of MZM degrades the performance of FFT-based CO-O-OFDM drastically when the power of message signal becomes sufficiently large, but only has negligible impact on the time-lens-based CO-O-OFDM. A periodical driving voltage has been proposed to set up the time lens such that the maximally required driving voltage level is kept low within the time frame. The advantages using the time-lens-based CO-O-OFDM are that (i) FT can be done in optical domain almost instantaneously, whereas the FFT in digital domain is slow and requires significant computational efforts, (ii) optical domain Fourier transform has a large bandwidth ($\sim$ THz) and therefore, FT/IFT can be performed at a large symbol rate.

In Chapter 7, the digital backward propagation (DBP) has been studied both in orthogonal frequency-division multiplexing (OFDM) and single-carrier (SC) fiber-optic transmission systems. 16 quadrature amplitude modulation (QAM) is used for both systems with the bit rate of 100 Gb/s. The results show that OFDM and SC with Nyquist pulses (SC-Nyquist) have a superior performance as compared to SC with raised-cosine pulses (SC-NRZ) when the DBP is used. The impact of electrical filter bandwidth and nonlinear phase/amplitude noise has also been investigated. The performance of perfect-BP-based OFDM/SC initially improves when the electrical filter bandwidth increases at high signal-to-noise ratio (SNR). The comparison of the effects of nonlinear phase/amplitude noise among OFDM, SC-Nyquist and SC-NRZ systems is made and it is shown that SC-NRZ systems significantly suffer from the effects of nonlinear phase/amplitude noise, which explains the performance advantage of OFDM/SC-Nyquist over SC-NRZ when the DBP used.

Acknowledgement

First, I would like to give my deepest gratitude to my beloved wife, Qiuyuan. I will never forget every single thing you have done for me. Thank you for your bearing my bad temper and capriciousness. Without you, whatever I have achieved in my life will become meaningless. Second, I would like to thank all my family. My dear mother Xiulian Li, father Yilin Yang, sister Ying Yang, huaibei mother Ling Jin and huaibei father Yazhou Huang, you give me strength and courage to face any difficulties in my life. Thank all of you for supporting me and taking care of me. I may not be the best son and brother, and sometimes make you upset, but please do believe that I am the one you can always rely on because I love you and that never changes. Third, I am deeply grateful to my supervisor, Dr. Shiva Kumar. We have been working together since 2004 when I came to MAC. You are not only my instructor, but also my friend. Please forgive me always calling you "Dr. Kumar", because you pay me and you are my boss. But, maybe soon after I will just call your name Shiva, like an old friend if you don't mind. Thank you so much for your financial support and academic supervision in the past six years. Last but not the least, I would like to thank Cheryl Gies, Helen Jachna and Alexa Huang at the Department of Electrical and Computer Engineering. Thank you for providing me all the conveniences and helps in my study.

The special thank and blessing to my angle, Lulu, who will be given birth to in March 2011. Mom and Dad are so excited and cannot wait to see you in next minute. You are just coming with the best timing like you know that Dad will finish PhD soon. You are the best award to Dad for the accomplishment of PhD. See you soon, my baby.

Contents

List of Figures

List of Tables

Chapter 1

Introduction

1.1 Evolution of Fiber-Optic Communications

A communication system transmits information data from one place to another, whether separated by a few kilometers or by transoceanic distances. Information is often carried by an electromagnetic carrier wave whose frequency can vary from a few megahertz to several hundred terahertz. Fiber-optic communication is a method of sending information-bearing lightwave pulses through an optical fiber. For a fiber-optic communication system, the high carrier frequencies (around 100 THz), in the visible or near-infrared regions of electromagnetic spectrum, are used. Compared to the microwave systems with the typical carrier frequency of $\sim$ 1 to 10 GHz, a fiber-optic communication system has much larger available bandwidth and therefore, it has been widely deployed to replace the copper wires in core networks in the past two decades for long-haul data transmission.

A point-to-point fiber-optic communication system consists of a transmitter, followed by the transmission channel (fiber), and then a receiver. The evolution of fiber-optic communications has always been promoted along with the advent of a technology breakthrough in either of the above three major components in a fiber-optic communication system. First, in 1960, the invention of the laser [2] provided a coherent optical source for transmitting information using lightwaves. After that, in 1979, the low loss fiber was realized at the operating wavelength of 1550 nm [3] with the loss of 0.2 dB/km, as compared to the initial value of over 1000 dB/km during the 1960s. The simultaneous feasibility of a stable optical source (laser) and a low-loss optical fiber led to an extensive research efforts and rapid development of fiber-optic communication systems. The drawbacks of 1550-nm systems in 1970s were that a large fiber dispersion occurs near the wavelength of 1550 nm, and the conventional InGaAsP semiconductor laser operating at 1550 nm oscillates multiple longitudinal modes simultaneously, which leads to large pulse broadening. Soon after, a dispersion-shifted single-mode silica fiber was designed and fabricated by Cohen et al. in 1979 [4]. For a dispersion-shifted fiber (DSF), the zero chromatic dispersion (CD) is shifted to the minimum-loss window at 1550 nm from 1300 nm by controlling the waveguide dispersion and dopant-dependent material dispersion, such that the transmission fiber with both low dispersion and low attenuation can be achieved. In 1983, an InGaAsP/InP semiconductor laser with single-mode linewidths of 10 kHz was demonstrated [5]. The DSFs in combination with lasers oscillating in a single longitudinal mode with narrow linewidths enabled long system reach for a fiber-optic communication system.

For a long-haul fiber-optic system, the loss limitation was initially overcome using optical-electrical-optical (OEO) repeaters in which the optical signal is first converted to the electrical current, and then regenerated using a transmitter. Such regenerating procedure is not suitable for multichannel lightwave systems because each single wavelength needs an OEO repeater, which leads to excessive system complexity. Another drawback of using OEO repeaters is that due to the high data rate in fiber-optical systems, the high-speed electronic devices are therefore required, but it is very hard and expensive to make extra-high speed electronics. An alternative approach is to use optical amplifiers that amplify the optical signal directly without the need of opto-electrical/electro-optical conversion. During the late 1980s when optical amplification became available, OEO repeaters were largely replaced by optical amplifiers due to its cost efficiency, especially for multichannel long-haul lightwave systems. The optical amplification was first realized using semiconductor laser amplifiers in 1983 [6], then Raman amplifiers in 1986 [7], and later using an optically pumped rare-earth-doped optical fibers, among which the most well-known candidate is the erbium-doped fibre amplifier (EDFA) in 1987. The optical fiber amplifier was invented by Shaw and Digonnet at Stanford University, California, in the early 1980s [8]. The EDFA was first demonstrated a couple of years later by D. N. Payne's group from the University of Southampton [9] and also by E. Desurvire et al. of AT&T Bell laboratories [10]. The characteristic of wideband amplification with low noise and high gain provided by EDFAs stimulated the development of transmitting signal through a single fiber channel using multiple carriers simultaneously, which can be implemented using a wavelength-division multiplexing (WDM) scheme. The use of optical amplification in combination with wavelength division multiplexing (WDM) started a new era in fiber-optic communications during the 1990s, and soon became available commercially by 1996.

WDM is basically the same as the frequency-division multiplexing (FDM), as the wavelength and the frequency are related by $c = f\lambda$, where c is the speed of light, f and λ are frequency and the corresponding wavelength of the light, respectively. For a WDM system, the channel multiplexing is realized by a multiplexer at the transmitter in which different wavelengths carrying different data are multiplexed. At the receiver, a demultiplexer is used to separate the wavelengths. The multiplexer and demultiplexer are realized using arrow waveguide grating (AWG). The WDM scheme led to a significant enhancement in capacity and therefore became very popular with telecommunication companies because the capacity of the network can be increased simply by increasing the number of channels without deploying more fibers. This concept was first discussed by Delange in 1970 [11], and by 1978 a WDM system with central wavelength in the range of 1-1.4 μm was demonstrated [12]. In this experiment, the demonstrated WDM system only combined two channels and transmitted these two channels in different windows of a optical fiber. The channel spacing was therefore quite large (250 nm) in this experiment. Afterwards, extensive research efforts were made to reduce the channel spacing in

WDM systems during the 1980s. By 1990, a channel spacing of less than 0.1 nm had been demonstrated [13]. Up to now, the modern WDM systems can handle 160 or more channels and they can expand a basic 10 Gb/s fiber-optic system to a total capacity of several Tb/s over a single fiber channel.

While WDM can greatly improve the capacity of a fiber-optic transmission system to some extent by increasing the number of channels, the achievable data rate in practice is limited by the bandwidth of optical amplifiers and ultimately by the fiber itself. Also, due to the fiber nonlinearity, the transmitted signal power cannot be arbitrarily large, and therefore it requires a high-sensitivity optical receiver for a noise-limited transmission system. Given a limited bandwidth and transmitted power, the challenge in the design of a fiber-optic communication system is how to transmit the highest data rate over the longest distance without signal regeneration. This issue could be addressed by simultaneously improving the spectral efficiency and the power efficiency. The spectral efficiency is measured in bit/s/Hz, and can be increased using various spectrally efficient modulation schemes, such as M-ray phase-shift keying (MPSK) and quadrature amplitude modulation (QAM), and/or polarization-division multiplexing (PDM) technique. The power efficiency can be improved by minimizing the required average signal power or signal-to-noise ratio(SNR) at a given level of bit error rate (BER). In a conventional fiber-optic communication system, the intensity of the optical carrier is modulated by the electrical information signal and at the receiver, the optical signal, transmitted through a fiber link, is directly detected by a photodiode acting as a square-law detector, and converted into the electrical domain. This is called the intensity modulation/direct detection (IMDD) scheme. Apparently, due to the power law of a photodiode, the phase information of the transmitted optical carrier is lost when direct detection is used, which prevents the use of the phase-modulated modulation schemes, like MPSK and QAM. Therefore, both spectral efficiency and power efficiency are limited in a fiber-optic system using direct detection.

In contrast, just as widely used in radio frequency (RF) and microwave communications, homodyne or heterodyne detection can be introduced in fiber-optic communications, and this kind of systems are referred to as coherent fiber-optic systems. The coherent optical communication systems have been extensively studied during the 1980s due to the high receiver sensitivity and the availability of introducing in-phase and quadrature multi-level modulation schemes. However, coherent communication systems were not commercialized because of the practical issues associated with polarization controllers and optical phase locked loops (PLLs) to align the phase of the local oscillator with the output of the fiber-optic link. With the advent of high speed digital signal processing (DSP) in early 2000s [28], coherent communication systems have gained renewed interest [29]-[31].

1.2 Time-Lens-Based Temporal Signal Processing Techniques

The analogy between the spatial diffraction and temporal dispersion has been known for many years [59]-[61]. In spatial domain, an optical wave propagating in free space diverges due to diffraction. As an analogue, in the temporal domain, an optical pulse propagating in a dispersive medium broadens due to dispersion. This space-time duality can also be extended to lenses. A conventional space lens converts the plane wave front into spherical

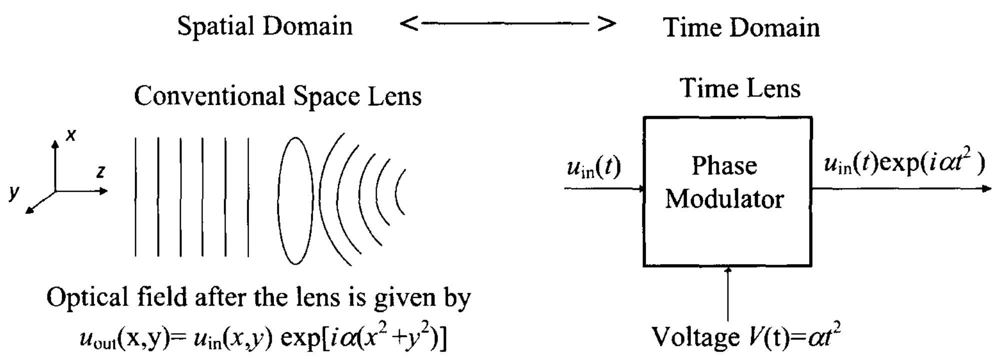

Figure 1.1: Space-time duality. Analogy between space lens and time lens.

wave front, as shown in Fig. 1.1. This is because of the spatial chirp introduced by the curvature of the lens. Similarly, a time lens introduces a temporal chirp factor (see Fig. 1.1) to a temporal signal. Simplest way to realize a time lens is by modulating the optical carrier by a phase modulator with quadratic drive voltage.

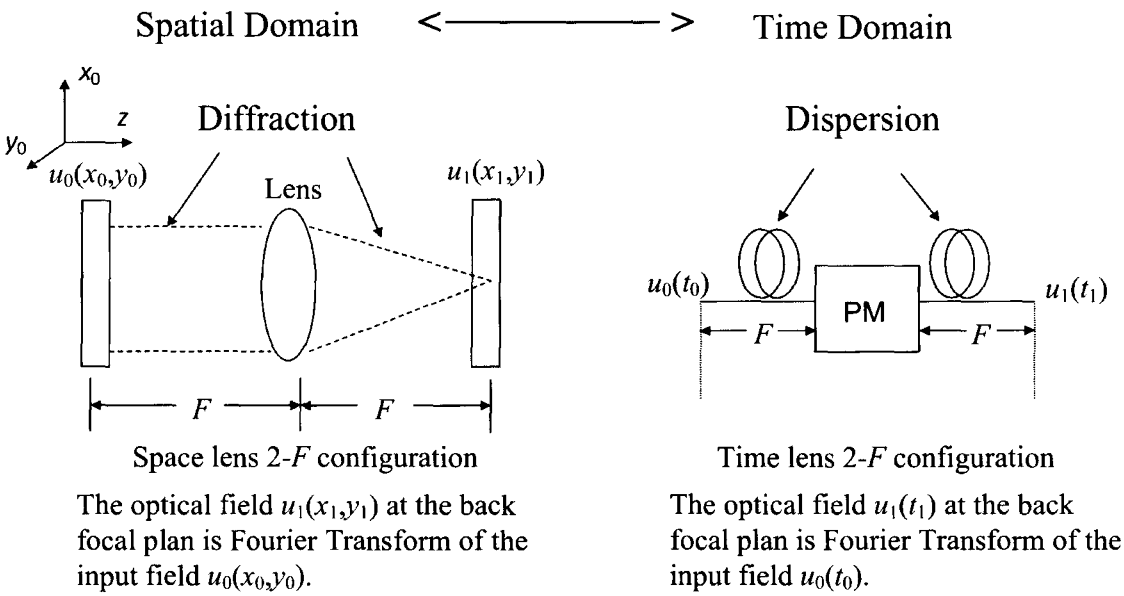

Figure 1.2: Spatial and temporal Foruier transformation. PM= Phase Modulator.

It is well known that the space lens produces the Fourier transform of the input spatial signal $u_0(x_0, y_0)$ (see Fig. 1.2) at the back focal plane. For example, if the input signal consists of parallel lines separated by δx, at the back focal plane ($u_1(x_1, y_1)$), we get bright spots at $x_1 = \pm k2\pi/\delta x$ (k is some constant) since the fundamental spatial frequency of the input signal is $2\pi/\delta x$. The propagation of the input signal u_0 to the lens and then from lens to the back focal plane is governed by diffraction. Using space-time analogy, the space lens is replaced by the time lens, and diffraction is replaced by dispersion and we could obtain the Fourier transform of the temporal signal (see Fig. 1.2). On this basis, the temporal filtering technique using time lenses was first proposed by Lohmann and Mendlovic in 1992 [62]. In their pioneering work, a temporal filter was introduced in a 4-F configuration consisting of time lenses. In the spatial domain, a conventional lens produces the Fourier transform (FT) at the back focal plane of an optical signal placed at the front focal plane, which is known as a 2-F configuration or 2-F subsystem (see Fig. 1.2). The spatial filter placed at the back focal plane modifies the signal spectrum, and a subsequent 2-F subsystem provides the Fourier transform of the modified signal spectrum, which returns the signal to the spatial domain with spatial inversion (see Fig. 1.3). As an analogue, in the case of temporal filtering, the spatial lens is replaced by a time

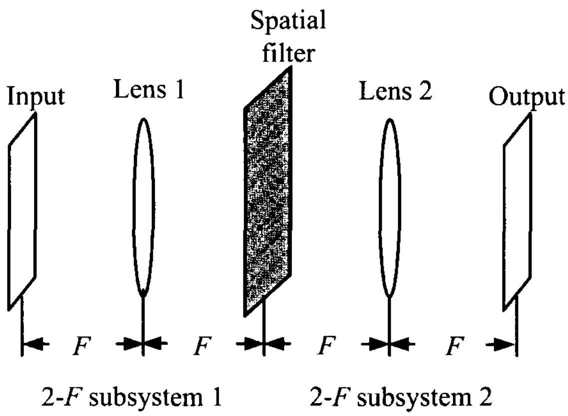

Figure 1.3: A schematic diagram of spatial filtering system.

lens (which is nothing but a phase modulator), and spatial diffraction is substituted with second-order dispersion of a fiber. The temporal filtering is implemented by inserting a temporal filter between two 2-F subsystems. A typical temporal filtering system is shown in Fig. 1.4. To compensate for the fiber dispersion using time-lens-based temporal

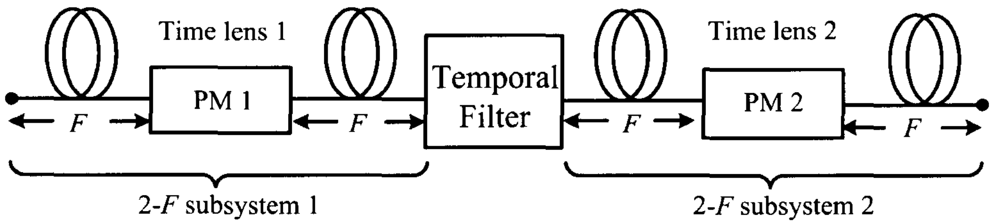

Figure 1.4: Schematic diagram of a typical 4-F system. PMj, $j = 1, 2$, are phase modulators in 2-F subsystems 1 and 2, respectively.

filtering technique, a temporal filter is introduced between two cascaded 2-F subsystems. This filter is realized by a phase modulator, of which the time domain transfer function has the same form as the frequency domain transfer function of fiber but the signs of dispersion coefficients are opposite. The optical signal distorted by fiber dispersion is fed into the first 2-F subsystem, and its time domain Fourier transformation is obtained before the temporal filter. At the temporal filter, the Fourier transformed input signal is multiplied by the time domain transfer function of the phase modulator so that fiber dispersion-induced phase shift is canceled out [63]. After passing through the second 2-F subsystem, the optical signal without dispersion-induced distortion is brought back to its time domain pulse shape. In principle, this time-lens-based dispersion compensator can be used to compensate for any order of fiber dispersion as long as the corresponding phase terms with opposite sign are generated in the inserted phase modulator. One of the most attractive advantages using optical fiber dispersion techniques is that the fiber dispersion is undone dynamically (online), and the inherently high bandwidth of the optical transmission link can be utilized as well.

Another important application of a time-lens-based system is to implement orthogonal frequency-division multiplexing (OFDM) in optical domain using the Fourier transforming property of 2-F subsystem [64]. Conventional optical OFDM systems use electronic devices to implements frequency-division multiplexing orthogonally, such as DSP-based fast Fourier transform (FFT), and therefore the data rate is limited by the availability of the maximum processing speed of DSP. In contrast, optical OFDM using time lenses implements Fourier transform in optical domain resulting in potentially high bandwidth compared to FFT-based OFDM. Optical OFDM has drawn significant research interest in the past several years due to its large tolerance to fiber dispersion and high spectral efficiency.

1.3 Orthogonal Frequency-Division Multiplexing

Orthogonal frequency-division multiplexing (OFDM) is a frequency-division multiplexing (FDM) scheme with closely spaced orthogonal sub-carriers, each of which is used to carry information data. The input data stream is first divided into several parallel data streams, one for each sub-carrier. Each sub-carrier is modulated with a conventional modulation scheme, such as on-off keying (OOK), phase-shift keying (PSK), or quadrature amplitude modulation (QAM), at a low symbol rate. The most attractive advantage of OFDM over the conventional FDM is that the sub-carriers in OFDM are orthogonal between each other and the corresponding spectra of the sub-channels are overlapped, which saves bandwidth significantly as compared to the normal FDM with non-overlapping multi-channels. Fig. 1.5 conceptually shows the bandwidth saving when OFDM is used. As

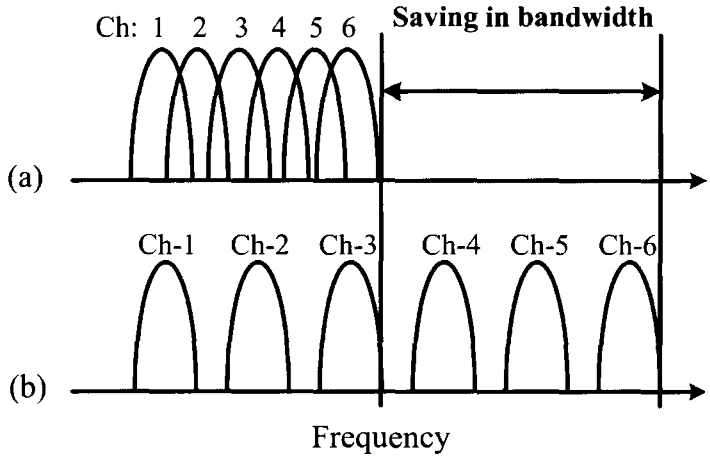

Figure 1.5: Schematic diagram of bandwidth usage in multi-carrier systems with total 6 sub-carriers. (a) OFDM, (b) FDM.

can be seen in Fig. 1.5, in a conventional FDM system, the carriers are separated with sufficiently large spacing between each other such that the signal in each channel can be received using the bandpass filter centered at the corresponding channel at the receiver. This multiplexing scheme is straightforward but waste the bandwidth. In contrast, when

OFDM is used, the sub-channels are overlapping leading to significant bandwidth saving (see Fig. 1.5). At the receiver, the orthogonality of the sub-carriers guarantees that the information signal transmitted through each sub-channel can be demodulated correctly. Another primary advantage of OFDM over normal FDM and single-carrier systems is its ability to counter severe channel conditions, such as frequency-dependent attenuation in copper wires and pulse spreading in dispersive channels, without complex equalization schemes. This is because the OFDM symbol is slowly-modulated signal with large symbol duration (low symbol rate) rather than the rapidly-modulated short pulses (high symbol rate), resulting in simple channel equalization.

The first paper on OFDM appeared in 1966 by Chang [65]. Soon after, a U.S. patent of OFDM data transmission system was filed and issued in 1970 [66]. In 1971, Weinstein and Ebert proposed an efficient OFDM scheme in which the discrete Fourier transform (DFT) was used and the guard interval was introduced to eliminate the inter-symbol interference (ISI) between OFDM symbols [67]. OFDM was first studied for high-speed modems and digital mobile communication in 1980s. In 1990s, it was utilized in wideband data communications over mobile frequency multiplexing (FM) channels, and high-bit-rate digital subscriber lines (DSLs). Just in the past decade, with the rapid advance in fiber-optic communication and coherent technologies, and the availability of high speed electronic devices, OFDM has arisen more and more research interest in optical communications due to its robustness against fiber dispersion and high spectral efficiency. The first paper on optical OFDM was presented by Pan and Green in 1996 [68]. Then, in 2001, Dixon et al. proposed the use of OFDM to suppress the modal dispersion in multi-mode fibers (MMFs) [69]. The optical OFDM applications in long-haul fiber-optic communications over standard single-mode fibers (SSMFs) have recently been studied by Shieh [70], Lowery [71] and Djordjevic [72]. One of the most attractive advantages of using OFDM is its high spectral efficiency. Spectral efficiency up to 3.57 bit/s/Hz has been demonstrated using optical OFDM [73]-[79], in combination with higher level modulation and polarization-division multiplexing (PDM). However, the aforementioned optical OFDM schemes are based on the implementation of Fourier transform (FT) in the electrical domain using DSP, in which the maximum achievable bit rate is limited by the availability of high-speed electronic devices. As an alternative, optical implementation of OFDM has been demonstrated by Lee et al [80] and Kumar and Yang [64] recently. Lee et al proposed a discrete Fourier transform (DFT) circuit that is designed using combinations of optical delays and phase shifters. In Ref. [64], it was proposed to use time lenses to implement OFDM with the Fourier transformation in the optical domain. The major difference between these two optical OFDM schemes is that the former requires a discrete input signal, while the latter works for the continuous signal. The all-optical OFDM, with its inherently high bandwidth, will become a promising candidate of transmission technique for the future high-speed all-optical networks.

One of the major drawbacks for optical OFDM is the high peak-to-average power ratio (PAPR) leading to significant performance degradation in a nonlinear fiber channel. The origin of high PAPR of an OFDM signal can be seen from its multi-carrier nature. When the independently modulated sub-carriers add up constructively at some time, the peak power is reached. Generally, the PAPR is over 10 dB. Such high level of PAPR for the OFDM signal can cause severe transmission impairments due to fiber nonlinearity. Therefore, the compensation schemes for fiber nonlinear effects in optical OFDM systems become important. There are several approaches which have been proposed to suppress the fiber nonlinear effects in optical OFDM systems, such as digital phase conjugation [81], and backward propagation (BP) [87]-[92]. The digital phase conjugation can compensate for even orders of dispersion and Kerr nonlinearity effects, but cannot compensate for odd orders of dispersion. However, digital BP can compensate for all orders of dispersion and Kerr nonlinearity.

1.4 Contributions of the Thesis

This thesis is organized as follows. In chapter 2, a literature background on the coherent transmission technology, dispersion compensation techniques, fiber nonlinearity and a novel equalization technique – digital backward propagation (DBP), is reviewed.

In chapter 3, the intra-channel four-wave mixing (IFWM) impairments in dispersion-managed coherent fiber-optic systems based on binary phase-shift keying (BPSK) are studied. The probability density function (PDF) of the received electrical signal for coherent fiber-optic transmission systems is derived. Both amplified spontaneous emission (ASE) noise and fiber nonlinearity are taken into account. The results show that the PDF of a bit '0' or '1' is asymmetric when intra-channel four-wave mixing (IFWM) is dominant. However, the PDF becomes nearly symmetric when the variance of ASE is much larger than that due to IFWM. The standard deviation of the fluctuations of the received signal due to IFWM is calculated analytically and validated using numerical simulations. It is shown that the variance varies quadratically with launch power. The optimum system scheme is also investigated, including optimum dispersion map and pre-compensation ratio, for the coherent fiber-optic systems based on analytically calculated variance of IFWM. The system design based on analytical calculations take significantly less time than the Monte-Carlo simulations.

In chapter 4, an improved optical signal processing scheme using time lenses is proposed. In a conventional 4-f configuration, the first 2-f subsystem consists of a dispersive element such as an optical fiber, a time lens and then another dispersive element, which provides the Fourier transform of the input signal. The second 2-f subsystem placed after the temporal filter typically has identical set-up as the first one, and therefore leads to the direct Fourier transform of the Fourier transform. As a result, the output signal is time-reversed when this 4-f configuration is used, which may be undesirable for a practical optical communication system. A technique to implement both direct and inverse Fourier transformation using time lenses is proposed, which has no spatial analogue. In the proposed scheme, the bit sequence at the output is not time-reversed. Two applications of the proposed scheme, a de-multiplexer for wavelength division multiplexing (WDM) systems and a higher-order dispersion compensators, have been discussed and numerically implemented. The advantage of the time-lens–based temporal filtering technique is that the transfer function of the temporal filter can be dynamically altered by changing the input voltage to the amplitude/phase modulator and therefore, this technique could have potential applications for switching and multiplexing in optical networks.

In chapter 5, an optical orthogonal frequency division multiplexing (O-OFDM) in a direct detection system is realized using time lenses. OFDM is a multiple carrier modulation scheme with orthogonal subcarriers. In the proposed time-lens-based optical OFDM scheme, the first 2-f subsystem modulates the serial input information signal to OFDM signal by producing inverse Fourier transform (IFT). At the receiver, the second 2-f subsystem provides the Fourier transform (FT) of the output signal after the transmission fiber link, and the demodulated OFDM signal is the product of the input signal and the transfer function of fiber link in the time domain. After the direct detection, the input information signal can be achieved without fiber-dispersion-induced phase shift due to the power-law detection. It is shown that using this configuration, the third- and higher-order dispersive effects can be considerably reduced for direct detection systems. The simulation results also show that the time-lens–based optical OFDM system scheme in direct detection systems has the tolerance to the fiber nonlinearity to some extent.

In chapter 6, an O-OFDM scheme with Fourier transform in optical domain using time lenses both at the transmitter and at the receiver in a coherent system is analyzed. The comparison of performance between this scheme with the optical OFDM scheme that utilizes fast Fourier transform (FFT) and inverse fast Fourier transform (IFFT) in electrical domain is made. The nonlinear effects induced by Mach-Zehnder modulator (MZM) as well as by the fiber are investigated for both schemes. Results show that the coherent OFDM using time lenses has almost the same performance as that using FFT when the electrical driving message signal voltages are low so that MZM operates in the linear region. The nonlinearity of MZM deteriorates the conventional coherent

OFDM based on FFT when the power of electrical driving signal increases significantly, but only has negligible impairment on the coherent OFDM using time lenses. Details of the time lens set up are provided and a novel scheme to implement the time lens without requiring the quadratic dependence of the driving voltage is presented. Important advantages of time-lens–based OFDM are that (i) FT can be done in optical domain almost instantaneously, whereas the FFT in digital domain is slow and requires significant computational efforts, (ii) optical domain Fourier transform has a large bandwidth ($\sim$ THz) and therefore, FT/IFT can be performed at a large system rate.

In chapter 7, the performance of orthogonal frequency-division multiplexing (OFDM) and single-carrier (SC) fiber-optic transmission systems with digital backward propagation (BP) are compared. 16 quadrature amplitude modulation (QAM) is used for both systems with the bit rate of 100 Gb/s. The results show that OFDM and SC with Nyquist pulses (SC-Nyquist) have a superior performance as compared to SC with raised-cosine pulses (SC-NRZ) when the digital BP is used. We also studied the impact of electrical filter bandwidth and nonlinear phase/amplitude noise on the performance. As the filter bandwidth increases, the performance improves for the case of ideal BP for both OFDM and SC systems when the signal-to-noise ratio (SNR) is large. The analysis of nonlinear phase/amplitude noise revealed that it causes significant impairments for SC-NRZ systems and least impact on OFDM and SC-Nyquist systems, which explains the performance advantage of OFDM/SC-Nyquist over SC-NRZ when the BP is used.

In chapter 8, conclusions of the present work and future plans are given. All references are placed at the end of the thesis.

The research work has resulted in the following refereed journals, book chapter and conference publications:

Journal Publications:

1. D. Yang and S. Kumar, "Investigation and Comparison of Digital Back-Propagation Schemes for OFDM and Single-Carrier Fiber-Optic Transmission Systems," Optical

Fiber Technology (OFT), submission number: OFT-10-121 (2010) (submitted).

2. D. Yang and S. Kumar, "Realization of optical OFDM using time lenses and its comparison with optical OFDM using FFT," Opt. Express 17, 17214 (2009).

3. D. Yang and S. Kumar, "Intra-channel four-wave mixing impairments in dispersion-managed coherent fiber-optic systems based on binary phase-shift keying," J. of Lightwave Tech. 27, 2916 (2009).

4. S. Kumar and D. Yang, "Optical implementation of orthogonal frequency- division multiplexing using time lenses," Opt. Lett. 33, 2002 (2008).

5. D. Yang, S. Kumar and H. Wang, "Temporal filtering with time lens in optical transmission systems," Opt. Comm. 281, 238 (2008).

Book Chapter:

1. D. Yang, S. Kumar and H. Wang, "Temporal filtering technique using time lenses for optical transmission systems," Chapter 6, Advances in Imaging and Electron Physics (AIEP), Vol. 158, pp. 203-232, 2009, Elsevier.

Conference Publications:

1. Nor Shahida, D. Yang and M. Matsumoto, "Amplitude Limiting of Time-Interleave-Multiplexed OOK and DPSK Signals Based on Four-Wave Mixing in a Fiber," to appear on the Proc. of Photonics Global Conference (PGC), Singapore, 2010.

2. S. Kumar and D. Yang, "Application of time lenses for high speed fiber-optic communication systems," Invited Talk, 4th International Conference on Computers & Devices for Communication (CODEC'09), Kolkata, India, Dec. 14-16, pp. 1-6, 2009.

3. D. Yang and S. Kumar, "Realization of optical OFDM using time lenses and its comparison with conventional OFDM for fiber-optic systems," 35th European Conference on Optical Communication (ECOC'09), Paper P4.21, Vienna, Austria, Sept. 20-24, 2009.

4. D. Yang and S. Kumar, "Space-mapping based optimization for fiber-optic transmission systems," Integrated Photonics and Nanophotonics Research and Applications and Slow and Fast Light 2007 Technical Digest (The Optical Society of America, Washington, DC, 2007), ITuH6.

Chapter 2

Literature Background

In the past decade, coherent transmission technology has revived in fiber-optic communications due to the availability of high-speed digital signal processing (DSP), and drawn a lot of research attention. In a coherent fiber-optic system, the spectrally efficient modulation and multiplexing techniques, such as quadrature amplitude modulation (QAM) and OFDM can be used and in combination with DSP, the impairments induced by the fiber dispersion and Kerr nonlinearity can also be effectively suppressed. The coherent optical communication technology has therefore become one of the most attractive candidates for the future high-speed fiber-optic communications. In this chapter, the background on the coherent transmission technology is first provided. Second, the literatures on the two major limiting factors of fiber transmission – dispersion and Kerr effect, and the corresponding suppression techniques are reviewed. Lastly, the digital backward propagation (DBP) technique, a novel equalization technique used to compensate both fiber dispersion and Kerr effect in a coherent fiber-optic communication system, is presented.

2.1 Coherent Transmission Technology

A coherent receiver linearly down-converts the optical signal to the electrical domain by using homodyne/heterodyne detection. A schematic diagram of a coherent receiver is shown in Fig. 2.1. The basic idea of the coherent detection is that the received

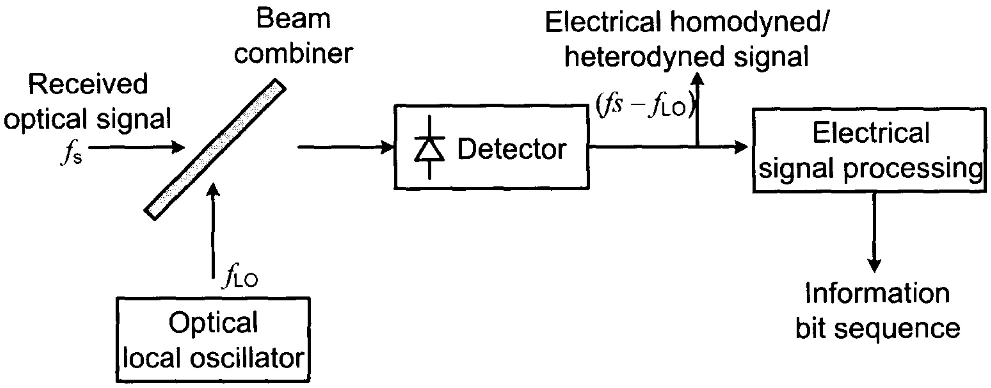

Figure 2.1: Schematic diagram of a coherent detection.

optical signal is mixed with a coherent local carrier signal before it passes through a photodetector. Suppose that the complex received optical signal is given by

$$E_r = A_0 \exp\left[-i\left(2\pi f_c t + \phi_0\right)\right], \tag{2.1}$$

where f_c is the carrier frequency, A_0 is the amplitude, and ϕ_0 is the phase. The electrical field of the local oscillator (LO) is given by

$$E_{LO} = A_{LO} \exp\left[-i\left(2\pi f_{LO} t + \phi_{LO}\right)\right], \tag{2.2}$$

where f_{LO}, A_{LO}, and ϕ_{LO} are the frequency, amplitude and phase of local carrier, respectively. The output electrical current of the photodetector can be written as

$$\begin{aligned} I(t) &= RP = R\left|E_r + E_{LO}\right|^2 \\ &= RP_0 + RP_{LO} + 2R\sqrt{P_0 P_{LO}} \cos\left(2\pi f_{IF} + \phi_0 - \phi_{LO}\right), \end{aligned} \tag{2.3}$$

where

$$P_0 = A_0^2, \quad P_{LO} = A_{LO}^2, \quad f_{IF} = f_0 - f_{LO}, \tag{2.4}$$

are the received optical signal power, the local carrier power and the intermediate frequency (IF), respectively. If $f_{IF} = 0$, it is called homodyne detection. If $f_{IF} \neq 0$, it is called heterodyne detection [1]. Ignoring the direct-current term in Eq. (2.3), the homodyne signal can be written as

$$I_{homo}(t) = 2R\sqrt{P_0 P_{LO}} \cos\left(\phi_0 - \phi_{LO}\right), \tag{2.5}$$

and the heterodyne signal can be written as

$$I_{heter}(t) = 2R\sqrt{P_0 P_{LO}} \cos\left(2\pi f_{IF} t + \phi_0 - \phi_{LO}\right). \tag{2.6}$$

As can be seen from Eqs. (2.5) and (2.6), the phase information of the optical carrier can be preserved using coherent detection. From Eq. (2.5), it can be seen that for the homodyne detection, the local-oscillator phase ϕ_{LO} is should be aligned with ϕ_0 so that the transmitted signal is not attenuated. In the past, optical phase locked loop (OPLL) was used to control ϕ_{LO}. But, it is not simple to implement such a loop in optical domain, which leads to high complexity of the design of a homodyne receiver. In contrast, when the local-oscillator frequency f_{LO} is deviating from the received optical signal carrier frequency f_c, as shown in Eq. (2.6), the optical signal is first converted into the microwave domain, which is called heterodyne detection. The intermediate frequency f_{IF} is typically falling in the region of GHz. For the heterodyne detection, the optical phase-locked loop is no longer needed. However, this merit is gained at the cost of 3-dB penalty in the receiver sensitivity as compared to the homodyne detection. It can be seen from Eq. (2.6) by taking the average of the power of electrical current,

$$\frac{1}{T}\int_{<T>} I_{heter}^2(t)dt = \frac{1}{T}\int_{<T>} 4R^2 P_0 P_{LO} \cos^2\left(2\pi f_{IF} t\right) dt = 2R^2 P_0 P_{LO}, \tag{2.7}$$

where ϕ_{LO} is assumed the same as ϕ_0 and $T = 1/f_{IF}$, and the corresponding electrical power output from the homodyne detection is given by

$$I_{homo}^2(t) = 4R^2 P_0 P_{LO}. \tag{2.8}$$

Recently, homodyne (or intradyne) detection is widely employed without optical PLL and the phase difference $\phi_0 - \phi_{LO}$ is estimated using digital signal processing (DSP). Another advantage of homodyne detection is the optical receiver bandwidth (and also the speed of A/D converter) is of the order of the symbol rate, B_s. In contrast, for heterodyne detection, the receiver bandwidth should be $\sim 2B_s$ centered around f_{IF}.

Since the coherent detection is linear in nature, the complex-valued electrical field with phase information can be achieved and therefore, the amplitude, phase and frequency of the optical carrier can all be utilized to carry the information data. There are several advantages for a coherent detection over a direct detection. First, the receiver sensitivity can be greatly improved by making the power of the local carrier P_{LO} sufficiently large. Second, the availability of introducing phase modulation/demodulation in a coherent system can further improve the receiver sensitivity compared to the conventional IMDD systems because of the increased distance between symbols in the constellation. Third, the heterodyning scheme allows closely spaced WDM channels as compared to the WDM of a few channels with wide spacings in the direct detection system. Last, the linearly detected signal by using coherent detection enables the post signal processing in the electrical domain with the help of the advanced DSP techniques. The electronic compensation schemes to suppress chromatic dispersion (CD), polarization-mode dispersion (PMD), and the fiber nonlinearity can be performed after the coherent detection.

The feasibility of heterodyne/homodyne detection for a coherent fiber-optic communication system was demonstrated in 1980 [14]-[19]. The significant improvement in receiver sensitivity by using coherent technology was also shown soon after in 1981 [20]. Although coherent fiber-optic communication systems were studied extensively in 1980's [21]-[26], their research and development were far behind the rapid progress in high-capacity WDM systems using EDFAs because of the requirement of an optical source with high stability and narrow-linewidth optical source at the transmitter, and sophisticated phase control techniques at the receiver for a coherent system. A semiconductor laser with external grating feedback was demonstrated operating at 1550 nm with the linewidth of 10 kHz [27]. In conjunction with an external optical modulator, a coherent transmitter was well established. But, the difficulty in efficiently implementing the phase control in coherent detection wasn't overcome until 2000's. The demonstration of digital carrier phase estimation in a coherent receiver in 2005 [28] has recently re-ignited a widespread interest in coherent fiber-optic communications [29]-[31]. The combination of coherent detection and DSP is expected to become a very important transmission technique for the next generation of fiber-optic communication systems due to its potential high capacity and flexibility with various post signal processing schemes in the electrical domain.

One of the most important advances in long-haul fiber-optic communication systems using a coherent detection combined with DSP is that the fiber dispersion can be effectively compensated at the receiver without deploying in-line dispersion compensation modules (DCMs). This can greatly reduce the system cost and also make the system design more flexible with adaptive receiver-based dispersion compensation techniques. In the following section, various dispersion compensation techniques are discussed, and their advantages and disadvantages are also compared.

2.2 Dispersion Compensation Techniques

One of major limiting factors in the long-haul 10Gb/s and beyond fiber-optic systems is the pulse broadening caused by fiber chromatic dispersion (CD), which leads to significant inter-symbol interference (ISI), and therefore severely degrades the performance. For a single-mode fiber, only the fundamental mode is supported when an optical pulse is launched into a fiber, and therefore, the intermodal dispersion is absent. However, the pulse broadening still occurs due to intra-modal dispersion which is described as follows. The group velocity associated with the fundamental mode depends on the frequency leading to different propagation speeds for the different frequency components of the optical pulse. This phenomenon is also called group-velocity dispersion (GVD), or chromatic dispersion to emphasize its wavelength-dependent nature.

Suppose that v_g is the group velocity at the angular frequency of ω, and the fiber length is L. The spectral component of a pulse at this frequency point arrives at the output of the fiber after a delay given by

$$T = \frac{L}{v_g}. \tag{2.9}$$

The group velocity v_g is associated with the propagation constant β as [32]

$$v_g = \left(\frac{d\beta}{d\omega}\right)^{-1}. \tag{2.10}$$

Assume the spectral width of the pulse is $\Delta\omega$, at the output of fiber, the pulse broadening can be estimated as [1]

$$\Delta T = \frac{\Delta T}{\Delta\omega}\Delta\omega \cong \frac{dT}{d\omega}\Delta\omega = \frac{d}{d\omega}\left(\frac{L}{v_g}\right)\Delta\omega = L\frac{d^2\beta}{d\omega^2}\Delta\omega = L\beta_2\Delta\omega, \tag{2.11}$$

where $\beta_2 = d^2\beta/d\omega^2$ is known as the GVD parameter. It can be seen from Eq. (2.11) that the pulse broadening occurs when $\beta_2 \neq 0$, and the amount of the pulse spreading is also determined by the spectral width of pulse $\Delta\omega$.

Ignoring the fiber nonlinearity and polarization-mode dispersion (PMD), the fiber can be characterized as a linear dispersive channel with the transfer function of $H_f(\omega)$. When the output of a continuous wave (CW) laser operating at frequency ω is incident on the fiber, the optical field distribution can be written as [33]

$$E(x, y, z, t) = \phi(x, y)A(\omega)\exp\left\{-j\left[\omega t - \beta(\omega)z\right]\right\}, \tag{2.12}$$

where $\phi(x, y)$ is the transverse field distribution, $A(\omega)$ is a weight coefficient at the frequency of ω, and $j = \sqrt{-1}$. If an optical fiber is excited with multiple frequencies, the total field distribution is the superposition of field induced at each single frequency, i.e.

$$E(x, y, z, t) = \phi(x, y)\sum_n A(\omega_n)\exp\left\{-j\left[\omega t - \beta(\omega)z\right]\right\}. \tag{2.13}$$

Further, if the incident field is a pulse with continuous frequency components, the summation in Eq. (2.13) can be replaced with an integral,

$$E(x, y, z, t) = \phi(x, y)\int_{-\infty}^{\infty}\widetilde{A}(\omega)\exp\left\{-j\left[\omega t - \beta(\omega)z\right]\right\}d\omega, \tag{2.14}$$

where

$$\widetilde{A}(\omega) = \lim_{\Delta\omega_n \to 0} \frac{A(\omega_n)}{\Delta\omega_n}. \tag{2.15}$$

For a pulse with the spectral width $\Delta\omega \ll \omega_0$, it is useful to expand the $\beta(\omega)$ in Eq. (2.14) in a Taylor series around the carrier frequency ω_0 and retain terms up to the third order. It is given by

$$\beta(\omega) \cong \beta_0 + \beta_1 \Delta\omega + \frac{\beta_2}{2}(\Delta\omega)^2 + \frac{\beta_3}{6}(\Delta\omega)^3, \tag{2.16}$$

where $\Delta\omega = \omega - \omega_0$ and $\beta_n = (d^n/d\omega^n)\beta(\omega)|_{\omega=\omega_0}$. Inserting Eq. (2.16) into Eq. (2.14), and using $\omega = \omega_0 + \Delta\omega$, Eq. (2.14) can be rewritten as

$$E(x, y, z, t) = \phi(x, y) \underbrace{\exp\left[-j\left(\omega_0 t - \beta_0 z\right)\right]}_{\text{optical carrier}} \underbrace{B(t, z)}_{\text{envelope}}, \tag{2.17}$$

where

$$B(t, z) = \int_{-\infty}^{\infty} \widetilde{B}(\Delta\omega) \times \exp\left[j\beta_1 \Delta\omega z + \frac{j\beta_2}{2}(\Delta\omega)^2 z + \frac{j\beta_3}{6}(\Delta\omega)^3 z\right] \exp\left(-j\Delta\omega t\right) d(\Delta\omega), \tag{2.18}$$

and

$$\widetilde{B}(\Delta\omega) = \widetilde{A}(\omega_0 + \Delta\omega). \tag{2.19}$$

Replacing $\Delta\omega$ with ω, Eq. (2.20) can be rewritten as

$$B(t, z) = \int_{-\infty}^{\infty} \widetilde{B}(\omega) \times \exp\left(j\beta_1 \omega z + \frac{j\beta_2}{2}\omega^2 z + \frac{j\beta_3}{6}\omega^3 z\right) \exp\left(-j\omega t\right) d\omega, \tag{2.20}$$

where

$$\widetilde{B}(\omega) = \mathcal{F}\left\{B(t, 0)\right\} \tag{2.21}$$

is the Fourier transform of the input optical field envelope at $z = 0$, and

$$H_f(\omega) = \exp\left(j\beta_1 \omega z + \frac{j\beta_2}{2}\omega^2 z + \frac{j\beta_3}{6}\omega^3 z\right) \tag{2.22}$$

is known as the linear transfer function of fiber. In the absence of dispersion ($\beta_2 = \beta_3 = 0$), the output optical filed envelope at the distance of z is given by

$$B(t, z) = B(t - \beta_1 z, 0), \tag{2.23}$$

which implies that β_1 only leads to the propagation delay of an optical pulse without changing its shape. The other two parameters β_2 and β_3 in the fiber transfer function $H_f(\omega)$ are the second- and third-order dispersions, respectively, and are responsible for pulse broadening. Therefore, finding a way to cancel the phase factors $\exp(j\beta_2\omega^2 z/2)$ and $\exp(j\beta_3\omega^3 z/6)$ is the basic idea of fiber dispersion compensation. The implementation of fiber dispersion compensation can be done at the transmitter, at the receiver, or within the fiber link.

For a transmitter-based dispersion compensation scheme, fiber dispersion can be canceled out by pre-distorting the input pulses before they are launched into a fiber link. Koch and Alferness presented a technique in 1985 to compensate for the fiber dispersion using the synthesis of pre-distorted signal for a high-speed ($>$ 10 Gb/s) time-division multiplexing (TDM) transmission [34]. The pre-chirped Gaussian pulses were obtained by using a frequency-modulated (FM) optical carrier as input to an external modulator for amplitude modulation (AM). The output optical pulse is a chirped Gaussian pulse with the chirp parameter $C > 0$ such that $C\beta_2 < 0$ in a single-mode fiber with typical $\beta_2 = -21$ ps^2/km. The dispersion-induced chirp is canceled out by the intentionally introduced chirp in the input pulses, and therefore the pulse broadening is suppressed at the output of fiber. An alternative to implement signal predistortion is making use of digital signal processing (DSP). With the advances in the performance of high-speed electronic devices during the 2000s, the signal predistortion can be done in electrical domain using DSP at a line rate of fiber-optical transmission (10 Gb/s and above) [35]-[37]. The digital filter is designed to have the transfer function in the form of

$$H_{tx} = A\exp\left(-\frac{j\beta_2\omega^2 z}{2}\right), \tag{2.24}$$

if only the second-order dispersion is considered, and A is some constant. The electrical signal, $u(t)$, passes through this filter and input to an optical-E-filed modulator, such as a Mach-Zehnder in-phase/quadrature (IQ) modulator, the transmitted optical field envelope is then given by

$$B(t,0) = \mathcal{F}^{-1}\left\{\widetilde{U}(\omega) \times H_{tx}(\omega)\right\}, \tag{2.25}$$

where $\mathcal{F}^{-1}$ denotes inverse Fourier transform, and $\widetilde{U}(\omega)$ is the Fourier transform of $u(t)$. Using Eq. (2.20), and ignoring β_1 and β_3, the output optical field envelope after propagation along the fiber can be written as

$$B(t,z) = \int_{-\infty}^{\infty} \widetilde{U}(\omega) \exp(-j\omega t)\, d\omega = u(t). \tag{2.26}$$

In principle, this dispersion pre-compensating technique can be used to undo any amount of fiber dispersion simply by generating the corresponding inverse quadratic phase in the pre-distorting digital filter. The disadvantage of pre-compensating scheme is that the exact dispersion compensation cannot be achieved without the knowledge of the transmission fiber link. Further, even the transfer function of the fiber link is fully known, the optimum performance of the dispersion compensation is still hard to reach by using pre-compensation because when an optical pulse propagates along a fiber link, other linear and nonlinear effects, such as PMD and self-phase modulation (SPM), interact with fiber dispersion and change the pulse shape further, and therefore make the performance of the dispersion pre-compensation imperfect. To avoid the requirement of prior-knowledge of fiber links and achieve the optimum dispersion compensation, the dispersion compensating module is moved from the transmitter to the receiver, and this is so-called dispersion post-compensation, or receiver-based dispersion compensation.

There are several receiver-based electrical dispersion compensation (EDC) approaches. A linear equalizer can be used between the receiver and the detector to compensate for the inter-symbol inference (ISI) caused by fiber dispersion, and its corresponding technique is called linear equalization. A transversal filter (tapped delay line) is often used as a linear equalizer [38], and its typical structure is shown in Fig. 2.2. As seen from Fig. 2.2, the equalized output can be written as

$$I(t = kT_b) = I_k = \sum_{i=0}^{L-1} w_i r_{k-i}, \tag{2.27}$$

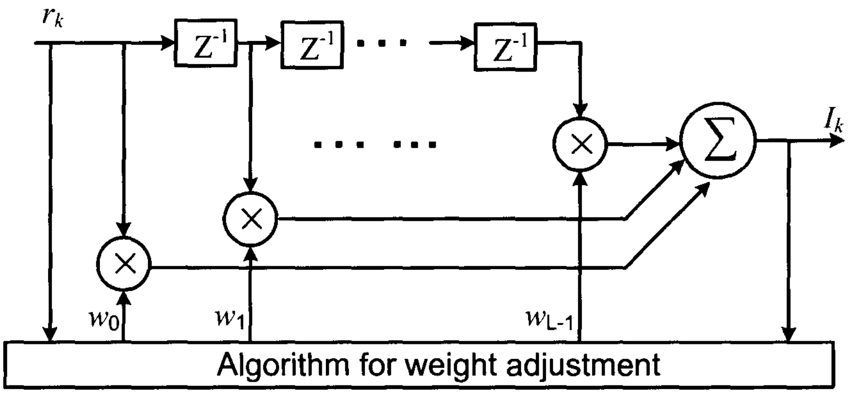

Figure 2.2: Schematic diagram of a tapped delay line. z^{-1} stands for a delay unit. w_j stands for the weight coefficient. r_k is the unequalized input and I_k is the equalized output at the sampling time kT_b.

where T_b is the bit interval. Suppose a dispersive fiber channel with ISI spanning over $L-1$ symbols, and r_k is the sampled received signal that is distorted by fiber-dispersion-induced ISI. By multiplying the current and previous $L-1$ received symbols by the corresponding weight coefficients, $w_i, i = 0, 1, \cdots (L-1)$ and summing them up at the end, the output is used as an estimation of the transmitted symbol. The weight coefficients can be adaptively adjusted using some algorithms. Two of the most widely used algorithms are least-mean square (LMS) algorithm [39], and zero-forcing algorithm [40], [41]. The essential difference between these two algorithms is that the LMS algorithm minimizes the variance of the error symbol $(I_k - x_k)$, where x_k is the transmitted symbols, while the zero-forcing algorithm minimizes the peak distortion (defined as the worst-case ISI at the output of the equalizer). Therefore, the zero-forcing based linear equalizer can only work well when the unequalized eye diagram is open (noise is small). In contrast, the LMS based linear equalizer can provide modest performance even when the eye diagram is close (noise is large) because it minimizes both the ISI and noise.

For a conventional fiber-optic communication system with direct detection, due to the power-law detection, the linear dispersion-induced distortion in optical domain becomes nonlinear in the electrical domain. As a result, the linear EDC techniques discussed above can only partially undo the fiber dispersion. Some of the nonlinear equalization techniques were therefore developed for the direct detection. One method is to cancel the nonlinear distortions using previously detected symbols and the estimates of symbols to be detected. In this method, the equalized output is linear summation of the previous and estimated symbols [42], and the optimum weight coefficients can be obtained using LMS or zero-forcing algorithms. Such an approach is called decision-feedback equalization. In another method, a lookup table was used to find the optimum decision threshold , and the transmission distance was demonstrated to be doubled by using this nonlinear equalization technique [43].

Maximum likelihood sequence estimation (MLSE), the optimum detection technique from the point of view of error probability, can be used to compensate for the fiber dispersion at the receiver in a fiber-optic communication systems. If the fiber-induced ISI spans over $L+1$ symbols, the MLSE is equivalent to the problem of estimating the state of of a discrete-time finite-state machine. When the symbols are M-ary, the state machine has M^L states. The Viterbi algorithm is used to implement a MLSE by searching for the most probable path through a M^L-state trellis [44]. MLSE-based receiver design in fiber-optic communications has drawn a lot of research interest due to its high robustness for nonlinear fiber channels, and it has been demonstrated that EDC using MLSE gives superior performance over linear equalization and DFE-based equalization [45]-[49], and therefore can be used as a BER lower bound estimation of a fiber-optic communication system.

For a fiber-optic communication system with direct detection, the nonlinearity induced by the power law of the detector makes the dispersion compensation scheme more complex and less efficient. With the development of powerful digital signal processing during the 2000s, the difficulty in tracking the received optical carrier phase in an optical coherent receiver was overcome by using digital carrier phase estimation circuit [28]. Hence, The coherent receiver combined with electronic dispersion compensation (EDC) using DSP has become more practical in the past decade. Since the phase information of the transmitted signal is preserved in a coherent system, or in other words, the complex-valued electrical filed is fully detected at the coherent receiver, more options for the dispersion compensation are available for a coherent optical system compared to the direct detection. First, most of the EDC schemes used in direct detection, such as the linear equalizer and DFE, can also be used in coherent systems without much modifications, and the performance of such compensation schemes is expected to be better than in direct detection systems since the nonlinear impairment introduced by power-law detection is absent in the coherent receiver. Second, the EDC schemes working with direct detection are typically done in time domain. In contrast, for a coherent system, the EDC can be implemented in frequency domain. The first step in the frequency domain equalization (FDE) is a fast Fourier transformation (FFT) block that takes the unequalized signal $r(t)$ into the frequency domain,

$$\mathcal{F}\{r(t)\} = \widetilde{U}(\omega)\widetilde{H}_f(\omega), \tag{2.28}$$

where $\widetilde{U}(\omega)$ is the Fourier transform of the information signal $u(t)$, and $\widetilde{H}_f(\omega)$ is the transfer function of a linear fiber channel that is given by

$$\widetilde{H}_f(\omega) = \exp\left(j\frac{\beta_2}{2}\omega^2 L + j\frac{\beta_3}{6}\omega^3 L\right), \tag{2.29}$$

where β_2 and β_3 are the second- and third-order dispersions, and L is the total transmission distance. Then, the signal is multiplied by an all pass filter with the frequency response of

$$\widetilde{H}_{eq}(\omega) = \exp\left(-j\frac{\beta_2}{2}\omega^2 L - j\frac{\beta_3}{6}\omega^3 L\right). \tag{2.30}$$

It can be noticed that the signs of the β_2 and β_3 in Eq. (2.30) are reversed compared to those in Eq. (2.29), and therefore after passing through this filter, the fiber dispersion is canceled out. Finally, the signal is brought back to the time domain using inverse fast Fourier transform (IFFT). The whole process discussed above can also be done in the time domain by the convolution. The impulse response of the all pass filter can be alternatively written as

$$h_{eq}(t) = \mathcal{F}^{-1}\{\widetilde{H}_{eq}(\omega)\}, \tag{2.31}$$

and the corresponding time domain equalization (TDE) is realized by

$$u(t) = r(t) \otimes h_{eq}(t), \tag{2.32}$$

where $\otimes$ denotes the convolution. The FDE has been reported less computational complexity than TDE because the convolution needs more computational effort compared to multiplication [50], [51]. One of the most attractive advantages of the receiver-based EDC over the transmitter-based schemes is that the fiber dispersion can be adaptively compensated without the knowledge of the transmission link. The dispersion parameters for a fiber channel given in Eq. (2.30) can be estimated adaptively, which is realized using some algorithms, such as least-mean square (LMS) [52] or the constant-modulus algorithm (CMA) [53]. A novel blind adaptive algorithm is proposed recently for coherent systems with low complexity and ability of precisely estimating arbitrarily large dispersion [54].

Before the development of the electronic-circuit-based high-speed, powerful DSP, the effective fiber dispersion compensation, especially for a long-haul system, was implemented along the transmission fiber link using in-line dispersion compensation modules (DCMs) in the optical domain. A DCM could be a dispersion compensating fiber (DCF) with reverse sign of the GVD parameter as that of the transmission fiber, typically a standard single-mode fiber (SSMF), or an optical filter with inverse transfer function of the fiber channel.

The use of a DCF to compensate for fiber dispersion was first proposed in 1980 by Lin et al [55]. But due to the relatively high loss of DCFs, this technique was not applied in practice until 1990's after the EDFA was present. A typical transmission fiber span with a DCF is shown in Fig. 2.3. The total transfer function of the SSMF cascaded with a DCF is given by

$$\widetilde{H}_{\text{span}}(\omega) = \exp\left[\frac{j}{2}\omega^2\left(\beta_{21}L_1 + \beta_{22}L_2\right)\right] \tag{2.33}$$

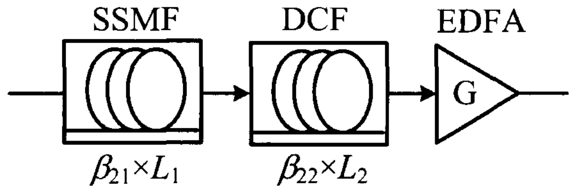

Figure 2.3: A transmission span with a DCF. β_{21}, L_1, and β_{22}, L_2 are the GVD parameter and length for SSMF and DCF, respectively.

It is evident from Eq. (2.33) that the perfect dispersion compensation is realized if

$$\beta_{21}L_1 + \beta_{22}L_2 = 0. \tag{2.34}$$

For a SSMF, the GVD parameter, $\beta_{21} < 0$, and therefore the DCF must have normal dispersion, i.e., $\beta_{22} > 0$, such that the accumulated fiber dispersion in Eq. (2.34) becomes zero. From the practical point of view, the DCF should have as large normal GVD parameter as possible such that L_2 is small. However, there are two major limiting factors for the use of DCFs. First, the extra insertion loss in the transmission link is introduced by the deployment of DCFs. Although it can be compensated by increasing the amplifier gain, the amplified spontaneous emission (ASE) noise is enhanced accordingly. Second, the DCF has small effective mode area leading to large nonlinear effects. These two shortcomings limits the use of DCF in the long-haul fiber links. For example, for a standard SMF with the length of 40 km, and dispersion $D = 17$ ps/(km $\cdot$ nm), the length of the DCF with dispersion of -100 ps/(km$\cdot$nm) will be 6.8 km. The performance degradation introduced by the ASE noise and nonlinear effects of DCFs become significant in this case. Another approach of fiber dispersion compensation in the optical domain is the use of optical filters. The basic idea of an optical equalizing filter is that making an all-pass filter with the transfer function of

$$H_{\text{opt}} = A\exp\left(-\frac{j}{2}\beta_2 L\omega^2\right), \tag{2.35}$$

where A is some constant, and $\beta_2 L$ is the accumulated fiber dispersion to be compensated. Hence, the optical field envelope passes through this kind of filter leading to the cancelation of fiber dispersion. The optical equalizing filter can be realized using a Fabry-Perot (FP) interferometer [56] or a Mach-Zehnder (MZ) interferometer [57] , or fiber Bragg gratings [58]. There are some disadvantageous factors limiting the use of optical equalizing filters. First, the the transfer function of these kinds of filters is not an exact inverse of the transfer function of a fiber. So, the dispersion can only be partially canceled using optical equalizing filters. Second, the relatively high loss and narrow bandwidth limit their use in the broad band fiber-optic communication systems.

With the rapidly increasing demand on the bandwidth, the fiber-optic communication tends to transmit high bit-rate information data on a single-carrier or through multi-carries, both of which will suffer from the distortions caused by the higher-order fiber dispersion due to their large bandwidth. Therefore, the compensation of higher-order dispersion becomes more important in the long-haul high-speed fiber-optic communication system. However, it is hard to handle the higher-order dispersion using DCFs and optical equalizing fibers. For this reason, in this thesis, a novel temporal filtering technique using time lenses was proposed to compensate for the any order of fiber dispersion in the optical domain.

2.3 Fiber Kerr Nonlinearities

The optical fiber medium can be approximated as a linear medium only when the launch power is sufficiently low. For the long-haul fiber-optic transmission and wideband WDM systems, to combat the accumulated noise along the transmission fiber link, the launch power must be increased to keep signal-to-noise ratio (SNR) high enough for the error-free detection at the receiver. As the launch power increases, the nonlinearity of fiber becomes significant leading to severe performance degradation. The fiber nonlinear effect (or Kerr effect) originates from the dependence of the refractive index on light intensity, which was discovered in 1875 by John Kerr. The refractive index can be written as

$$n(\omega, P) = n_0(\omega) + n_2 \frac{P}{A_{\text{eff}}}, \tag{2.36}$$

where n_0 is the linear part of refractive index, n_2 is the Kerr coefficient with typical value of 2.2-3.4 $\times 10^{-20}$ m^2/W, P is the optical power, and A_{eff} is the effective core area. The dependence of the refractive index on the light intensity results in the propagation constant β varying as the light intensity due to $\beta = 2\pi n/\lambda$, and the propagation constant can be written as

$$\beta(\omega, P) = \beta_0(\omega) + \frac{2\pi n_2}{\lambda A_{\text{eff}}} P, \tag{2.37}$$

where $\beta_0(\omega)$ is related to fiber dispersion, and

$$\frac{2\pi n_2}{\lambda A_{\text{eff}}} = \gamma, \tag{2.38}$$

is known as the fiber nonlinear coefficient. The phase shift induced by the nonlinear effect occurs when the optical signal propagates along the fiber. The total nonlinear phase shift after the distance L is given by

$$\phi_{NL} = \int_0^L [\beta - \beta_0]\, dz. \tag{2.39}$$

Substituting Eq. (2.37) in Eq. (2.39), and using Eq. (2.38) and

$$P(z) = P_0 \exp(-\alpha z), \tag{2.40}$$

where P_0 is the launch power, and α is the fiber loss coefficient, we obtain [82]

$$\phi_{NL} = \int_0^L \gamma P_0 \exp(-\alpha z) dz = \gamma P_0 \frac{1 - \exp(-\alpha L)}{\alpha} = \frac{L_{\text{eff}}}{L_{NL}}, \tag{2.41}$$

where

$$L_{\text{eff}} = \frac{1 - \exp(-\alpha L)}{\alpha} \tag{2.42}$$

is the effective length, and

$$L_{NL} = \frac{1}{\gamma P_0} \tag{2.43}$$

is the nonlinear length. It can seen from Eq. (2.41) that the fiber nonlinear effect enhances when L_{NL} decreases, or equivalently P_0 increases. There are three types of fiber nonlinearities due to the Kerr effect. Type (I) self-phase modulation (SPM), (II) cross-phase modulation (XPM), and (III) four-wave mixing (FWM). The SPM, imposing the nonlinear phase shift on the pulses as shown in Eq. (2.41), is responsible for spectral broadening of optical pulses. Interacting with fiber dispersion, the SPM can cause temporal pulse broadening (normal dispersion ($\beta_2 > 0$)), or pulse compression (anomalous dispersion $\beta_2 < 0$). The well-known interaction of the SPM with anomalous dispersion is the formation of optical solitons [83]. The cross-phase modulation (XPM) causes the nonlinear phase shift including the contribution of the optical pulses from other channels, or the overlapping pulses in a single channel, which is called intrachannel XPM (IXPM). In XPM, the nonlinear phase shift in k-th channel can be written as

$$\phi_{NL}(k) = \gamma L_{\text{eff}} P_0^{(k)} + 2 \sum_{h=1, h \neq k}^{N} \gamma L_{\text{eff}} P_0^{(h)}, \tag{2.44}$$

where $P_0^{(k)}$ is the pulse peak power in k-th channel. The first term in Eq. (2.44) is the SPM and the second term denotes the contribution of XPM. It can be seen from Eq. (2.44) that the XPM induced phase shift is twice that of SPM when the optical powers of all the channels are equal. XPM causes asymmetric spectral broadening of the optical pulses, and timing jitter and amplitude distortion in time domain. The four-wave mixing (FWM) is another effect that generates optical signal at new frequencies. For a WDM system, with carrier frequencies of f_i, f_j and f_k, the signal at new frequency $f_h = f_i + f_j - f_k$ can be generated by FWM, which leads to serious performance degradation when the newly generated frequency component falls into the WDM channels. For a single carrier system, the nonlinear mixing of overlapped pulses generates ghost pulses due to intra-channel four-wave mixing (IFWM), which is one of the dominant penalties for high bit rate (above 40 Gb/s) fiber-optic systems [84]-[86]. The studies of suppressing the impairments induced by SPM, XPM and FWM for long-haul and wideband fiber-optic communications have become important.

2.4 Backward Propagation (BP)

The approach of digital backward propagation (BP) in fiber-optic communications for the compensation of fiber nonlinearity has drawn significant research interest recently owing to its ability to undo fiber linear and nonlinear impairments [87]-[92]. The basic idea behind BP can be understood from the governing equation of fiber propagation. The electrical filed envelope of an optical signal, $u(t, z)$, is governed by the nonlinear Schrödinger equation (NLSE)[33]

$$\frac{\partial u}{\partial z} = \left[\hat{D} + \hat{N}\right] u, \tag{2.45}$$

where $\hat{D}$ denotes the linear operator given by

$$\hat{D} = -i\frac{\beta_2(z)}{2}\frac{\partial^2}{\partial t^2} + \frac{\beta_3(z)}{6}\frac{\partial^3}{\partial t^3} - \frac{\alpha(z)}{2}, \tag{2.46}$$

and $\hat{N}$ denotes the nonlinear operator given by

$$\hat{N} = i\gamma(z)|u|^2, \tag{2.47}$$

$\beta_2(z)$, $\beta_3(z)$, $\alpha(z)$ and $\gamma(z)$ are the profiles of second-order, third-order fiber dispersion coefficients, loss/gain and nonlinear coefficient, respectively. Eq. (2.45) is invertible in the absence of noise. If the sign of z in Eq. (2.45) is reversed, and the received signal is taken as the input signal, Eq. (2.45) can be rewritten as

$$\frac{\partial u}{\partial z} = \left[-\hat{D} - \hat{N}\right] u, \tag{2.48}$$

which is equivalent to sending the received signal through a virtual fiber with opposite-signed dispersion and fiber nonlinearity. The transmitted signal can therefore be fully recovered in this way. This is so-called "backward propagation". Eq. (2.48) can be numerically solved using split-step Fourier method (SSFM) in digital domain. The performance of BP-based compensation scheme is limited by the noise and the step size used in SSFM for backward propagation. In principle, in the absence of noise, BP can completely cancel both fiber dispersion and nonlinearity when the step size used for solving

Eq. (2.48) is chosen small enough. However, when the noise is present, the transmitted signal cannot be fully recovered using BP whatever the step size is chosen because the noise-induced impairments, such as nonlinear phase/amplitude noise, cannot be undone using BP. On the other hand, the computational cost in digital BP increase as the step size decreases. As a result, in practice, the step size should be so chosen that the computational effort at the transmitter/receiver is affordable. Backward propagation operates on the complex-valued electrical field envelope, $u(t, z)$ directly and therefore, the coherent detection is required, which also allows the use of BP for any modulation formats and multi-carrier systems, such as OFDM with QAM. The compensation of fiber nonlinearity using BP has been demonstrated to enable larger launch power and longer transmission distance in optical OFDM systems [89].

Chapter 3

Intra-channel Four-Wave Mixing Impairments in Dispersion-Managed Coherent Fiber-Optic Systems based on Binary Phase-Shift Keying

3.1 Introduction

The statistical characteristic of received bits is a fundamental concern in communication systems. In long-haul fiber-optic communication systems, because of the fiber nonlinearity, it is usually hard to obtain the exact analytical expression for the probability density function (PDF) of received bits. The pulsewidth and amplitude of pulse fluctuate due to intra-pulse self-phase modulation (ISPM) and also the nonlinear interaction of adjacent pulses causes phase modulation of the probe pulse due to intra-channel cross-phase modulation (IXPM), which is translated to timing delay because of dispersion [93]-[95]. Furthermore, the nonlinear mixing of overlapped pulses generates ghost pulses due to intra-channel four-wave mixing (IFWM), which is one of the dominant penalties for high bit rate fiber-optic systems (≥ 40 Gb/s) [96, 105]. Suppose we have three consecutive bits of '1' centered at $t = -2T_b$, $-T_b$ and 0. The ghost pulse generated by the nonlinear mixing (IFWM) of pulses at $-2T_b$ and $-T_b$ interferes with the pulse at $t = 0$. This interference leads to the amplitude jitter of the pulse at $t = 0$. In this chapter, we consider the impact of ISPM, IXPM and IFWM in a coherent fiber-optic system based on binary phase-shift keying (BPSK).

In many occasions fiber links can be seen as quasi-linear systems, if transmitted power is well controlled such that the nonlinear effect of fiber is not too large. Our work is based on this assumption and the nonlinearity of a fiber is described by the first-order perturbation approximation [99], [105]. In this chapter, we derive analytical expressions for PDFs and variances of bit '0' and bit '1' for dispersion-managed coherent fiber-optic systems based on BPSK. Our results show that the probability density functions for both bit '1' and bit '0' are of asymmetric shape when fiber nonlinearity is dominant impairment over amplified spontaneous emission (ASE) noise. One might expect that the PDFs should be symmetric since bit '0' (amplitude -1) and bit '1' (amplitude 1) occur with equal probability for systems based on BPSK. But the conditional PDF of the received signal given that bit '1' (or bit '0') is sent, is calculated by fixing the bit '1' (or bit '0') in the bit slot 0 and other bit slots carry bit '1' or bit '0' with equal probability. The non-degenerate symmetric four-wave mixing triplet involving the pump pulse in bit slot 0 (which is fixed) is responsible for making the PDFs asymmetric. However, the PDFs become nearly symmetric as ASE noise increases. Recently, auto correlation functions and approximate probability density function of IFWM induced phase noise have been obtained in [107] using a different approach. After numerically validating our analytical expression for the variance of IFWM, we used it as a design tool to optimize the various parameters such as pre-, post- and inline- dispersion compensation and launch power of a dispersion-managed coherent fiber-optic transmission system. Our results show that as the average dispersion of the dispersion managed transmission fiber becomes large, the optimum dispersion compensation ratio approaches 0.5. This implies that dispersion compensation at the transmitter (pre-compensation) should be roughly same as that at the receiver (post-compensation) for all the dispersion maps analyzed in this chapter when the average dispersion of the fiber-optic link (excluding pre- and post- compensation) is large.

The ASE noise introduced by an amplifier fluctuates the energy of a pulse. The fiber nonlinearity translates the energy fluctuations into phase fluctuations leading to nonlinear phase noise or Gordon-Mollenauer phase noise [108]. In this chapter, we ignore the nonlinear phase noise and mainly focus on the amplitude fluctuations due to IFWM. It is likely that the dispersion map that minimize the IFWM impairments would also minimize nonlinear phase noise. However, this would be the subject of a future investigation.

In section 3.2, mathematical derivation of PDF is given, in which first-order perturbation theory is used to solve the nonlinear Schrödinger equation (NLS). In section 3.3, the variance of IFWM is analytically calculated. In section 3.4, simulations based on the given analytical PDF are implemented and the results are compared with those from Monte-Carlo simulations. In addition, the optimum dispersion map is investigated based on the analytically calculated variance of IFWM for coherent fiber-optic systems. Finally, in section 3.5, the results and contributions are concluded.

3.2 Mathematical Derivation of PDF

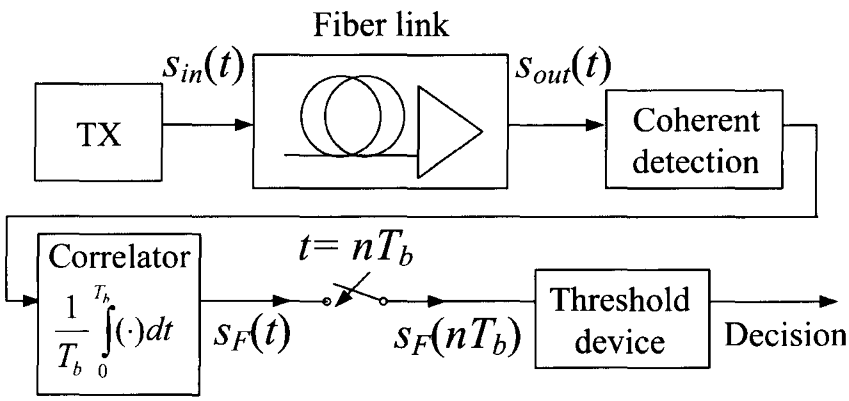

Figure 3.1: Coherent fiber-optic system.

In this section, we derive the PDF of received bits for a BPSK coherent fiber-optic system. Fig. 3.1 shows the scheme of the coherent fiber-optic system based on BPSK. Suppose the input to the fiber link is

$$s_{in}(t) = \sum_{n=-\infty}^{\infty} a_n \sqrt{P_0} f(t - nT_b) \tag{3.1}$$

where a_n is a random variable which takes values 1 and -1 with equal probability, P_0 is the peak power, $f(t)$ represents a basic pulse shape and T_b is the bit interval. We assume that the fiber channel is quasi-linear. Under this assumption, the output field of the fiber link can be evaluated using first-order perturbation theory [99], [105]. The evolution of the optical field envelope is described by the nonlinear Schrödinger equation in the lossless form,

$$i\frac{\partial u}{\partial z} - \frac{\beta_2(z)}{2}\frac{\partial^2 u}{\partial t^2} + \gamma \exp\left[-w(z)\right] |u|^2 u = 0, \tag{3.2}$$

where γ is the fiber nonlinear coefficient,

$$w(z) = \int_0^z \alpha(s) ds, \tag{3.3}$$

$\alpha(s)$ is the fiber loss/gain profile and $\beta_2(s)$ is the dispersion profile. Fig. 3.2 shows the typical dispersion and loss/gain profiles of a long-haul dispersion-managed fiber-optic system. The solution to Eq. (3.2) can be written as

$$u(t,z) = u_0(t,z) + \gamma u_1(t,z) + \gamma^2 u_2(t,z), \tag{3.4}$$

where $u_0(t,z)$ is the solution of the linear Schrödinger equation given by [106]

$$\begin{aligned} u_0(t,z) &= \mathcal{F}^{-1}\left[\widetilde{s}_{in}(\omega)\exp\left(i\omega^2 s(z)/2\right)\right] \\ &= \sqrt{P_0}\mathcal{F}^{-1}\left[\sum_n a_n \widetilde{f}(\omega)\exp\left(i\omega n T_b + i\omega^2 s(z)/2\right)\right] \end{aligned} \tag{3.5}$$

where $\mathcal{F}^{-1}$ denotes the inverse Fourier transform,

$$s(z) = \int_0^z \beta_2(s) ds, \tag{3.6}$$

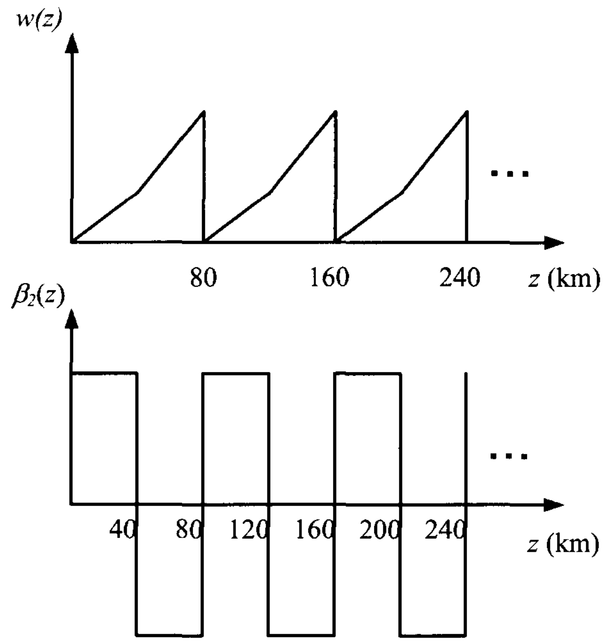

Figure 3.2: Typical dispersion and loss/gain profiles of the dispersion-managed fiber. Pre- and post- compensation are not shown.

$\widetilde{s}_{in}(\omega)$ and $\widetilde{f}(\omega)$ are the Fourier transform of $s_{in}(t)$ and $f(t)$, respectively. Substituting Eq. (3.4) in Eq. (3.2) and collecting the terms proportional to γ, we obtain

$$i\frac{\partial u_1}{\partial z} - \frac{\beta_2(z)}{2}\frac{\partial^2 u_1}{\partial t^2} = -\exp\left[-w(z)\right]|u_0|^2 u_0 \tag{3.7}$$

$u_1(t,z)$ represents the first order correction to Eq. (3.5) due to fiber nonlinearity. The nonlinear mixing of pulses in bit slots l, m and n leads to a ghost pulse in bit slot 0 if $l+m-n=0$. Without loss of generality, let us focus on the nonlinearly generated ghost pulses $u_1(t,z)$ at bit slot 0. Taking the Fourier transform of Eq. (3.7), we obtain

$$\begin{aligned} i\frac{\partial \widetilde{u}_1}{\partial z} + \frac{\beta_2(z)}{2}\omega^2\widetilde{u}_1 = &-\exp\left[-w(z)\right]\times \\ &\left[\widetilde{u}_0(\omega,z)\otimes\widetilde{u}_0^*(-\omega,z)\right]\otimes\widetilde{u}_0(\omega,z) \end{aligned} \tag{3.8}$$

Substituting Eq. (3.5) in Eq. (3.8) and considering only the four-wave mixing triplets that satisfy the condition $l+m-n=0$, we obtain

$$\gamma u_1(t,z) = P_0^{3/2}\sum_m\sum_n a_m a_n a_{m+n} X_{mn}(t,z) \tag{3.9}$$

where

$$\begin{aligned} X_{mn}(t,L) = &-\frac{i}{2\pi}\int_0^L\int_{-\infty}^{\infty}\mathcal{K}_{mn}(\omega,z) \\ &\times\exp\left\{i\left[s(L)-s(z)\right]\omega^2/2 - i\omega t\right\}d\omega dz, \end{aligned} \tag{3.10}$$

$$\begin{aligned} \mathcal{K}_{mn}(\omega,z) = &-\gamma\exp\left[-w(z)\right]\times \\ &\left[\widetilde{f}(\omega)r_m(\omega)\otimes\widetilde{f}(\omega)r_n(\omega)\right]\otimes\left\{\widetilde{f}^*(-\omega)r_{m+n}^*(-\omega)\right\}, \end{aligned} \tag{3.11}$$

$$r_m(\omega) = \exp\left[i\omega m T_b + i\omega^2 s(z)/2\right], \tag{3.12}$$

and L is the total transmission distance. We assume that the accumulated dispersion is zero at the receiver, $s(L)=0$. Using Eqs. (3.5) and (3.9) in Eq. (3.4) and ignoring the terms involving γ^n, $n > 1$, optical field envelope at the end of the transmission line for the bit slot 0 is

$$\begin{aligned} s_{out}(t) &= a_0\sqrt{P_0}f(t) + P_0^{3/2}\sum_m\sum_n a_m a_n a_{m+n} X_{mn}(t) \\ &+n(t) \end{aligned} \tag{3.13}$$

where $n(t)$ is a Gaussian white noise due to optical amplifiers. When

$$f(t) = \exp\left(-\frac{t^2}{2T_0^2}\right), \tag{3.14}$$

dispersion β_2 and loss coefficient α are constants, and dispersion of the transmission fiber is linearly compensated such that $s(L) = 0$, Eq. (3.10) reduces to that derived in [99], [105],

$$\begin{aligned} X_{mn}(t,L) = i\gamma \int_0^L &\exp\left(-\frac{t^2}{6T_0^2} - \alpha z\right) \\ \times &\frac{1}{\sqrt{1 + 2i\beta_2 z/T_0^2 + 3\left(\beta_2 z/T_0^2\right)^2}} \\ \times &\exp\left\{-\frac{3\left(2t/3 - nT_b\right)\left(2t/3 - mT_b\right)}{T_0^2\left(1 + 3i\beta_2 z/T_0^2\right)}\right. \\ &\left.-\frac{(m-n)^2 T_b^2}{T_0^2\left\{1 + 2i\beta_2 z/T_0^2 + 3\left(\beta_2 z/T_0^2\right)^2\right\}}\right\} dz \end{aligned} \tag{3.15}$$

After passing through the ideal unit gain coherent detector, the output signal $s_{out}(t)$ is multiplied by the $\sqrt{P_0}f^*(t)$ and integrated over one bit interval which is equivalent to the matched filter receiver. The output of the correlator is

$$\begin{aligned} s_F(T_b) &= a_0\frac{P_0}{T_b}\int_0^{T_b} |f(t)|^2\, dt \\ &+\frac{P_0^2}{T_b}\sum_m\sum_n a_m a_n a_{m+n}\int_0^{T_b} X_{mn}(t) f^*(t) dt \\ &+\frac{\sqrt{P_0}}{T_b}\int_0^{T_b} n(t) f^*(t) dt \end{aligned} \tag{3.16}$$

If $Re\left\{s_F(T_b)\right\} > 0$, it will be decided that bit '1' is transmitted. Otherwise, bit '0' is transmitted. Let

$$\begin{aligned} I &= Re\{s_F(T_b)\} \\ &= a_0 P_{av} + \sum_m \sum_n a_m a_n a_{m+n} y_{mn} + n_F \end{aligned} \tag{3.17}$$

where

$$P_{av} = \frac{P_0}{T_b} \int_0^{T_b} |f(t)|^2 \, dt \tag{3.18}$$

is the average power of the transmitted bit '1' or bit '0',

$$y_{mn} = \frac{P_0^2}{T_b} Re \left\{ \int_0^{T_b} X_{mn}(t) f^*(t) dt \right\}, \tag{3.19}$$

and

$$n_F = \frac{\sqrt{P_0}}{T_b} Re \left\{ \int_0^{T_b} n(t) f^*(t) dt \right\} \tag{3.20}$$

The characteristic function of random variable I is given by

$$\Psi_I(\xi) = E\{\exp(i\xi I)\} = \int_{-\infty}^{\infty} \exp(i\xi I)\, p(I) dI \tag{3.21}$$

where E denotes expectation and $p(I)$ is the conditional probability density function of received current I when bit '1' or bit '0' is sent. Because I is a function of transmitted random binary variables $a_{-N}, a_{-N+1}, \cdots, a_N$ and noise n_F, Eq. (3.21) can be rewritten as

$$\begin{aligned} \Psi_I(\xi) &= \int_{-\infty}^{+\infty} \cdots \int_{-\infty}^{+\infty} \exp\left[i\xi I \left(a_{-N}, a_{-N+1}, \cdots, a_N, n_F \right) \right] \\ &\quad \times p\left(a_{-N}, a_{-N+1}, \cdots a_N, n_F \right) \, da_{-N} da_{-N+1} \cdots da_N dn_F, \end{aligned} \tag{3.22}$$

where $p(a_{-N}, a_{-N+1}, \cdots a_N, n_F)$ is the joint probability density function of random variables $a_{-N}, a_{-N+1}, \cdots a_N, n_F$. When they are independent and identically distributed (i.i.d.) random variables, the joint probability density function in Eq. (3.22) becomes the products of probability functions of each random variable. Here, we assume that the ISI induced by fiber nonlinearity is only contributed by the neighboring N bits on both sides of the central bit, i.e., $(m, n) \in [-N, N]$. To calculate the conditional PDF given bit

'1', we assume that the bit in slot 0 is a '1', i.e., $a_0 = +1$, and the transmitted information bits are independent and with the equal probability being '1' or '0'. The characteristic function can be rewritten as

$$\begin{aligned}\Psi_I(\xi) &= \int_{-\infty}^{+\infty} \cdots \int_{-\infty}^{+\infty} \exp\left[i\xi\left(P_{av} + n_F\right.\right.\\ &\quad \left.\left. + \sum_m \sum_n a_m a_n a_{m+n} y_{mn}\right)\right]\\ &\quad \times p(a_{-N})p(a_{-N+1}) \cdots p(a_N)p(n_F)\\ &\quad \times da_{-N} da_{-N+1} \cdots da_N dn_F, \end{aligned} \tag{3.23}$$

where

$$p(n_F) = \frac{1}{\sqrt{2\pi}\sigma} \exp\left(-\frac{n_F^2}{2\sigma^2}\right), \tag{3.24}$$

where σ^2 is the variance of the Gaussian noise field n_F and it is proportional to the variance of the ASE noise $n(t)$, and

$$p(a_i) = \frac{1}{2}\left[\delta(a_i - 1) + \delta(a_i + 1)\right], \tag{3.25}$$

where $i \neq 0$ and $i \in [-N, N]$. Inserting Eqs. (3.24) and (3.25) into Eq. (3.23), we obtain

$$\begin{aligned}\Psi_I(\xi) = &\sum_{\substack{a_{-N}=-1\\ \text{or } 1}} \sum_{\substack{a_{-N+1}=-1\\ \text{or } 1}} \cdots \sum_{\substack{a_N=-1\\ \text{or } 1}} \int_{-\infty}^{+\infty} \frac{1}{2^{2N}\sqrt{2\pi}\sigma}\\ &\times \exp\left[i\xi\left(P_{av} + \sum_m \sum_n a_m a_n a_{m+n} y_{mn} + n_F\right)\right]\\ &\times \exp\left(-\frac{n_F^2}{2\sigma^2}\right) dn_F \end{aligned} \tag{3.26}$$

Taking the Fourier transform of Eq. (3.26), the probability density function of received electrical signal for bit '1' is obtained as

$$\begin{aligned} p_1(I) = &\frac{1}{2^{2N}\sqrt{2\pi}\sigma} \sum_{\substack{a_{-N}=-1\\ \text{or } 1}} \sum_{\substack{a_{-N+1}=-1\\ \text{or } 1}} \cdots \sum_{\substack{a_N=-1\\ \text{or } 1}}\\ &\exp\left[-\frac{\left(I - P_{av} - \sum\limits_m \sum\limits_n a_m a_n a_{m+n} y_{mn}\right)^2}{2\sigma^2}\right] \end{aligned} \tag{3.27}$$

Simplifying Eq. (3.27), we obtain

$$p_1(I) = \frac{1}{2^{2N}\sqrt{2\pi}\sigma} \sum_{x=1}^{2^{2N}} \exp\left[-\frac{(I - I_x^1)^2}{2\sigma^2}\right] \tag{3.28}$$

where

$$I_x^1 = P_{av} + \sum_m \sum_n a_m a_n a_{m+n} y_{mn} \tag{3.29}$$

and x is the index corresponding to each possible bit pattern in total 2^{2N}. Then, we expand I_x^1 as

$$\begin{aligned} I_x^1 &= P_{av} + y_{00} + 2 \sum_{m=-N,\neq 0}^{N} y_{m0} \\ &+ \sum_{m=-N,\neq 0}^{N} \sum_{n=-N,\neq 0}^{N} a_m a_n a_{m+n} y_{mn} \end{aligned} \tag{3.30}$$

In Eq. (3.30), the first term represents the average power of the transmitted bit, the second term represents the ISPM, the third term represents IXPM and the last term represents the IFWM. ISPM and IXPM are independent of bit pattern and only lead to deterministic changes to the first order. When the launch power is too large, the depletion of the pump pulses due to IFWM can not be ignored and as a result, the peak powers of the pulses vary leading to IXPM penalty which is bit pattern dependent. However, under the first order perturbation approximation, ISPM and IXPM effects are independent of bit pattern. Therefore, we finally obtain

$$I_x^1 = P' + \sum_{m=-N,\neq 0}^{N} \sum_{n=-N,\neq 0}^{N} a_m a_n a_{m+n} y_{mn} \tag{3.31}$$

where

$$P' = P_{av} + y_{00} + 2 \sum_{m=-N}^{N} y_{m0} \tag{3.32}$$

Calculation of the PDF of bit '0' is similar and proceeding as before, we obtain

$$p_0(I) = \frac{1}{2^{2N}\sqrt{2\pi}\sigma} \sum_{x=1}^{2^{2N}} \exp\left[-\frac{(I - I_x^0)^2}{2\sigma^2}\right] \tag{3.33}$$

where

$$\begin{aligned} I_x^0 &= -P_{av} - y_{00} - 2\sum_{m=-N}^{N} y_{m0} \\ &+ \sum_{m=-N,\neq 0}^{N}\sum_{n=-N,\neq 0}^{N} a_m a_n a_{m+n} y_{mn} \end{aligned} \tag{3.34}$$

3.3 Variance of IFWM

Suppose the bit '1' is sent, i.e., $a_0 = +1$. Eq. (3.17) can be rewritten as

$$\begin{aligned} I &= P_{av} + y_{00} + 2\sum_{m=-N,\neq 0}^{N} y_{m0} \\ &+ \sum_{m=-N,\neq 0}^{N}\sum_{n=-N,\neq 0}^{N} a_m a_n a_{m+n} y_{mn} + n_F \end{aligned} \tag{3.35}$$

where the first three terms are deterministic, and therefore they don't contribute to the variance. The fourth term involving a_m, a_n and a_{m+n}, leads to random fluctuations of the received signal. Then we can rewrite Eq. (3.35) as

$$I = P' + \delta I_{\text{FWM}} + n_F \tag{3.36}$$

where

$$P' = P_{av} + y_{00} + 2\sum_{m=-N,\neq 0}^{N} y_{m0}, \tag{3.37}$$

$$\delta I_{\text{FWM}} = \sum_{m=-N,\neq 0}^{N}\sum_{n=-N,\neq 0}^{N} a_m a_n a_{m+n} y_{mn} \tag{3.38}$$

Considering that the random bit sequence is independent of the Gaussian noise n_F, the variance of bit '1' can be written as

$$\sigma_1^2 = \sigma_{\text{IFWM}}^2 + \sigma_{n_F}^2 \tag{3.39}$$

where $\sigma_{n_F}^2$ is the variance of ASE noise after the matched filter. The variance of δI_{FWM} can be written as

$$\sigma_{\text{IFWM}}^2 = E\left\{\delta I_{\text{FWM}}^2\right\} - E^2\left\{\delta I_{\text{FWM}}\right\} \tag{3.40}$$

where E denotes the ensemble average.

For BPSK signal, we have

$$E\{a_m a_n\} = \begin{cases} 1, & \text{if} \quad m = n \\ 0, & \text{otherwise} \end{cases} \tag{3.41}$$

we have

$$E\{a_m a_n a_{m+n}\} = \begin{cases} 1, & \text{if} \quad m = 0 \quad \text{or} \quad n = 0 \\ 0, & \text{otherwise} \end{cases} \tag{3.42}$$

and therefore we obtain

$$E\{\delta I_{\text{FWM}}\} = 0 \tag{3.43}$$

Then Eq. (3.40) becomes

$$\begin{aligned} \sigma^2_{\text{IFWM}} &= E\left\{\delta I^2_{\text{FWM}}\right\} \\ &= E\left\{ \sum_{m=-N,\neq 0}^{N} \sum_{n=-N,\neq 0}^{N} a_m a_n a_{m+n} y_{mn} \right. \\ &\quad \left. \times \sum_{l=-N,\neq 0}^{N} \sum_{k=-N,\neq 0}^{N} a_l a_k a_{l+k} y_{lk} \right\} \\ &= \sum_{m=-N,\neq 0}^{N} \sum_{n=-N,\neq 0}^{N} \sum_{l=-N,\neq 0}^{N} \sum_{k=-N,\neq 0}^{N} \\ &\quad E\left\{a_m a_n a_{m+n} a_l a_k a_{l+k}\right\} y_{mn} y_{lk} \end{aligned} \tag{3.44}$$

Noticing that in Eq. (3.44), $m \neq 0$, $n \neq 0$ and

$$E\{a_m a_n a_{m+n} a_l a_k a_{l+k}\} = \begin{cases} 1, & \text{if} \quad m = l \quad \text{and} \quad n = k \\ 1, & \text{if} \quad m = k \quad \text{and} \quad n = l \\ 0, & \text{otherwise} \end{cases} \tag{3.45}$$

we finally obtain

$$\sigma^2_{\text{IFWM}} = 2 \sum_{m=-N,\neq 0}^{N} \sum_{n=-N,\neq 0}^{N} \sum_{m \neq n} y^2_{mn} + \sum_{m=-N,\neq 0}^{N} y^2_{mm} \tag{3.46}$$

We use Eq. (3.46) in section (3.4) to calculate the impact of various dispersion maps on the intrachannel impairments.

3.4 Simulations and Results

3.4.1 Probability density function

In this section, we implement the simulations based on the analytical PDF given in Eq. (3.28) and also the Monte-Carlo simulations to verify the results obtained from the analytical formula. The De Bruijn bit sequence of length 2^{13} is used as input in Monte-Carlo simulations and the lumped amplification is assumed throughout this paper. The critical simulation parameters are listed in Table 3.1. We consider a dispersion-managed

Table 3.1: Simulation parameters

Bit rate	40 Gb/s
Pulse width (FWHM)	7.5 ps
Pulse shape	Gaussian
Peak power	0 dBm
Amplifier spacing	80 km
Transmission distance	400 km
N (Effective neighboring bit slots)	10
No. of bits in Monte-Carlo sim.	2^{13}
Computational bandwidth	1600 GHz

fiber with two segments. The first segment is a standard SMF of 40 km length and dispersion $D_1 = 17$ ps/(km·nm) and this is followed by a reverse dispersion fiber of equal length and dispersion $D_2 = -17$ ps/(km·nm). The fiber loss for these two kinds of fibers are 0.2 dB/km and 0.25 dB/km, respectively. We consider two cases. In the first case, ASE noise is turned off and, dispersion and nonlinear effects are the only impairments. In Fig. 3.3(a) and 3.3(b), PDFs of bit '1' and bit '0' are shown, respectively for this case. $\sigma = 0$ in Eq. (3.28) leads to Dirac-Delta function instead of Gaussian function. In our simulation, the rectangular function with very narrow width $\Delta = 10^{-3}$ for the normalized current and height $1/\Delta = 10^3$ is used to approximate the Dirac-Delta function to implement the analytical calculation of PDF. One would expect the PDFs of intra-channel impairments to be symmetric since bit '1' and bit '0' are represented by optical field amplitudes 1 and -1, respectively and they occur with equal probability. But the conditional PDF of the received signal when bit '1' (or bit '0') is sent, is calculated by fixing the bit '1 (or bit '0') in the bit slot 0 and other bit slots carry bit '1' or bit '0' with equal probability. The non-degenerate symmetric IFWM triplet of the type $u_j u_{-j} u_0^*$, $j \neq 0$, involves the pump pulse u_0 in bit slot 0 and this is responsible for making the PDFs asymmetric. If the pusles in all the bit slots were to be of amplitudes $+1$ and -1 with equal probability, the PDFs would be symmetric.

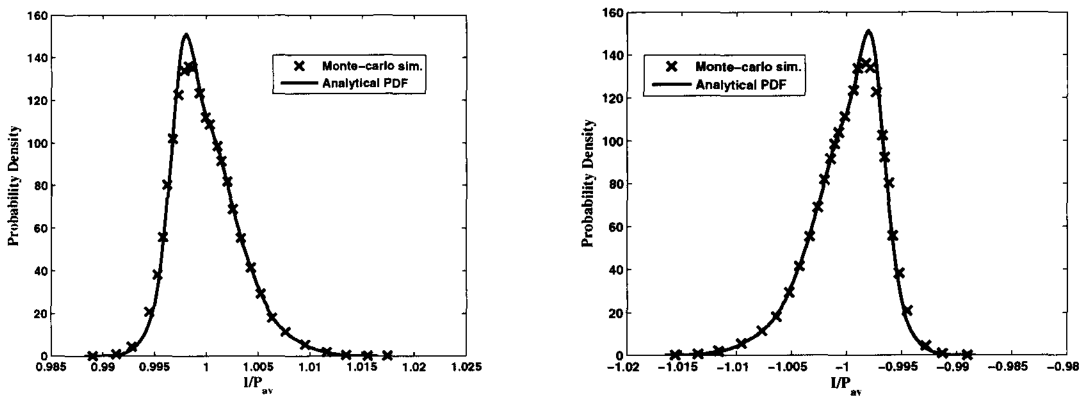

(a) (b)

Figure 3.3: (a) PDF of bit '1'. (b) PDF of bit '0'.

In the second case, nonlinear impairments are weaker than that due to ASE. In Fig. 3.4, the cross marks show the PDF from Monte-Carlo simulation and the solid line shows the analytically calculated PDF that agrees well with the numerically calculated PDF. The noise figure of amplifiers is set to 4.5 dB in this simulation. As can be seen, the PDF becomes nearly symmetric since ASE is the dominant noise process in this example. Fig. 3.5 shows the standard deviation of bit '1'. The solid line with triangles shows the result from the Monte-Carlo simulation and the the dashed line with circles shows that from the

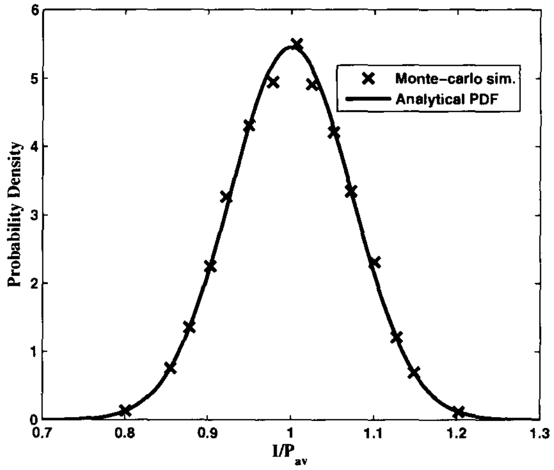

Figure 3.4: PDF of bit '1' with ASE noise. PDF of bit '0' is similar to that of bit '1'.

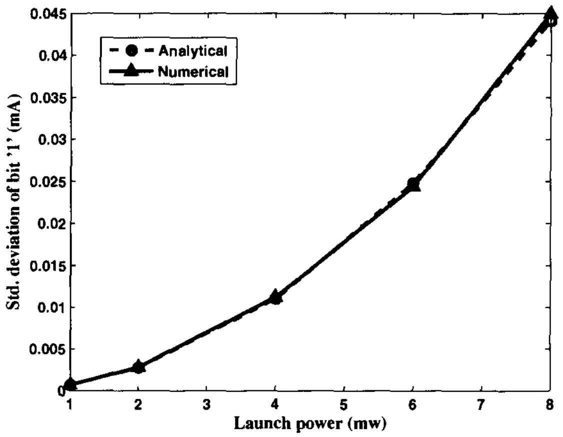

Figure 3.5: Normalized standard deviation of bit '1'.

analytical formula (Eq. (3.46)) and both of them match each other very well.

3.4.2 Optimum dispersion maps

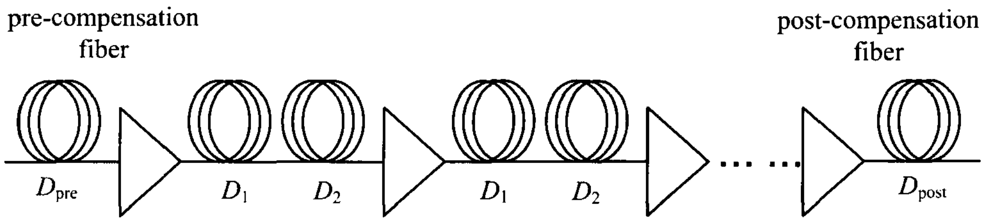

Figure 3.6: Dispersion-managed fiber link with pre- and post- dispersion compensation.

Fig. 3.6 shows the fiber link consisting of pre-, post- and inline dispersion compensation. We assume the same parameters as before except that average dispersion of the transmission fiber, total transmission distance, pre- and post- compensation are variables. In this section, we will investigate the optimum dispersion map and also the optimum dispersion compensation ratio (DCR) for the fiber-optic coherent system based on the analytical formula given in Eq. (3.46).

We define the average dispersion within each amplifier spacing as

$$D_{av} = (D_1 L_1 + D_2 L_2) / (L_1 + L_2) \tag{3.47}$$

where D_j and L_j, $j = 1, 2$, are the dispersion and length of the fiber section j between amplifiers. We assume that total accumulated dispersion at the receiver is zero. The dispersion compensation ratio (DCR) is defined as

$$\text{DCR} = \frac{\text{Accum. disp. of pre-compensation fiber}}{\text{Accum. disp. of pre- and post- compensation fibers}} \tag{3.48}$$

The dispersion of the compensating fiber used at the transmitter and receiver is -100 ps/(km·nm) in this study. The compensating fiber loss is 0.5 dB/km. The loss of anomalous dispersion fiber (D_1) and normal dispersion fiber (D_2) are 0.2 dB/km and 0.25 dB/km, respectively. The variance of IFWM changes with the dispersion map, pre-compensation ratio and also the transmission distance. Combining all these three factors, we then study the optimum dispersion compensation scheme for the fiber-optic coherent system.

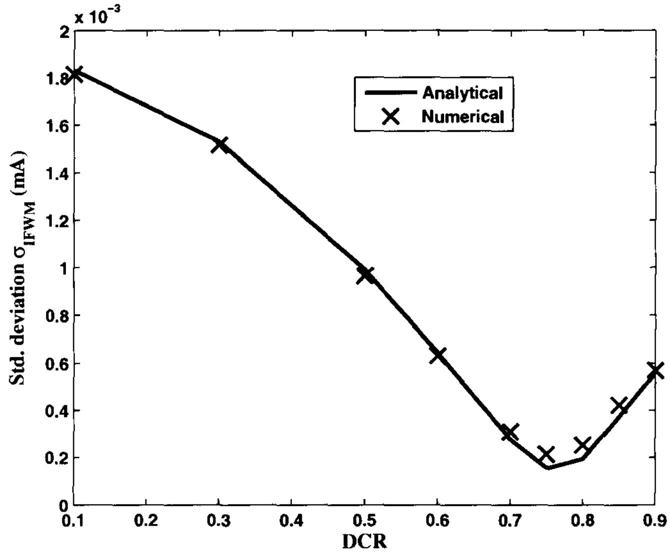

Figure 3.7: Comparison of standard deviation of IFWM between analytical expression and numerical simulation at $L = 800$ km and $D_{av} = 1.25$ ps/(km·nm).

The solid line in Fig. 3.7 shows the standard deviation of IFWM obtained analytically and the $\times$ shows the numerical simulation of nonlinear Schrődinger equation. It can be seen that σ_{IFWM} can be significantly reduced if 75% of the dispersion of the transmission fiber is compensated at the transmitter. Fig. 3.8 shows the optimum DCR at three different transmission distances, $L = 800, 1200$ and 1600 km, respectively, with $D_{av} = 1.25$ ps/(km·nm). From Fig. 3.8, we see that at smaller transmission distances, it is advantageous to do the dispersion compensation mostly at the transmitter (DCR close to 0.8). However, as transmission distance increases, optimum DCR approaches 0.5 for the dispersion-managed fiber-optic link. Fig. 3.9 shows the optimum DCR as a function of the average dispersion, D_{av}. The optimum DCR is that DCR which minimizes the variance of IFWM and it is found using line search method. It can be seen that as D_{av} increases, optimum DCR approaches 0.5 for the dispersion-managed fiber-optic link. Fig.

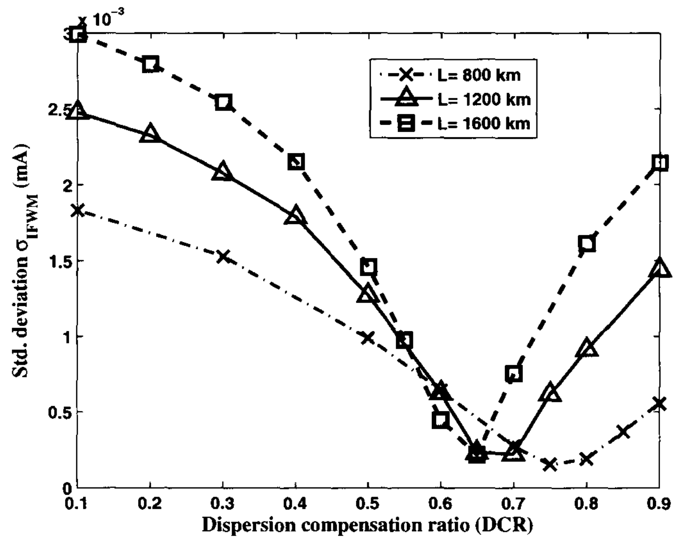

Figure 3.8: Standard deviation of IFWM as a function of DCR at $D_{av} = 1.25$ ps/(km·nm).

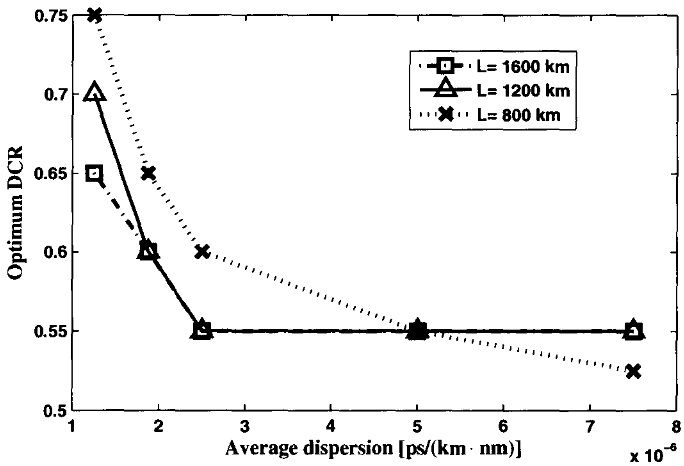

Figure 3.9: Optimum DCR v.s. Average dispersion.

3.10 shows the dependence of standard deviation of IFWM on average dispersion. We see that the system scheme with larger average dispersion has better performance. This is because the frequency components of the pulses walk off quickly as D_{av} increases. As a result, the ghost pulses generated in different amplifier spans do not add up coherently.

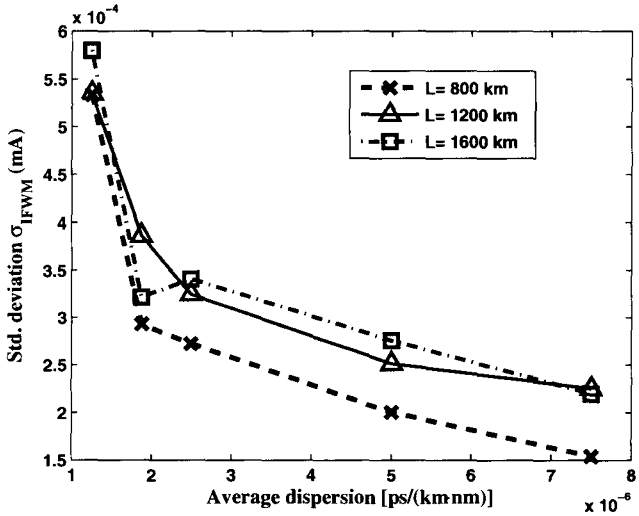

Figure 3.10: Standard deviation of IFWM varying as a function of average dispersion at optimum DCR.

The numerical simulation of NLS is time-consuming, however, the analytical method based on solving NLS under the first-order perturbation approximation is a quite efficient, and therefore, the analytical PDF and variance can be obtained more easily without requiring extensive computational efforts, and also with fairly good accuracy for quasi-linear systems.

3.5 Conclusion

We have derived analytical expressions for the PDFs and variances of bit '1' and bit '0' in a dispersion managed coherent fiber-optic system based on BPSK. The analytical expressions are in good agreement with numerical simulations. We have shown that PDFs of bit '1' and bit '0' become asymmetric when IFWM is dominant impairment over ASE. But the PDFs become nearly symmetric as the variance of ASE increases. The analytical formula for the variance of IFWM is used as a design tool to investigate the optimum dispersion maps for coherent fiber-optic systems based on BPSK. Our results show that the optimum dispersion compensations ratio approaches 0.5 as the average dispersion of the dispersion managed transmission fiber becomes large for all the dispersion maps analyzed in this chapter.

Chapter 4

Temporal Filtering Technique using Time Lenses for Optical Transmission Systems

4.1 Introduction

It is well known that there exits an analogy between the spatial diffraction and temporal dispersion [59]-[61]. In the spatial domain, an optical wave propagating in free space diverges due to diffraction. As an analogue, in the temporal domain, an optical pulse propagating in a dispersive medium broadens due to dispersion. This space-time duality can also be extended to lenses. A space lens generates quadratic phase modulation on the transverse profile of the input beam and its analogue, a time lens, simply applies a quadratic phase modulation to a temporal optical waveform. On this basis, several temporal analogues to spatial systems based on thin lenses have been created and many real-time optical signal processing applications, including temporal imaging, pulse compression, and temporal filtering using time lenses have been proposed [62], [109]-[111]. In 1992, Lohmann and Mendlovic first proposed the temporal filtering technique [62]. A temporal filter was introduced in a 4-f configuration consisting of time lenses in their pioneering work. In the spatial domain, a conventional lens produces the Fourier transform (FT) at the back focal plane of an optical signal placed at the front focal plane, which is known as a *2-f configuration* or *2-f subsystem*. The spatial filter placed at the back focal plane modifies the signal spectrum, and a subsequent 2-f subsystem provides the Fourier transform of the modified signal spectrum, which returns the signal to the spatial domain with spatial inversion.

An exact analogy exists between spatial filtering and temporal filtering techniques. In the case of temporal filtering, the spatial lens is replaced by a time lens (which is nothing but a phase modulator), and spatial diffraction is substituted with second-order dispersion. Figure 4.1 shows a modified 4-f system consisting of two time lenses. In this 4-f configuration, the subsystem T1 provides the Fourier/inverse FT of the input signal. The signs of chirp and dispersion coefficients are reversed in the 2-f subsystem T2 after the temporal filter. In contrast, Lohmann and Mendlovic proposed the 4-f configuration in which the signs of the dispersion coefficients of the 2-f subsystems are identical [62]. This implies that the second 2-f subsystem provides the Fourier transform of the modified signal spectrum leading to a time-reversed bit pattern, whereas in the approach we proposed in 2008 [63], it provides the IFT so that the output bit pattern is not reversed in time. This approach has no spatial analog since the sign of spatial diffraction cannot be changed [112].

In this chapter, based on the 4-f configuration consisting of time lenses, two applications have been numerically implemented. One of them is a tunable wavelength division demultiplexer [63]. The wavelength division multiplexing demultiplexer is realized using the temporal band pass filter in a 4-f system. The temporal filter is realized using an amplitude modulator, and the channel to be demultiplexed can be dynamically changed by changing the input voltage to the amplitude modulator. The passband of the temporal filter is chosen to be at the central frequency of the desired channel with a suitable bandwidth such that only the signal carried by the channel to be demultiplexed passes through it with the least attenuation. The wavelength division multiplexed signal passes through the 2-f subsystem T1 (see Figure 4.1 and its FT in the time domain is obtained. After the temporal filter, the signals in any other undesired channels are blocked and the signal in the desired channel then passes through the 2-f subsystem T2, which finally produces the demultiplexed signal as its original bit sequence by the exact IFT.

The other application of the 4-f temporal filtering scheme is a higher-order dispersion compensator [63]. The temporal filter in this application is realized by a phase modulator. To compensate for fiber dispersion, the time domain transfer function of the phase modulator has the same form as the frequency domain transfer function of fiber but the signs of dispersion coefficients are opposite. At the temporal filter, the Fourier transformed input signal is multiplied by the time domain transfer function of the phase modulator so that fiber dispersion–induced phase shift is canceled out.

4.2 Configuration of a Time-Lens–Based Optical Signal Processing System

Figure 4.1 shows the modified 4-f system based on time lenses [63]. This 4-f system consists of two cascaded 2-f subsystems T1 and T2, each of which contains a time lens and two segments of single-mode fibers (SMFs) that are symmetrically placed on both sides of the time lens. A time lens is a temporal analog of a space lens and it is realized by an electro-optic phase modulator that can generate quadratic phase modulation. The signal spectrum can be modified using a temporal filter. The temporal filter can be realized using an amplitude and/or phase modulator. The transfer function of the temporal filter can be changed by changing the input voltage to the amplitude and/or phase modulator.

For the proper operation of this system, two phase modulators and the temporal filter should be properly synchronized. If T_k is the absolute time at the phase modulator k, $k = 1, 2$, then they are related by

$$T_2 = T_1 + f_1/v_{g1} + f_2/v_{g2}, \tag{4.1}$$

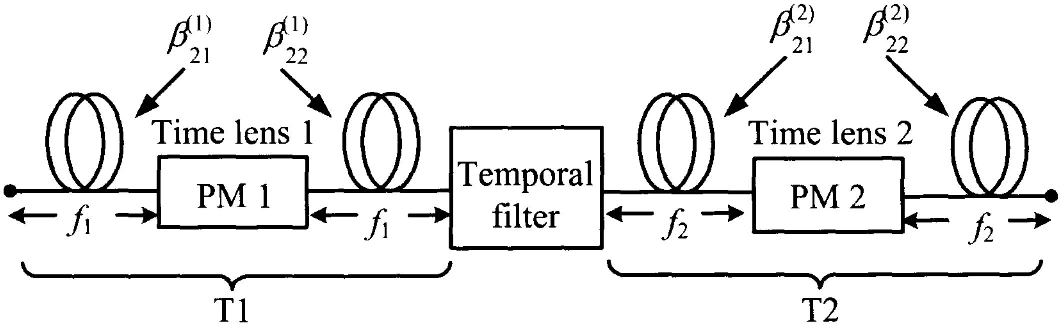

Figure 4.1: Scheme of a typical 4-f system. PM= Phase modulator.

where v_{g1} and v_{g2} are the group speeds of the fibers after the time lens 1 and just before the time lens 2, respectively. f_1 and f_2 are the fiber lengths as shown in Figure 4.1. This delay between the driving voltages of the phase modulators can be achieved using a microwave delay line. Similarly, the absolute time T_f at the temporal filter is related to T_1 by

$$T_f = T_1 + f_1/v_{g1}, \tag{4.2}$$

where f_1 is the length of the SMF in T1.

Propagation of the optical signal in a system consisting of a dispersive SMF and the time lens (such as the 2-f subsystem T1 in Figure 4.1) results in the FT of the input signal at the length $2f_1$. We use the following definitions of FT pairs:

$$\tilde{U}(\omega) = \mathcal{F}\{u(t)\} = \int_{-\infty}^{+\infty} u(t)\exp(i\omega t)dt \tag{4.3}$$

$$u(t) = \mathcal{F}^{-1}\{\tilde{U}(\omega)\} = \frac{1}{2\pi}\int_{-\infty}^{+\infty} \tilde{U}(\omega)\exp(-i\omega t)d\omega, \tag{4.4}$$

where $u(t)$ is a temporal function and $\tilde{U}(\omega)$ is its FT. The time lens is implemented using an optical phase modulator whose time domain transfer function is given by

$$h_j(t) = \exp\left(iC_j t^2\right), \quad j = 1, 2, \tag{4.5}$$

where C_j is the chirp coefficient of the phase modulator j in the 2-f subsystem T_j, $j = 1, 2$, and t is the time variable in a reference frame that moves with an optical pulse. Using

Eq. (4.5) in Eq. (4.3), we obtain the FT of the transfer function $h_j(t)$:

$$\tilde{H}_j(\omega) = \sqrt{i\pi/C_j}\exp\left(-i\frac{\omega^2}{4C_j}\right), \; j = 1, 2. \tag{4.6}$$

Suppose that the field envelope of the input signal is $u(t, 0)$, and the corresponding FT is $\tilde{U}(\omega, 0)$. Let $\beta_{21}^{(k)}$ and $\beta_{22}^{(k)}$ be the dispersion coefficients of the first and second fibers in the subsystem T_k, $k = 1, 2$, respectively, and f_k be the length of the SMF in T_k, $k = 1, 2$. Before the time lens of T1 ($z = f_{1-}$), the temporal signal is [1]

$$u(t, f_{1-}) = \frac{1}{2\pi}\int_{-\infty}^{+\infty}\tilde{U}(\omega, 0)\exp\left(\frac{i}{2}\beta_{21}^{(1)}f_1\omega^2 - i\omega t\right)d\omega. \tag{4.7}$$

The behavior of the time lens is described as follows:

$$u(t, f_{1+}) = u(t, f_{1-})\; h_1(t). \tag{4.8}$$

Because the product in the time domain becomes a convolution in spectral domain, taking the Fourier transform of Eq. (4.8), we obtain

$$\begin{aligned}\tilde{U}(\omega, f_{1+}) &= \mathcal{F}\left\{u(t, f_{1-})h_1(t)\right\} \\ &= \frac{1}{2\pi}\int_{-\infty}^{\infty}\tilde{U}\left(\omega - \omega', f_{1-}\right)\tilde{H}_1(\omega')d\omega',\end{aligned} \tag{4.9}$$

where $\tilde{U}(\omega, f_{1-})$ is the FT of $u(t, f_{1-})$. Hence, at the end of the first 2-f subsystem T1, we obtain

$$u(t, 2f_1) = \frac{1}{2\pi}\int_{-\infty}^{\infty}\tilde{U}(\omega, f_{1+})\exp\left(\frac{i}{2}\beta_{22}^{(1)}f_1\omega^2 - i\omega t\right)d\omega. \tag{4.10}$$

Substituting Eq. (4.9) into Eq. (4.10), by choosing the focal length as [62]

$$f_1 = 1\Big/\left(2\beta_{22}^{(1)}C_1\right), \tag{4.11}$$

and after some algebra (see A.1), we obtain the following:

$$u(t, 2f_1) = \frac{\sqrt{i\pi/C_1}}{2\pi\left|\beta_{22}^{(1)}f_1\right|}\tilde{U}\left(\frac{t}{\beta_{22}^{(1)}f_1}, 0\right)\exp\left(-i\phi_{res}\right), \tag{4.12}$$

where the residual phase term is given by

$$\phi_{res} = \left[\frac{1}{\beta_{22}^{(1)}f_1} - \frac{\left(\beta_{21}^{(1)} + \beta_{22}^{(1)}\right)}{2\left(\beta_{22}^{(1)}\right)^2 f_1}\right]t^2. \tag{4.13}$$

Let us consider the case when the temporal filter is absent. This can be divided into two cases.

Case 1: $\beta_{22}^{(1)} = \beta_{21}^{(1)} = \beta_2^{(1)}$

In this case, $\phi_{res} = 0$ and

$$u(t, 2f_1) = \frac{\sqrt{i\pi/C_1}}{2\pi\left|\beta_2^{(1)} f_1\right|}\, \tilde{U}\left(\frac{t}{\beta_2^{(1)} f_1}, 0\right). \tag{4.14}$$

Choosing $\beta_{21}^{(2)} = \beta_{22}^{(2)} = \beta_2^{(2)}$ and $f_2 = 1\Big/\left(2\beta_{22}^{(2)} C_2\right)$ in the 2-f subsystem T2 and noting that

$$\mathcal{F}\{\tilde{U}(t/\beta_2^{(1)} f_1, 0)\} = \left(2\pi\left|\beta_2^{(1)} f_1\right|\right) u\left(-\beta_2^{(1)} f_1 \omega, 0\right), \tag{4.15}$$

we finally obtain (see A.2)

$$u(t, 2f_1 + 2f_2) = u\left(-\frac{\beta_2^{(1)} f_1}{\beta_2^{(2)} f_2}\, t, 0\right), \tag{4.16}$$

where $2f_1 + 2f_2$ is the total length of the time-lens system. For the 4-f configuration proposed by Lohmann and Mendlovic, the magnification factor is defined as

$$M = -\frac{C_2}{C_1} = -\frac{\beta_2^{(1)} f_1}{\beta_2^{(2)} f_2}. \tag{4.17}$$

If $\text{sgn}\left(\beta_2^{(1)}\right) = \text{sgn}\left(\beta_2^{(2)}\right)$, from Eq. (4.16) it follows that M is negative. Defining a positive stretching factor $m = |M|$, Eqs. (4.17) and (4.16) can be rewritten as

$$\beta_2^{(1)} f_1 = m\beta_2^{(2)} f_2 \quad \text{and} \quad C_2 = mC_1 \tag{4.18}$$

and

$$u\left(t, 2f_1 + 2f_2\right) = u\left(-mt, 0\right), \tag{4.19}$$

which shows that T2 provides the scaled FT of its input and then leads to an inverted image of the signal input of the 4-f configuration [62]. If $M = -1$, T2 provides the exact FT and this leads to the reversal of the bit sequence within a frame, which requires additional signal processing in the optical/electrical domain to recover the original bit sequence.

In our work, the 4-f system of Lohmann and Mendlovic is reconfigured. Suppose $\mathrm{sgn}\left(\beta_2^{(1)}\right) = -\mathrm{sgn}\left(\beta_2^{(2)}\right)$, Eqs. (4.17) and (4.16) can be rewritten as

$$\beta_2^{(1)} f_1 = -m\beta_2^{(2)} f_2 \quad \text{and} \quad C_2 = -mC_1 \tag{4.20}$$

and

$$u(t, 2f_1 + 2f_2) = u(mt, 0), \tag{4.21}$$

which shows that the 2-f subsystem T2 provides the scaled IFT so that the signal at the end of the 4-f system is not time-reversed. If $M = 1$, the output signal is identical to the input signal. We note that in spatial optical signal processing, it is not possible to obtain both direct and inverse Fourier transformation since the sign of diffraction cannot be changed [112]. Table 4.1 lists the signs of fiber dispersions and chirp coefficients of subsystems T1 and T2 to produce signals with and without time reversal.

Table 4.1: Comparison of fiber dispersions and phase coefficients for different time-lens systems.

Parameters	PM1	PM2	T1		T2		Function
	C_1	C_2	$\beta_{21}^{(1)}$	$\beta_{22}^{(1)}$	$\beta_{21}^{(2)}$	$\beta_{22}^{(2)}$	
Case 1	+	+	+	+	+	+	Time reversal
	-	-	-	-	-	-	Time reversal
	+	-	+	+	-	-	No time reversal
	-	+	-	-	+	+	No time reversal
Case 2	+	-	-	+	-	+	No time reversal
	-	+	+	-	+	-	No time reversal

Case 2: $\beta_{22}^{(1)} = -\beta_{21}^{(1)}$

In this case,

$$\phi_{res} = \exp\left(-i\frac{t^2}{\beta_{22}^{(1)} f_1}\right) \tag{4.22}$$

and

$$u(t, 2f_1) = \frac{\sqrt{i\pi/C_1}}{2\pi\left|\beta_{22}^{(1)} f_1\right|}\,\tilde{U}\left(\frac{t}{\beta_{22}^{(1)} f_1}, 0\right)\exp\left(-i\frac{t^2}{\beta_{22}^{(1)} f_1}\right). \tag{4.23}$$

If we configure the 2-f subsystem T2 with reversed parameters,

$$\beta_{21}^{(2)} f_2 = -\beta_{22}^{(1)} f_1, \; C_2 = -C_1, \; \beta_{22}^{(2)} f_2 = -\beta_{21}^{(1)} f_1, \tag{4.24}$$

then we find that the input signal of T1 can be exactly recovered at the end of T2 (see A.3),

$$u(t, 2f_1 + 2f_2) = u(t). \tag{4.25}$$

Lines 5 and 6 in Table 4.1 present two possible configurations of **Case 2**. The result of Eq. (4.25) has a simple physical explanation. When $\beta_{21}^{(2)} f_2 = -\beta_{22}^{(1)} f_1$, the accumulated dispersion of the second fiber of T1 is compensated by that of the first fiber of T2, leading to unity transfer function. After that, since chirp coefficients C_1 and C_2 are of opposite sign, they cancel each other too, making the transfer function from PM1 to PM2 (see Figure 4.1) to unity. Finally, the accumulated dispersion of the first fiber of T1 is compensated by that of the second fiber of T2 when $\beta_{22}^{(2)} f_2 = -\beta_{21}^{(1)} f_1$. Thus, the total transfer function of the 4-f system is unity.

By inserting a temporal filter between two 2-f subsystems (see Figure 4.1), we can easily fulfill various kinds of optical signal processing in the time domain. The important advantage of the time-lens–based temporal filtering technique is that the transfer function of the temporal filter can be dynamically altered by changing the input voltage to the amplitude/phase modulator and therefore, this technique could have potential applications for switching and multiplexing in optical networks. Next, we provide two examples of optical signal processing based on this time-lens temporal filtering technique to show the potential advantages of this temporal filtering technique. One example is a tunable wavelength division demultiplexer and the other is a higher-order fiber dispersion compensator.

4.3 Wavelength Division Demultiplexer

For fiber-optic networks, tunable optical filters are desirable so that center wavelengths of the channels to be added or dropped at a node can be dynamically changed. Tunable optical filters are typically implemented using directional couplers or Bragg gratings. We discuss a temporal filtering technique for the implementation of a tunable optical filter. As an example, let us consider the case of a 2-channel WDM system at 40 Gb/s channel with a channel separation of 200 GHz. Let the input to the 4-f system be the superposition of two channels as shown in Figure 4.2 (b). Here we ignore the impairments caused by the fiber-optic transmission and assume that the input to the 4-f system is the same as the transmitted multiplexed signal. In this example, we have simulated a random bit pattern consisting of 16 bits in each channel. The bit '1' is represented by a Gaussian pulse of width 12.5 ps. We assume that the bit rate is 40 Gb/s and therefore the signal bandwidth for each channel is approximately 80 GHz (Return-to-zero (RZ) signal with duty cycle of 0.5). Thus, the channel separation of 200 GHz is wide enough to avoid channel interference. Assume that channel 1 is centered at the optical carrier frequency ω_0 and channel 2 is centered at $\omega_0 + 2\Delta\omega$, where $2\Delta\omega$ is the channel separation. A band pass filter that is also centered at ω_0 and with double-side bandwidth of $2\Delta\omega$ can allow channel 1 to transmit while it blocks the channel 2. In this case, the temporal band pass filter is realized using an amplitude modulator—for instance, an electroabsorption modulator (EAM), with a time domain transfer function

$$H(t) = \begin{cases} 1, & |t/\beta_2^{(1)} f_1| \leq \Delta\omega \\ 0, & \text{otherwise} \end{cases}, \tag{4.26}$$

where $\beta_{21}^{(1)} = \beta_{22}^{(1)} = \beta_2^{(1)}$ is the dispersion coefficient of the SMF in the 2-f subsystem T1 and $\Delta\omega/2\pi = 100$ GHz. In this section and in Section 4.4, we assume that $\beta_{21}^{(j)} = \beta_{22}^{(j)} = \beta_2^{(j)}$, $j = 1, 2$, and $M = 1$ unless otherwise specified. Considering the realistic implementation of the high-speed amplitude modulator, we need to choose the parameters of the 4-f system carefully. The state-of-the-art EAM operates up to a bit rate of 40 Gb/s

[113, 114], which implies that it can be turned on and off with a temporal separation of 25 ps. From Eq. (4.26), we see that the amplitude modulator should be turned on for a duration

$$\Delta T = 2\left|\beta_2^{(1)} f_1\right| \Delta\omega \tag{4.27}$$

and then it is turned off. Setting $\Delta T \geq 25$ ps, we find that

$$\left|\beta_2^{(1)} f_1\right| \geq 20 \text{ ps}^2. \tag{4.28}$$

Eq. (4.28) can be satisfied using a dispersion compensation module (DCM) with dispersion coefficient $\beta_2^{(1)} = 123$ ps^2/km and length $f_1 = 1$ km. From Eq. (4.27), we find $\Delta T = 155$ ps. To implement IFT in T2, we use a standard SMF with dispersion coefficient $\beta_2^{(2)} = -21$ ps^2/km and length $f_2 = 5.86$ km, which leads to $\beta_2^{(2)} f_2 = -\beta_2^{(1)} f_1$ and $M = 1$.

Figure 4.2 shows a wavelength division demultiplexer based on a 4-f time-lens system. After the 2-f subsystem T1, we obtain the FT of the multiplexed signal in time domain, given by

$$q(t, 2f_{1-}) = \left[\tilde{U}_1(\omega) + \tilde{U}_2(\omega)\right]\Big|_{\omega = t/\left(\beta_2^{(1)} f_1\right)}, \tag{4.29}$$

where $\tilde{U}_1$ and $\tilde{U}_2$ are the spectra of the signals for channel 1 and channel 2, respectively. Then it passes through the temporal filter defined by Eq. (4.26), and the output is given by

$$\begin{aligned} q(t, 2f_{1+}) &= H(t)\left[\tilde{U}_1(\omega) + \tilde{U}_2(\omega)\right]\Big|_{\omega = t/\left(\beta_2^{(1)} f_1\right)}, \\ &= \tilde{U}_1(\omega)\Big|_{\omega = t/\left(\beta_2^{(1)} f_1\right)} \end{aligned} \tag{4.30}$$

and as shown in Figure 4.2 (c), the signal from channel 2 is blocked. Thus, at the input end of the 2-f subsystem T2, only the signal from channel 1 is retained. Finally, we obtain the demultiplexed signal for channel 1 at the output of the 2-f subsystem T2 as shown in Figure 4.2 (d). According to Eq. (4.21), it is $q(t, 2f_1 + 2f_2) = u_1(t)$ for $m = 1$, which is identical to the original input of the channel 1. As can be seen, the data in channel 1 can be successfully demultiplexed.

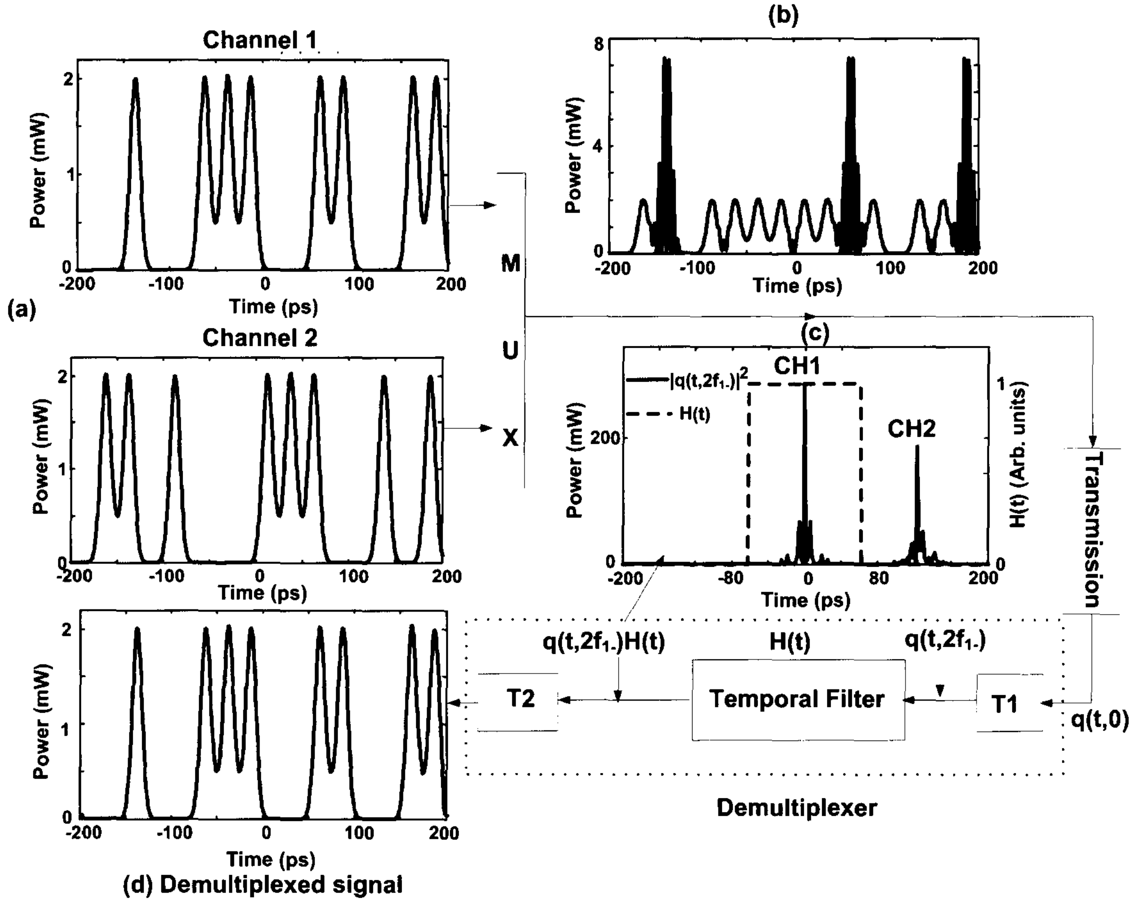

Figure 4.2: A WDM demultiplexer based on a 4-f time-lens system ($M = 1$). (a) Input signals from channel 1 and channel 2. (b) Multiplexed output signal. (c) Combined signals before and after the temporal filter. (d) Demultiplexed signal in channel 1.

For a practical implementation, the quadratic phase factor of Eq. (4.5) cannot increase indefinitely with time and therefore, a periodic time lens is introduced in Ref. [115]. It is given by

$$h_j(t) = \sum_{n=-\infty}^{+\infty} h_{0j}\left(t - nt_f\right), \tag{4.31}$$

where

$$h_{0j}(t) = \begin{cases} \exp\left(iC_j t^2\right), & |t| < \frac{t_f + t_g}{2} \\ \text{otherwise} \end{cases}, \quad j = 1, 2, \tag{4.32}$$

where t_f is the frame time and t_g is the guard time between the frames. Based on the periodic time lenses, we redo the above simulation with a random bit pattern consisting of 3 frames (= 48 bits) in each channel. We assume the frame time t_f = 400 ps and therefore, a frame consists of 16 bits. Figure 4.3 (a) shows the input bit sequence of channel 1. Figures 4.3 (b) and 4.3 (c) show the demultiplexed signals for $M = -1$ (time reversal) and $M = 1$ (without time reversal), respectively. For the case of $M = -1$, we choose the same parameters as for the case of $M = 1$ except that $\beta_2^{(1)} f_1 = \beta_2^{(2)} f_2$. From Figure 4.3 (b), we see that the pulses at the edges of frames are distorted, whereas the output pulses without time reversal as shown in Figure 4.3 (c) suffer only some minor distortions. As discussed in Ref. [115], the time-reversal system introduces distortion if there is no guard time between the frames because the bits at the left and right edges of a frame are imaged by the neighboring (in time domain) time lenses. As $\left|\beta_2^{(1)}\right|$ increases, the distortion also increases because pulses at the edges of a frame broaden more due to high dispersion of the 2-f subsystems and occupy the neighboring frames. In this modified 4-f configuration ($M = +1$), the distortion is less (Figure 4.3 (c)) than with $M = -1$ (Figure 4.3 (b)). This is probably because the distortion introduced by the first 2-f system is suppressed by that due to the second 2-f system since the signs of the dispersions are reversed. These distortions can be avoided by introducing a guard time between frames, as shown in Figure 4.4. Figure 4.4 (a) shows the input bit sequence with a guard time of

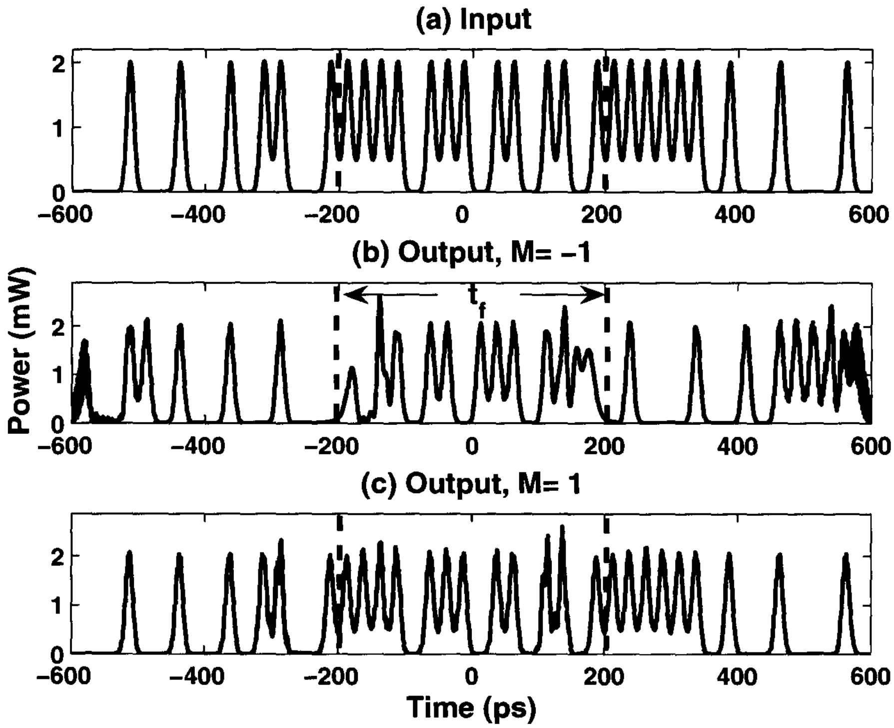

Figure 4.3: Input and output bit sequences of the WDM demultiplexer based on a 4-f time-lens system. (a) Input. (b) Output with time reversal, $M = -1$. (c) Output without time reversal, $M = +1$. Guard time $t_g = 0$ and $t_f = 400$ ps.

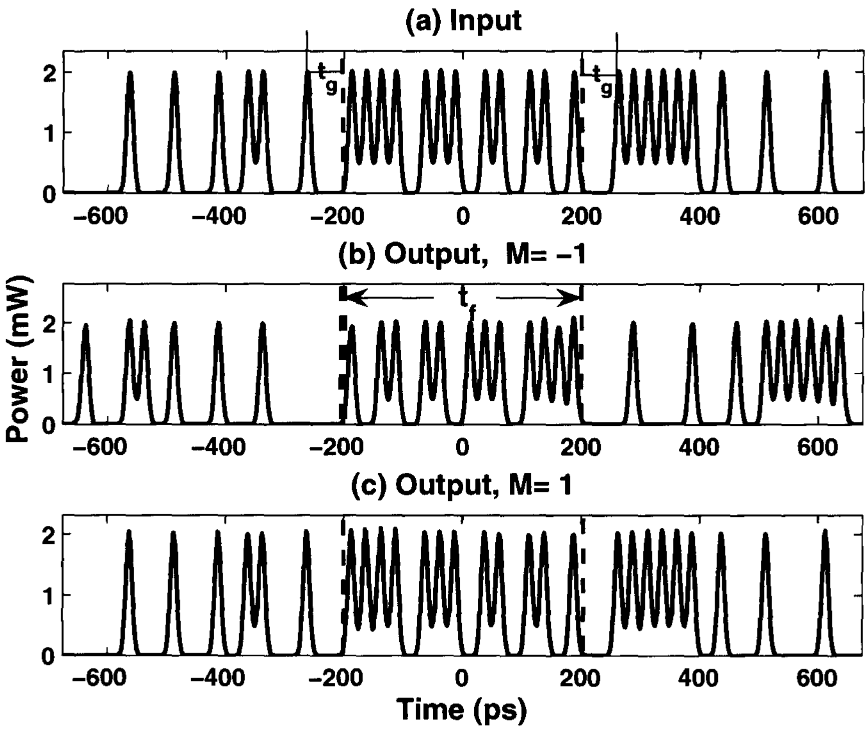

Figure 4.4: Input and output bit sequences of the WDM demultiplexer based on a 4-f time-lens system. (a) Input. (b) Output with time reversal, $M = -1$. (c) Output without time reversal, $M = +1$. Guard time $t_g = 50$ ps and $t_f = 400$ ps.

50 ps. Figures 4.4 (b) and 4.4 (c) show the output signals with and without time reversal, respectively. From Figures 4.4 (b) and 4.4 (c), we find that the distortion is effectively eliminated by adding the guard time between frames.

The advantage of this scheme is that the channels to be demultiplexed at a node can be dynamically reconfigured. For example, if channel 1 has to be blocked instead of channel 2, the transmittivity of the amplitude modulator [Eq. (4.26)] can be dynamically changed to

$$H(t) = \begin{cases} 1, & \left|\frac{t}{\beta_2^{(1)} f_1} - 2\Delta\omega\right| \leq \Delta\omega \\ 0, & \text{otherwise} \end{cases} \tag{4.33}$$

such that channel 1 is in the stop band of the temporal filter and channel 2 is in the passband.

4.4 Dispersion Compensator

The following example is the implementation of a higher-order fiber dispersion compensator based on the temporal filtering technique. As the bit rate of a single channel increases, its spectrum broadens and the higher-order dispersion leads to pulse distortion in such a transmission system that limits the system performance. Various dispersion compensation techniques have been developed. The most commercially advanced technique is negative-dispersion fiber-based dispersion compensation, but the disadvantage is that, in practice, it is hard to design and manufacture a dispersion-compensating fiber with negative dispersion slope due to its higher sensitivity to waveguide profile fluctuations [116].

We discuss a dispersion compensation technique based on the time-lens–based temporal filtering technique that can compensate for any order of fiber dispersion in fiber-optic transmission systems. In this application, the temporal filter is realized using a phase modulator instead of an amplitude modulator and its time domain transfer function is

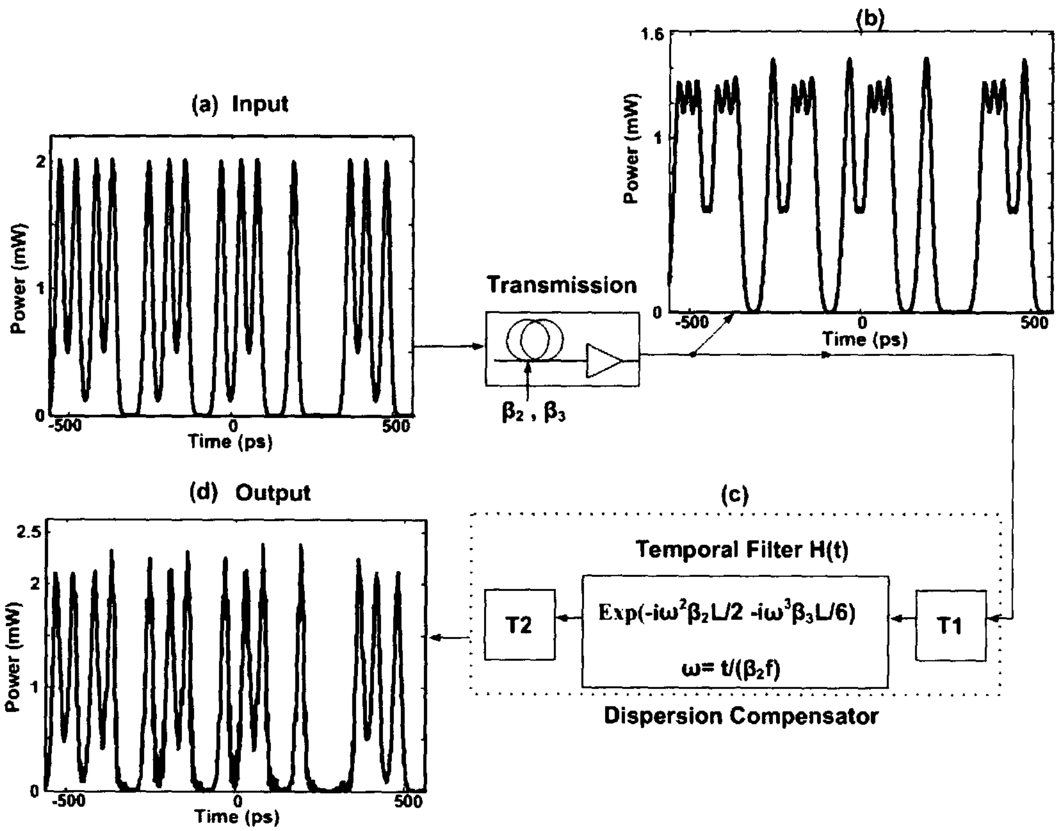

Figure 4.5: A dispersion compensator based on a 4-f time-lens system. t_f = 100 ps, t_g = 12 ps, and M = 1. (a) Input signal. (b) Output signal after fiber propagation. (c) Dispersion compensator based on the time-lens system. (d) Output after the dispersion compensator.

given by

$$H(t) = \exp\left(-iL\sum_{n\geq 2}\frac{\omega^n}{n!}\frac{d^n\beta}{d\omega^n}\right)\Bigg|_{\omega=t/(\beta_2^{(1)}f_1)}, \tag{4.34}$$

where $d^n\beta/d\omega^n$ is the nth order dispersion. To realize the transfer function given by Eq. (4.34), an arbitrary waveform generator (AWG) is required to drive the phase modulator. Considering that the bit sequence is processed frame by frame, if the frame time is t_f, then for each frame, the frequency resolution is given by

$$\Delta f = \frac{1}{t_f}. \tag{4.35}$$

Before using the temporal filter we obtain the Fourier transform of the input signal in the time domain as $\tilde{U}\left(t\left/\beta_2^{(1)}f_1\right.\right)$. Therefore, the corresponding time resolution is given by

$$\Delta t = \left|\beta_2^{(1)}f_1\right|(2\pi\Delta f). \tag{4.36}$$

The maximum achievable bandwidth, B_{max}, of an AWG using the current technology is $\sim$ 12.5 GHz [117]. Therefore, we obtain

$$\Delta t \geq \frac{1}{B_{max}} = 80 \text{ ps}. \tag{4.37}$$

Using Eqs. (4.35) and (4.36) in Eq. (4.37), we obtain the following constraint on the parameters of the time-lens system:

$$\left|\beta_2^{(1)}f_1\right| \geq \frac{t_f}{2\pi B_{max}}. \tag{4.38}$$

From Eq. (4.38), we see that if the frame is too wide, the fiber with higher dispersion coefficient is required when the bandwidth of AWG is fixed. However, on the other hand, if the frame is too narrow, synchronization of various modulators should be done at a higher frame rate ($= 1/t_f$). Usually synchronization is done by extracting the clock from the signal [118] and synchronization is easier at lower frame rates. From Eq. (4.38), we see that if the bandwidth of the AWG is too small, we need a fiber with large dispersion. We choose dispersion coefficient $\beta_2^{(1)} = 123$ ps^2/km and the frame time $t_f = 100$ ps. From Eq.

(4.38), we find $f_1 = 10.4$ km. With the above choice of frame time, the synchronization of the frame needs to be done by extracting a clock at 10 GHz ($= 1/t_f$).

Without loss of the generality, in this example only the second- and third-order fiber dispersion effects are taken into account. Therefore, the temporal filter is simplified to

$$H(t) = \exp\left(-i\omega^2\beta_2 L/2 - i\omega^3\beta_3 L/6\right)\Big|_{\omega=t/\left(\beta_2^{(1)}f_1\right)}, \tag{4.39}$$

where β_2 and β_3 are the second- and third-order dispersions of the transmission fiber, respectively. L is the transmission distance. $\beta_2^{(1)}$ is the dispersion coefficient of the SMF in the 2-f subsystem T1. In the simulation, we ignore the nonlinear effect and amplifier noise. The bit '1' is represented by a Gaussian pulse with width of 25 ps, and the input bit sequence is shown in Figure 4.5 (a). We simulate a random bit pattern with 20 bits (10 frames), and the bit rate is 20 Gb/s such that there are two bits within each frame in this case. The guard time is chosen as $t_g = 12$ ps. The second-order dispersion of the transmission fiber is $\beta_2 = -21$ ps^2/km and the transmission distance is 10 km. To highlight the effect of the third-order dispersion, we set $\beta_3 = 20$ ps^3/km, rather than the standard value of 0.1 ps^3/km, but it does not affect the generality of this dispersion compensation technique. After propagation along the transmission fiber with both the second- and third-order dispersions, each bit has been broadened beyond its bit interval and hence the output signal after fiber transmission is distorted as shown in Figure 4.5 (b), which is then input to the 4-f system. As analyzed previously, the 2-f subsystem T1 provides the FT of the signal input to the 4-f system in the time domain such that

$$q(t, 2f_{1-}) = \tilde{U}(\omega)\exp\left(i\omega^2\beta_2 L/2 + i\omega^3\beta_3 L/6\right)\Big|_{\omega=t/\left(\beta_2^{(1)}f_1\right)}, \tag{4.40}$$

where $\tilde{U}(\omega)$ is the FT of the launched bit sequence as shown in Figure 4.5 (a) and the exponential part is the linear transfer function of the fiber transmission system. Thus, combining Eqs. (4.39) and (4.40), after the temporal filter we obtain

$$\begin{aligned} q(t, 2f_{1+}) &= q(t, 2f_{1-})H(t) \\ &= \tilde{U}(\omega)\Big|_{\omega=t/\left(\beta_2^{(1)}f_1\right)}, \end{aligned} \tag{4.41}$$

and it is shown from Eq. (4.41) that the phase shift caused by the transmission fiber has been completely canceled out by the temporal filter. Since $M = 1$, the 2-f subsystem T2 provides the exact IFT of $q(t, 2f_{1+}) = \tilde{U}(t/\beta_2^{(1)} f_1)$ so that $q(t, 2f_1 + 2f_2) = u(t, 0)$, where $u(t, 0)$ is the input signal of the fiber transmission system. Figure 4.5 demonstrates the process of the dispersion compensation undertaken by the time-lens–based temporal filtering system. Figure 4.5 (d) shows that there is some distortion of the output signal since the guard time (= 12 ps) used in this simulation is quite small. To avoid this distortion, we use the guard time $t_g = 24$ ps and redo the above simulation. Figure 4.6 shows the simulation results with $t_g = 12$ ps and $t_g = 24$ ps and the rest of the parameters is the same as that used in Figure 4.5. Figure 4.6 (a) shows the input bit sequence (the same as Figure 4.5 (a)). Figures 4.6 (b) (the same as Figure 4.5 (d)) and 4.6 (c) show the output signals for the cases of $t_g = 12$ ps and $t_g = 24$ ps, respectively. As can be seen, the distortion is more effectively suppressed in the case of $t_g = 24$ ps compared with the case of $t_g = 12$ ps.

4.5 Conclusions

Various issues in the design of a time-lens–based optical signal processing system are discussed. The 2-f subsystem T2 is chosen to be anti-symmetric with respect to the 2-f subsystem T1; that is, $\beta_2^{(2)} = -\beta_2^{(1)}$ and $C_2 = -C_1$ so that the 2-f subsystem T2 provides the exact inverse Fourier transform, and as a result the bit sequence at the output is not time-reversed. In contrast, as for the 4-f configuration in previous work [62], the sign of dispersion of the fiber in the 2-f subsystem T2 is identical to that in T1 and therefore, T2 provides the Fourier transform of its input, which leads to a time-reversed output bit pattern and therefore, additional signal processing in the optical/electrical domain to recover the original bit sequence is required.

We have discussed two applications using the time-lens–based optical signal processing scheme. One is a tunable wavelength division demultiplexer. The temporal filter in this

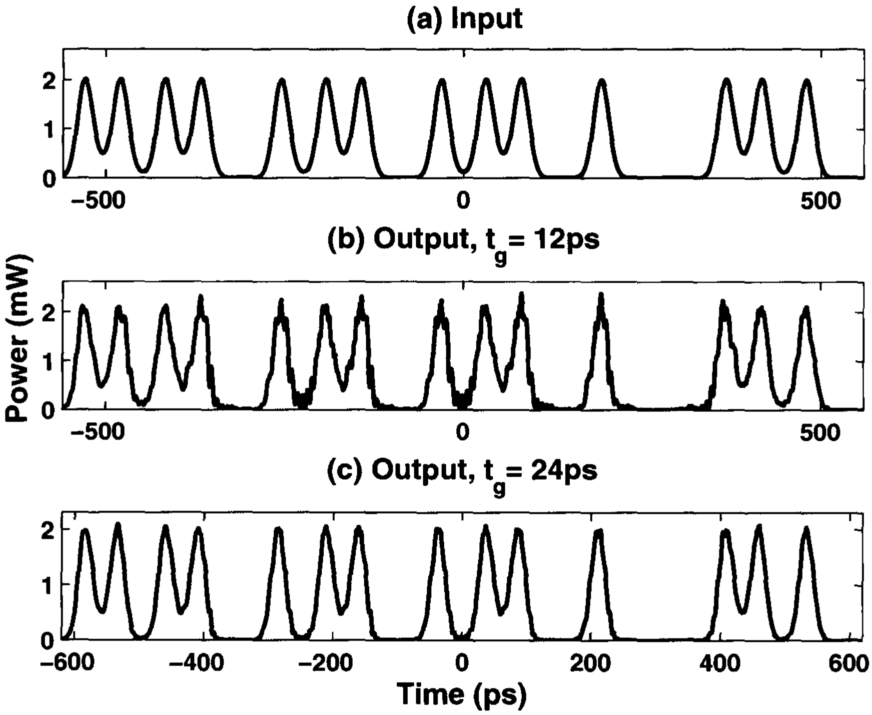

Figure 4.6: Input and output bit sequences of the dispersion compensator based on a 4-f time-lens system ($M = 1$ and $t_f = 100$ ps). (a) Input. (b) Output with guard time $t_g = 12$ ps. (c) Output with guard time $t_g = 24$ ps.

example is an amplitude modulator. The advantage of this time-lens–based wavelength division multiplexing demultiplexer is that the channels to be demultiplexed at a node of an optical network can be dynamically chosen by changing the passbands of the temporal filter. The other application is a higher-order fiber dispersion compensator. In this case, the temporal filter is realized by a phase modulator. The transfer function of the filter can be expressed as a summation of several independent terms, each of which corresponds to the amount of the phase shift caused by the certain order of fiber dispersion. This dispersion compensation technique can flexibly compensate for any order of fiber dispersion by simply modifying the transfer function of the temporal filter.

Chapter 5

Realization of OFDM using Time Lenses in Direct Detection Systems

5.1 Introduction

Orthogonal frequency division multiplexing (OFDM) has been widely used in wireless communication systems and recently has drawn significant research interest in fiber-optic communications owing to its large dispersion tolerance and high spectral efficiency [70]-[81], [119, 120], [122]-[124]. OFDM is a form of multiple subcarrier multiplexing technique in which subcarriers are orthogonal. In a typical OFDM scheme, a large number of closely spaced orthogonal subcarriers are used to carry information data. Each subcarrier can be modulated with the conventional modulation schemes such as QAM or PSK at a lower symbol rate, and the total data rate is as same as that in a single-carrier modulation scheme. We proposed an optical implementation of OFDM using time lenses in a direct detection system [64]. The first 2-f subsystem provides the inverse Fourier transform (IFT) of the input signal that carries the information. This input signal is obtained by the optical/electrical time division multiplexing of several channels. The kernel of the IFT is of the form $\exp(i2\pi ft)$ and therefore, IFT operation can be imagined as the multiplication of the signal samples of several channels by the optical subcarriers.

These subcarriers are orthogonal and therefore, the original signal can be obtained by a Fourier transformer at the receiver, which acts as a demultiplexer. The second 2-f subsystem provides the Fourier transform (FT) of the output from the fiber link so that the convolution of the input optical signal and the fiber transfer function in time domain is converted into the product of the FT of both, but still in time domain. The output of the Fourier transformer is the product of the original input signal (input signal of T1) and the phase correction due to the fiber transfer function. The photodetector responds only to the intensity of the optical signal and therefore, the deleterious effects introduced by the fiber that appear as the phase correction are removed by the photodetector in a direct detection system without extra signal processing. This occurs because the fiber transfer function due to dispersive effects is of the type $\exp\left[i\beta(f)\right]$. In the absence of fiber nonlinearity, optical carriers are orthogonal and the Fourier transformer at the receiver demultiplexes the subcarriers without introducing any penalty. However, strong nonlinear effects can destroy the orthogonality of the optical subcarriers. The simulations in our work show that the time-lens-based optical OFDM system scheme has the tolerance to the fiber nonlinearity to some extent.

5.2 Optical Implementation of Orthogonal Frequency-Division Multiplexing using Time Lenses

Figure 5.1 shows an example of a fiber-optic communication system based on OFDM. Single-channel input data are converted into N parallel data paths using serial-to-parallel conversion. Let the symbol interval of the input to the inverse fast Fourier transform (IFFT) be T_{block} and each of the parallel data channels consists of a complex data $a_k, k = 1, 2, \ldots N$, within each block. These signals are multiplied by subcarriers and multiplexed together using IFFT, which processes data on a block-by-block basis. The subcarriers are sinusoids with frequencies that are integer multiples of $1/T_{block}$, which makes them orthogonal to each other. The output of IFFT is up-converted to the radio frequency

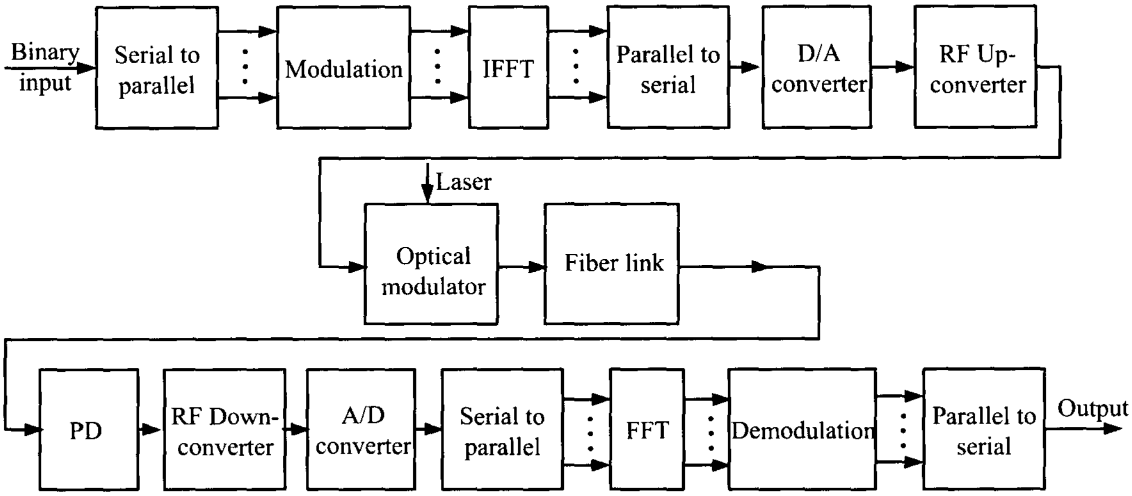

Figure 5.1: Block diagram of a conventional OFDM system.

(RF) domain after parallel-to-serial and digital-to-analog (D/A) conversion. An optical carrier is intensity modulated by the RF signal consisting of an OFDM band using optical modulator. At the receiver, the RF signal is down-converted to baseband and the input complex data a_k can be recovered from the output of fast-Fourier transform (FFT). The signals in adjacent blocks could interfere with each other due to fiber dispersion leading to interblock interference, which can be avoided by introducing guard intervals between blocks [119, 120]. Figure 5.2 shows an optical implementation of OFDM using time lenses for direct detection. The input electrical signals for each subchannel, $1, 2, \cdots, M$, are first multiplexed in time domain before the optical modulation. Let the input optical field envelope be $\tilde{u}_{in}(t')$. We define the Fourier transform pairs as

$$\tilde{u}(t') = F[u(t); t \to t'] = \int_{-\infty}^{\infty} u(t) \exp(-i2\pi t' t) dt, \tag{5.1}$$

and

$$u(t) = F^{-1}[\tilde{u}(t'); t' \to t] = \int_{-\infty}^{\infty} \tilde{u}(t') \exp(i2\pi t' t) dt'. \tag{5.2}$$

The IFT and FT are implemented using time lenses. Propagation of an input optical field envelope in a 2-f system consisting of dispersive elements and a phase modulator (time lens) results in either FT or IFT of the input signal at the output of the 2-f system

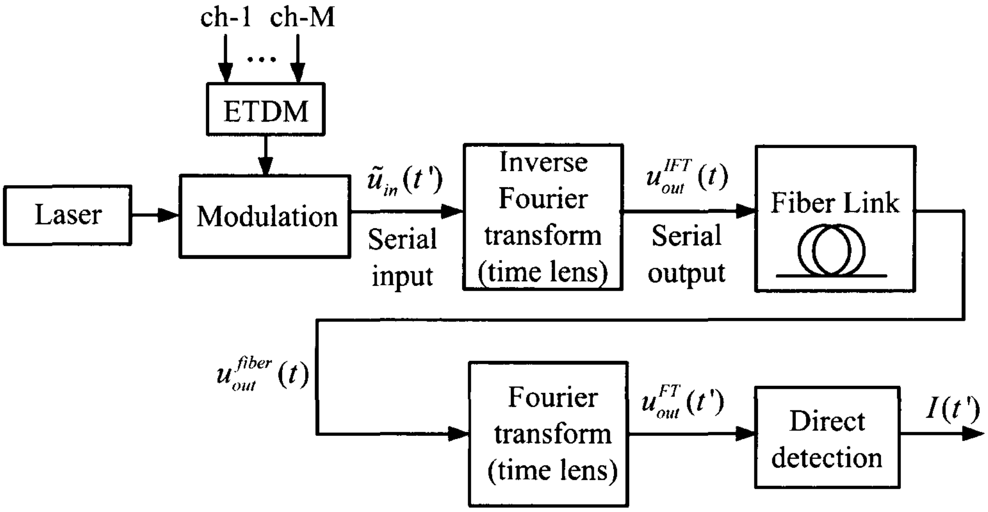

Figure 5.2: Block diagram of the time-lens-based direct-detection OFDM scheme. ETDM= electrical time-division multiplexer.

[62], [121]. The output of the 2-f system can either be the FT or IFT depending on the signs of second-order dispersion coefficients and chirp factors of the phase modulator [63].

We choose

$$\begin{aligned}\beta_{21}^{(1)} f_1 &= \beta_{22}^{(1)} f_1 = \beta_2^{(1)} f_1, \\ \beta_{21}^{(2)} f_2 &= \beta_{22}^{(2)} f_2 = -\beta_2^{(1)} f_1, \end{aligned} \tag{5.3}$$

so that the first 2-f subsystem provides the IFT and the second 2-f subsystem provides the direct FT. Define the $S_j = \beta_2^{(j)} f_j, j = 1, 2$ as the accumulated second order dispersion coefficient of the 2-f subsystems T1 and T2, respectively, we have $S_1 = -S_2$. The temporal filter in this application is characterized as a transfer function of fiber link. Using the time-lens–based 2-f system, the IFT of the input field envelope, $\tilde{u}_{in}(t')$ is given by [62]

$$\begin{aligned}u_{out}^{IFT}(t) &= F^{-1}[\tilde{u}_{in}(t'); t' \to t/(2\pi S_1)]/\sqrt{-i2\pi S_1}, \\ &= u_{in}(t/(2\pi S_1))/\sqrt{-i2\pi S_1}. \end{aligned} \tag{5.4}$$

The input and output of the IFT (T1) are serial and therefore, there is no need for serial-to-parallel and parallel-to-serial conversion. The signal $u_{out}^{IFT}(t)$ is transmitted over the fiber-optic link and at the receiver, the output of the fiber-optic link, $u_{out}^{fiber}(t)$ passes through a Fourier transformer (T2) whose output is

$$\begin{aligned}\tilde{u}_{out}^{FT}(t') &= \frac{1}{\sqrt{-i2\pi S_2}} F[u_{out}^{fiber}(t); t \rightarrow t'/(2\pi S_2)], \\ &= \tilde{u}_{out}^{fiber}(t'/(2\pi S_2))/\sqrt{-i2\pi S_2}.\end{aligned} \tag{5.5}$$

After passing through the direct-detection optical receiver, the photodiode current is given by

$$I(t') = |\tilde{u}_{out}^{FT}(t')|^2, \tag{5.6}$$

assuming unity responsivity of the photodiode. Consider the optical OFDM signal $u_{out}^{IFT}(t)$ propagating in a fiber whose linear transfer function is [1]

$$H_f(f) = \exp[i\theta(f)L], \tag{5.7}$$

where

$$\theta(f) = \beta_2(2\pi f)^2/2 + \beta_3(2\pi f)^3/6 + \beta_4(2\pi f)^4/24 + \ldots, \tag{5.8}$$

L is the fiber length, and β_n is the nth-order dispersion coefficient. In the absence of noise and nonlinearity, the fiber output is

$$u_{out}^{fiber}(t) = u_{out}^{IFT}(t) * h_f(t), \tag{5.9}$$

where $*$ denotes convolution and $h_f(t) = F^{-1}[H_f(f)]$ is the fiber impulse response function. Convolution in the time domain becomes a product in frequency domain and therefore, after the Fourier transformer (see Figure 5.2), the output signal can be written as

$$\tilde{u}_{out}^{FT}(t') = \frac{1}{\sqrt{-i2\pi S_2}} F\{u_{out}^{IFT}(t); t \rightarrow t'/(2\pi S_2)\} F\{h_f(t); t \rightarrow t'/(2\pi S_2)\}. \tag{5.10}$$

Using Eqs.(5.4) and (5.7), we obtain

$$u_{out}^{FT}(t') = \tilde{u}_{in}(t') \exp[iL\theta(t'/(2\pi S_2))]. \tag{5.11}$$

From Eq. (5.6), the photocurrent is

$$I(t') = |\tilde{u}_{in}(t')|^2. \tag{5.12}$$

Thus, we see that the effect of fiber dispersion is a mere phase shift [Eq. (5.11)] in this system and therefore, dispersive effects completely disappear after direct detection and the photocurrent is directly proportional to the input power.

So far we have assumed that the aperture of the time lens is infinite. To process the input signal block-by-block basis, periodic time lenses with finite aperture should be introduced [63], [115]. In this case, the phase modulator multiplies the incident optical field envelope by a function

$$h(t) = \sum_{n=-\infty}^{\infty} h_0(t - nT_{ofdm}), \tag{5.13}$$

$$\begin{aligned} h_0(t) &= \exp(i\alpha t^2) \quad \text{for } |t| \leq T_{block/2} \\ &= 0, \qquad\qquad \text{elsewhere} \end{aligned} \tag{5.14}$$

and input signal is of the form

$$\tilde{u}_{in}(t') = \sum_{n=-\infty}^{\infty} u_n(t' - nT_{ofdm}), \tag{5.15}$$

$$\begin{aligned} u_n(t') &= f_n(t') \quad \text{for } |t'| \leq T_{block}/2 \\ &= 0, \qquad \text{elsewhere} \end{aligned} \tag{5.16}$$

where $f_n(t')$ is an arbitrary input signal in the block n and T_{ofdm} is the total width of the OFDM signal. The difference T_{ofdm}-T_{block} is the guard time introduced between consecutive blocks to ensure that interblock interference is not significant.

Consider the input signal $u_n(t')$, which is limited to the interval $[-T_{block}/2, T_{block}/2]$. Let the highest-frequency component of the signal $u_n(t')$ be f_{max}. After passing through the IFT, the corresponding signal should be confined within the interval $[-T_{block}/2, T_{block}/2]$. Using Eq. (5.4), the above condition leads to

$$|S_1| \leq T_{block}/(2f_{max}), \tag{5.17}$$

which gives an upper bound for $|S_1|$.

There are a few differences between the conventional OFDM and the scheme discussed here (see Figure 5.2). First, the conventional OFDM uses the discrete FT, whereas the scheme of Figure 5.2 uses continuous FT. Second, conventional OFDM requires high-speed digital signal processors to compute FFT and IFFT and computational time increases as the aggregate bit rate becomes higher. In contrast, the FT and IFT operations of Figure 5.2 are almost instantaneous except for the small propagation delays in the dispersive elements. This time-lens–based scheme should not be considered a method to compensate for second-order dispersion of the transmission fiber. This is because the dispersive elements of the FT and IFT should have both positive and negative second-order dispersion coefficients. This technique can be used to compensate for third- and higher-order dispersion coefficients. To illustrate this point, numerical simulations of a dispersion-managed transmission system is carried out using the following parameters: bit rate = 320 Gb/s, second- (β_2), third- (β_3) and fourth- (β_4) order dispersion of the transmission fiber (SMF) are -21.6 ps^2/km, 0.05 ps^3/km, and 1.69×10^{-4} ps^4/km, respectively, and total transmission distance = 400 km. The commercially available dispersion-compensating module (DCM) has a zero dispersion slope. Therefore, we choose $\beta_2 = 128$ ps^2/km, $\beta_3 = 0$ and $\beta_4 = 0$ for the DCM. The nonlinear coefficients of SMF and DCM are set to zero. Fiber losses are 0.2 dB/km and 0.5 dB/km for SMF and DCM, respectively. Fiber losses are fully compensated by amplifiers that are placed 80 km apart. The amplifiers are assumed to be noiseless to see the impact of dispersion clearly. The second-order dispersion of the SMF is fully compensated by the inline DCM placed just before each amplifier. $u_n(t')$ is a random bit sequence consisting of Gaussian pulses with FWHM of 1.56 ps, $T_{block} = 6.4$ ns, $T_{ofdm} = 7.2$ ns, and $S_1 = 397$ ps^2. The dotted line, crosses and solid line in Figure 5.3 show the input power($|u_{in}(t')|^2$), output power $((I(t'))$ with FT and IFT, and output power without FT and IFT, respectively. In Figure 5.3, the amplifiers are assumed to be noiseless to see the impact of dispersion clearly. Four blocks of data are simulated and Figure 5.3 shows a part of the data within a block. As can be seen, there is a significant distortion due to β_3 and β_4 when FT and IFT are not used, and higher-order dispersive

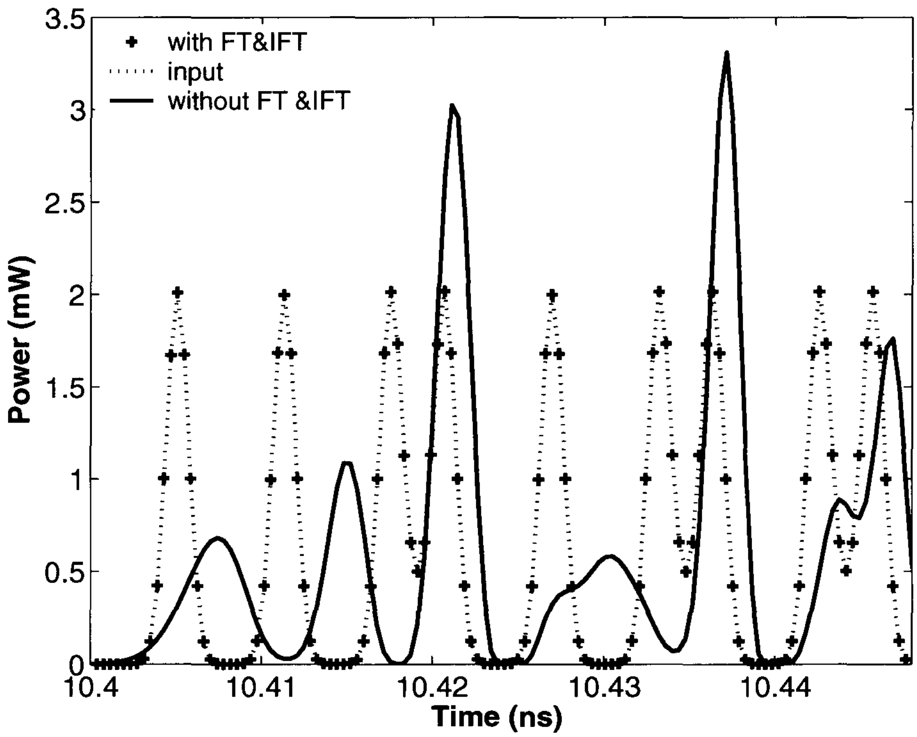

Figure 5.3: Plot of input and output powers vs time. The solid line denotes output power without using FT and IFT. The dotted line shows input power and the crosses show output power with FT and IFT.

effects can be suppressed using the scheme of Figure 5.2. The transmission distance can further be increased without distortion by increasing T_{block}.

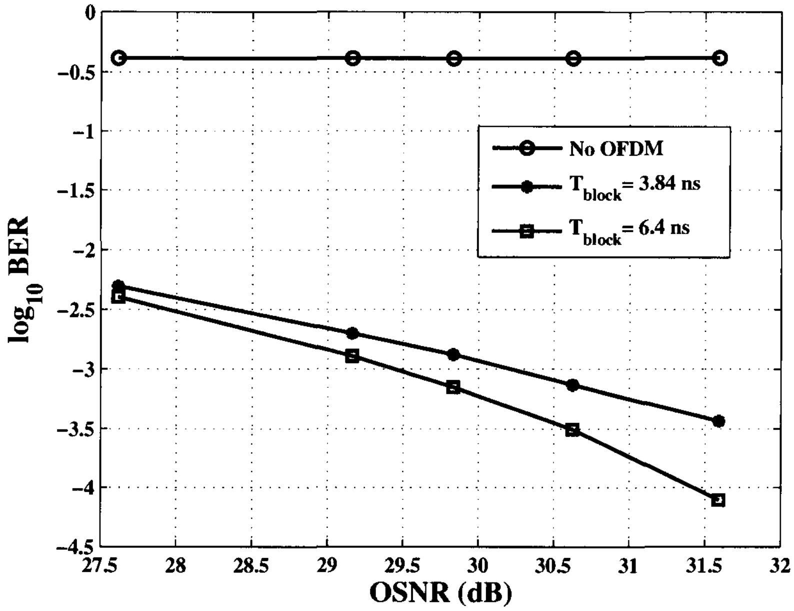

Figure 5.4: Comparison of BER between OFDM-based systems with different T_{OFDM} and the conventional OOK system.

In Figure 5.4, we compare the bit error rate (BER) of the time-lens–based scheme (see Figure 5.2) and the system without using FT and IFT. In this simulation, amplifier noise is turned on and 4 million bits are used at the input; all the other parameters are kept the same as in Figure 5.3, except T_{block} is changing. Optical signal-noise ratio (OSNR) is calculated using a bandwidth of 0.1 nm. In the absence of FT and IFT, from Figure 5.4 we see that BER is nearly independent of OSNR, indicating that degradation is mainly due to higher-order dispersion. As OFDM symbol interval increases, BER reduces, since larger T_{block} corresponds to lower subchannel bit rates and therefore higher dispersion tolerance.

Figure 5.5 shows the evolution of pulses in the presence of fiber nonlinearity. The

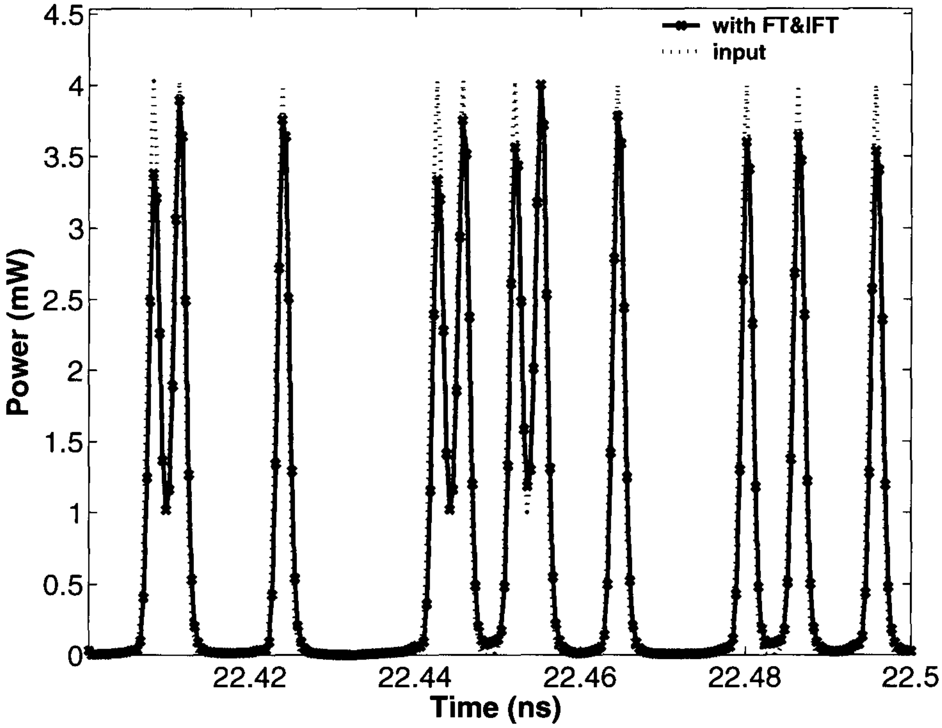

Figure 5.5: Nonlinear performance of the time-lens–based scheme.

parameters are same as in Figure 5.2 except that nonlinear coefficients of SMF and DCF are 1.25 $W^{-1}km^{-1}$ and 5 $W^{-1}km^{-1}$, respectively, and the launch peak power is 4 mW. As can be seen, there is a pulse distortion due to intrachannel nonlinear impairments, which should be expected since this time-lens-based scheme does not compensate for nonlinear impairments. Note that the FT and IFT should be properly synchronized to ensure that they process the data on a block-by-block basis. However, the synchronization needs to be done only at the OFDM symbol rate ($= 1/T_{ofdm}$), which is much lower than the aggregate bit rate.

5.3 Conclusions

An implementation of orthogonal frequency-division multiplexing in the optical domain using Fourier transforming properties of time lenses in direct detection systems is discussed. The first 2-f subsystem (T1) takes role of an inverse Fourier transformer and the second 2-f subsystem (T2) works as a Fourier transformer. The temporal filter between T1 and T2 is characterized as the transfer function of a fiber-optic link with nonlinearity. The output of the Fourier transformer is the original input signal of IFT (T1) multiplied by a phase factor due to fiber dispersive effects. Since the photocurrent is proportional to the absolute square of the optical field, dispersive effects are easily eliminated in direct detection systems. Using this configuration, the third- and higher-order dispersive effects can be considerably reduced. Results also show that the time-lens-based optical OFDM system scheme in a direct detection system has the tolerance to the fiber nonlinearity to some extent.

Chapter 6

Realization of Optical OFDM using Time Lenses in Coherent Detection Systems

6.1 Introduction

In this chapter, we investigate the possibility of introducing time lenses for coherent OFDM systems. Recently, Refs. [64] and [80] have proposed to realize Fourier transform (FT) and inverse Fourier transform (IFT) in optical domain. In Ref. [80], the discrete Fourier transform (DFT) circuit is designed using combinations of optical delays and phase shifters. The time-domain Fourier transformation of a single Gaussian pulse is experimentally demonstrated in Ref. [125]. The advantage of the optical domain realization of FT is that high speed digital signal processing needed for FFT and IFFT implementation is now replaced by optical signal processing by time lenses which have inherently high bandwidth. Due to inherently high peak-to-average power ratio (PAPR) of OFDM signal, fiber nonlinearity causes serious performance degradation. Therefore, the impact of fiber nonlinearity in optical OFDM systems and its mitigation have drawn significant attention, recently [127]-[137]. The effects of MZM nonlinearity on optical OFDM systems both for coherent detection [138, 139] and for direct detection [140, 141] have also been investigated and digital clipping and pre-distortion processes were applied to compensate for the nonlinear impairments introduced by in-phase and quadrature MZMs in Ref. [139]. In this chapter, the nonlinear tolerance of a coherent optical OFDM system using time lenses is studied. The nonlinear effects induced by MZM are also investigated and compared with the OFDM scheme based on FFT. Results show that the nonlinearity of MZM significantly degrades the performance of the conventional coherent OFDM using FFT as the power of the driving message signal increases, while it only has minor impairment on the coherent OFDM using time lenses. This is because MZM is placed after IFFT for the conventional OFDM, and the output signal of IFFT has the property of high peak to average power ratio (PAPR), such that some part of the input signal to MZM with high instant peak power falls into the nonlinear region of MZM, and therefore, the output of MZM is distorted by the nonlinear response of MZM. At the receiver end, the received OFDM sub-channels are no longer orthogonal and therefore, after FFT the demodulated signal cannot be recovered without errors. In contrast, for the coherent OFDM using time lenses, the MZM is placed before FT, so that, in the absence of fiber dispersion, nonlinearity and ASE noise, the signal after FT at the receiver end is identical to the output signal of MZM at the transmitter end. This implies that the nonlinear distortion induced by MZM is applied directly to the message signal while it does not affect the OFDM modulation and demodulation. The simulation results show that the nonlinearity of MZM does not have significant impairment on the coherent optical OFDM system using time lenses. One of the drawbacks of the scheme proposed in Ref. [64] is that to realize FT and IFT, one would need fibers with anomalous as well as normal dispersion and therefore, the dispersion tolerance of such a scheme becomes questionable. Instead, in this chapter, an alternative scheme is considered, in which FTs are introduced both at the transmitter and at the receiver so that the SMF can be used as a dispersive element of the time-lens setup. As a result, the received sequence gets time reversed within a frame. But it can be easily corrected using the digital signal processing at the receiver. To realize the time lens, a quadratic phase chirp should be introduced using a phase modulator. As the frame time increases, one would expect that the driving voltage increases quadratically with time and at the edge of the time frame, the required driving voltage becomes unreasonably large. But, it is shown in this chapter that it is possible to realize the time lens even with low driving voltage by making use of the periodic property of the sinusoidal transfer function of the phase modulator.

6.2 System Modeling and Time-Lens Setup

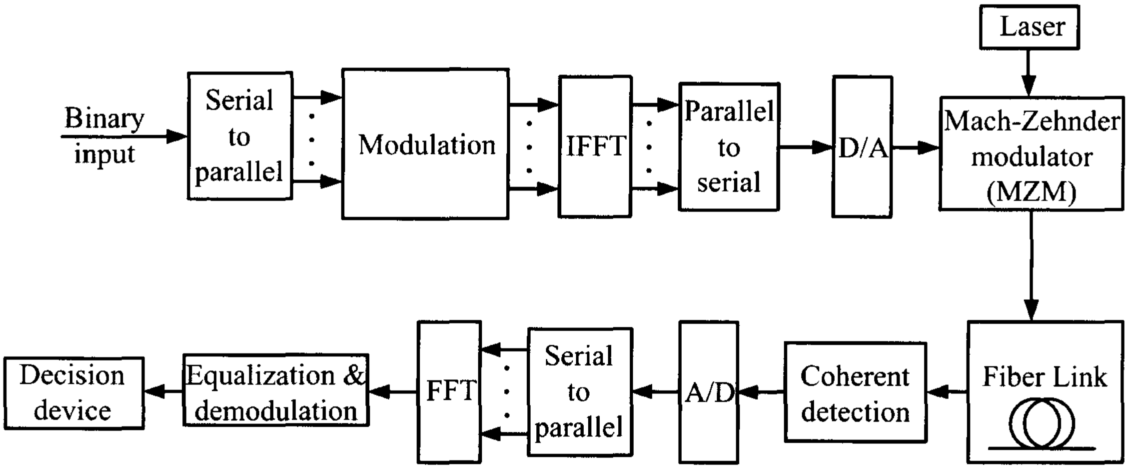

Figure 6.1: Block diagram of a coherent optical OFDM system using FFT.

Fig. 6.1 shows a typical optical OFDM scheme for coherent detection, in which the Fourier transform (FT)/inverse FT is implemented in the electrical domain using fast Fourier transform (FFT). The electrical OFDM signal is brought into optical domain after the Mach-Zehnder modulator. At the receiver, the coherent detection is used to recover both amplitude and phase of the OFDM signal. DSP is used after the coherent receiver to demodulate the OFDM signal, including FFT, equalization and demodulation.

In this chapter, we discuss an optical OFDM scheme with Fourier transform implemented in optical domain using time lenses. Fig. 6.2 shows a block diagram of fiber-optic

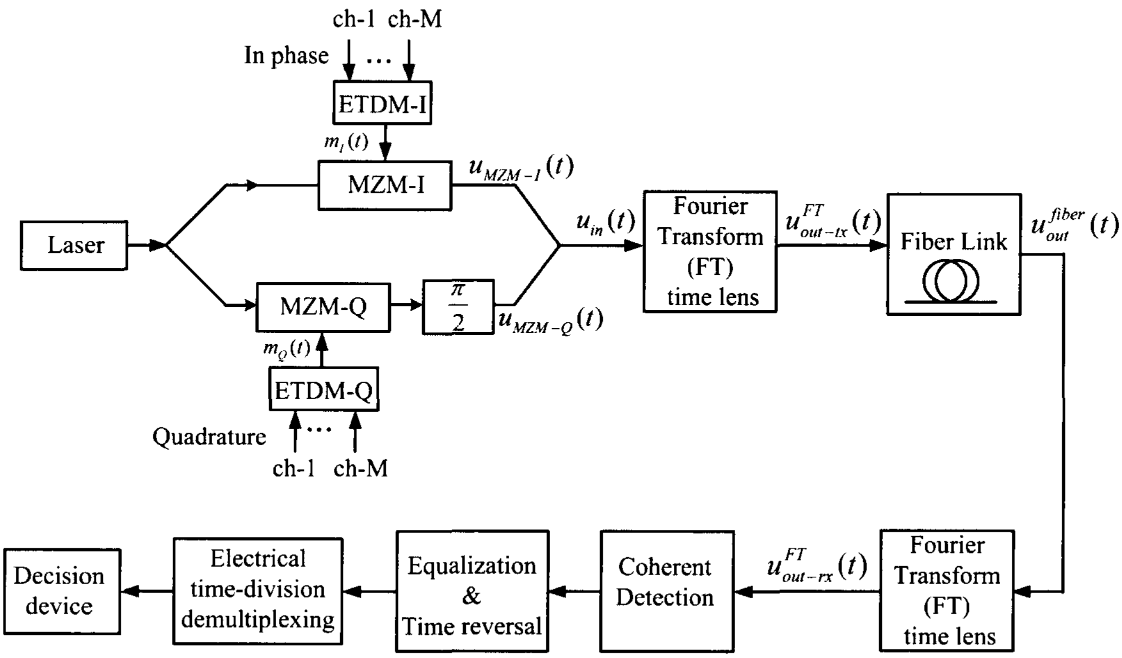

Figure 6.2: Block diagram of a coherent optical OFDM system using time lenses. MZM= Mach-Zehnder modulator, ETDM= electrical time division multiplexer. I and Q denote in-phase and quadrature components, respectively.

communication system based on optical OFDM using time lenses. In this scheme, the in-phase and quadrature components of the message signals from various channels are combined using electrical time division multiplexing (ETDM) units ETDM-I and ETDM-Q, respectively. The outputs of ETDM-I and ETDM-Q drive the in-phase and quadrature Mach-Zehnder modulators (MZM), MZM-I and MZM-Q, respectively. In contrast, in the case of conventional OFDM [72, 70], [122, 123], message signals from various channels modulate the sub-carriers through IFFT. The outputs of the MZMs are combined and pass through the FT block. The output of the FT block is launched to the fiber-optic link and then to another FT block at the receiver. Since the Fourier transform of a Fourier transform leads to time reversal within an OFDM frame, the transmitted signal can be recovered by introducing time reversal using digital signal processing. In the case of coherent optical/electrical OFDM, a phase chirp is introduced across the frame due to fiber dispersive effects which can be canceled using equalization algorithms [123]. The optical field envelope at the MZM-I and MZM-Q outputs can be written as [126]

$$u_{\text{MZM-I}}(t) = A_c \cos\left\{\frac{\pi}{2V_\pi}\left[m_I(t) - V_{bias}\right]\right\}, \tag{6.1}$$

$$u_{\text{MZM-Q}}(t) = iA_c \cos\left\{\frac{\pi}{2V_\pi}\left[m_Q(t) - V_{bias}\right]\right\}, \tag{6.2}$$

where $m_I(t)$, $m_Q(t)$ are in-phase and quadrature components of message signal, respectively, V_{bias} is a constant bias voltage, is known as the half-wave voltage, and A_c is the amplitude of optical carrier. When $V_{bias} = V_\pi$, and $m_I(t), m_Q(t) \ll V_\pi$, we have

$$u_{\text{MZM-I}}(t) = A_c \frac{\pi}{2V_\pi} m_I(t), \tag{6.3}$$

$$u_{\text{MZM-Q}}(t) = iA_c \frac{\pi}{2V_\pi} m_Q(t). \tag{6.4}$$

The input of the Fourier transformer under these conditions is

$$u_{in}(t) = \frac{A_c \pi m(t)}{2\sqrt{2}V_\pi}, \tag{6.5}$$

where

$$m(t) = m_I(t) + im_Q(t). \tag{6.6}$$

Here, we define the Laser power, P_c , in-phase/quadrature message signal average power, P_m , and average input power launched to fiber, P_{in} as

$$P_c = |A_c|^2, \tag{6.7}$$

$$P_m = < m_I^2(t) >=< m_Q^2(t) >, \tag{6.8}$$

$$P_{in} = < \left|u_{out-rx}^{FT}\right|^2 >= \frac{P_c P_m \pi^2}{4V_\pi^2}, \tag{6.9}$$

where < > denotes the temporal average and u_{out-rx}^{FT} is the input signal to fiber-optic link, as shown in Fig. 6.2.

Next, let us consider the implementation of the Fourier transformation using time lenses. Let the input optical field envelope be $u_{in}(t)$. The FT pairs are defined as

$$\widetilde{u}_{in}(f) = \mathcal{F}\left[u_{in}(t); t \to f\right] = \int_{-\infty}^{\infty} u_{in}(t) \exp\left(i2\pi f t\right) dt, \tag{6.10}$$

$$u_{in}(t) = \mathcal{F}^{-1}\left[\widetilde{u}_{in}(f); f \to t\right] = \int_{-\infty}^{\infty} \widetilde{u}_{in}(f) \exp\left(-i2\pi f t\right) df. \tag{6.11}$$

A time-lens-based Fourier transformer is shown in Fig. 6.3. β_2^F and F are the second-

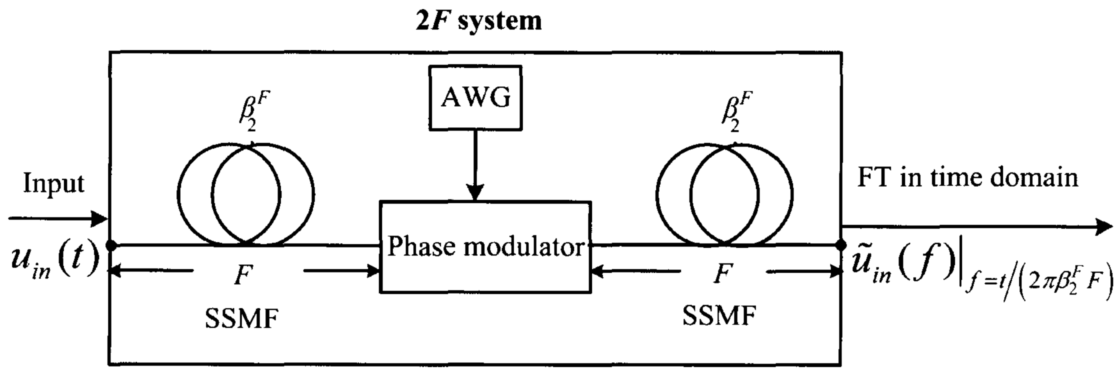

Figure 6.3: Fourier transform using the time lens. AWG= Arbitrary waveform generator, SSMF= Standard single-mode fiber.

order dispersion of the standard single-mode fiber (SMF) and the length of the fiber, respectively. The accumulated second-order dispersion of the dispersive fiber of the time lens is defined as $S_1 = \beta_2^F F$. Propagation of an input optical field envelope in a $2F$

system (see Fig. 6.3) consisting of dispersive elements (fibers) and a phase modulator (time lens) results in either FT or IFT of the input signal at the output of $2F$ system [62], depending on the signs of second-order dispersion coefficients and chirp factors of the phase modulator [63]. The phase modulator multiplies the incident optical field envelope by a function

$$h(t) = \exp\left[\frac{iV(t)\pi}{V_\pi}\right], \tag{6.12}$$

where $V(t) = V_0 t^2$ is the driving voltage and the chirp $C = \pi V_0 / V_\pi$ is related to S_1 by

$$C = \frac{1}{2S_1}. \tag{6.13}$$

The output of FT at the transmitter is given by

$$u_{out-tx}^{FT}(t) = \mathcal{F}\left[u_{in}(t); t \to t/\left(2\pi S_1\right)\right] = \frac{1}{\sqrt{i2\pi\left|S_1\right|}}\widetilde{u}_{in}\left(\frac{t}{2\pi S_1}\right). \tag{6.14}$$

Then, $u_{out-tx}^{FT}(t)$ is transmitted over the fiber-optic link, and the output of the fiber-optic link, $u_{out}^{fiber}(t)$ passes through the Fourier transformer at the receiver whose output is

$$u_{out-rx}^{FT}(t) = \mathcal{F}\left[u_{out}^{fiber}(t); t \to t/\left(2\pi S_1\right)\right] = \frac{1}{\sqrt{i2\pi\left|S_1\right|}}\widetilde{u}_{out}^{fiber}\left(\frac{t}{2\pi S_1}\right). \tag{6.15}$$

Consider the optical OFDM signal propagating in a fiber whose linear transfer function is

$$H_F(f) = \exp\left[i\phi(f)L\right]. \tag{6.16}$$

where

$$\phi(f) = \beta_2\left(2\pi f\right)^2/2 + \beta_3\left(2\pi f\right)^3/6 + \beta_4\left(2\pi f\right)^4/24 + \cdots, \tag{6.17}$$

L is the fiber length, and β_n is the nth-order dispersion coefficient. In the absence of fiber nonlinearity and noise, the fiber output is

$$u_{out}^{fiber}(t) = u_{out-rx}^{FT}(t) \otimes h_F(t), \tag{6.18}$$

where $\otimes$ denotes convolution and $h_F(t) = \mathcal{F}\left[H_F(f)\right]$ is the fiber impulse response function. Convolution in the time domain becomes a product in the frequency domain and therefore, after FT at the receiver, the output signal given in Eq. (6.15) can be rewritten as

$$u^{FT}_{out-rx}(t) = \frac{1}{\sqrt{i2\pi\,|S_1|}}\left[\widetilde{u}^{FT}_{out-tx}(f) \times H_F(f)\right]\big|_{f=t/2\pi S_1}. \tag{6.19}$$

Using Eqs. (6.14) and (6.16) in Eq. (6.19), we obtain

$$u^{FT}_{out-rx}(t) = -iu_{in}(-t)\exp\left[iL\phi\left(\frac{t}{2\pi S_1}\right)\right]. \tag{6.20}$$

From Eq. (6.20), we see that the effect of fiber dispersion is a mere phase shift in the time-lens-based OFDM system and therefore, dispersive effects completely disappear if direct detection is used since the photocurrent is directly proportional to the incident optical power. In the case of coherent detection, the phase shift introduced by the fiber dispersion is canceled using electrical equalizers. Note that the received signal is time-reversed in both detection schemes which can be easily undone in electrical domain.

Since the input signal to the time-lens-based system is processed in block-by-block basis, periodic time lenses with finite aperture should be introduced [64], [115, 63]. Suppose that the time frame of Fourier transform (FT) is T_{FT}, the OFDM bandwidth is f_s, the number of sub-channels is n_{sc}, and Δf_s is the frequency space between OFDM sub-channels, then we have

$$f_s = n_{sc}\Delta f_s, \tag{6.21}$$

$$T_{FT} = \frac{1}{\Delta f_s}. \tag{6.22}$$

The phase modulator multiplies the incident optical field envelope by a function

$$h(t) = \sum_{n=-\infty}^{\infty} h_0(t - nT_{FT}), \tag{6.23}$$

$$h_0(t) = \exp\left[\frac{iV(t)\pi}{V_\pi}\right], \tag{6.24}$$

$$V(t) = \begin{cases} V_0 t^2, & \text{for } |t| < T_{FT}/2, \\ 0, & \text{otherwise.} \end{cases} \tag{6.25}$$

The input signal to the time-lens-based Fourier transformer is of the form

$$u_{in}(t) = \sum_{n=-\infty}^{\infty} u_n(t - nT_{FT}), \tag{6.26}$$

$$u_n(t) = \begin{cases} m_n(t), & \text{for } |t| < T_{FT}/2, \\ 0, & \text{otherwise}, \end{cases} \tag{6.27}$$

where $m_n(t)$ is the message signal in the n-th block. Consider the input signal $u_n(t)$, which is limited to the interval $[-T_{FT}/2, T_{FT}/2]$. To see the spectrum of the OFDM signal, taking the FT of Eq. (6.14) and using Eq. (6.26), we obtain

$$\widetilde{u}^{FT}_{out-tx}(f) \propto u_n(t), \tag{6.28}$$

where

$$t = -2\pi S_1 f. \tag{6.29}$$

Eq. (6.28) implies that the desirable OFDM spectrum, $\widetilde{u}^{FT}_{out-tx}(f)$ can be obtained by appropriately shaping the input message signal $u_n(t)$ in time domain and the time axis, t is related to the frequency axis, f by Eq. (6.29). For the given frequency space, Δf_s between the sub-channels, the corresponding time spacing for the time-lens-based system is

$$\Delta t_s = 2\pi |S_1| \Delta f_s. \tag{6.30}$$

In other words, the samples of the message signals corresponding to adjacent subcarriers should be separated by Δt_s. For the OFDM signal with bandwidth of f_s , the frequency f in Eq. (6.28) should be confined to $[-f_s/2, f_s/2]$ and the time frame boundary $T_{FT}/2$ should correspond to the maximum frequency, $f_s/2$. Using Eq. (6.29), we obtain

$$|S_1| = \frac{T_{FT}}{2\pi f_s}. \tag{6.31}$$

Substituting Eq. (6.31) in Eq. (6.30) and using Eq. (6.22), we obtain

$$\Delta t_s = \frac{1}{f_s}. \tag{6.32}$$

The driving voltage of the phase modulator in the time lens set up could be very high if the duration of OFDM symbol is getting large, which can be seen from Eq. (6.25). Using Eqs. (6.13), (6.21), (6.22), (6.25) and (6.31), the maximum phase shift introduced by the phase modulator in frame-by-frame basis is given by

$$\frac{V_0 \pi}{V_\pi}\left(\frac{T_{FT}}{2}\right)^2 = \frac{\pi}{4} n_{sc}, \tag{6.33}$$

which means that the maximum phase shift increases linearly with the number of sub-channels. Since is generally a very large number, the maximum phase shift could be unreasonably large. To avoid the large driving voltage, we utilize the periodic property of sinusoidal function,

$$\exp(ix) = \exp[i(x + 2n\pi)], \quad n = \pm 0, 1, 2, \dots \,. \tag{6.34}$$

Because of the periodic property, the driving voltage needs not increase quadratically with time. The broken line in Fig. 6.4 shows the normalized driving voltage increasing quadratically with time and the solid line in Fig. 6.4 shows the driving voltage that provides the same amount of phase shift. For example, when $t = T_{FT}/2 = 25.6$ ns, the driving voltage with quadratic dependence is $256V_\pi$, whereas the voltage shown in the solid line of Fig. 6.4 does not increase beyond $2V_\pi$. Because of the periodic property, the maximum driving voltage becomes independent of T_{FT}. The required driving voltage shown in the solid line of Fig. 6.4 can be obtained using arbitrary waveform generator (AWG). Typically, the commercially available AWG has a bandwidth less than 10 GHz. For the example shown in Fig. 6.4, the required bandwidth is around 2 GHz.

For the proper operation of the proposed scheme, the driving voltage of the phase modulator should be synchronized with OFDM frames. This can be achieved by extracting a clock at the frame rate which would be used at the AWG electronics to synchronize the driving voltage with the OFDM frame. Similar techniques have been used to reduce the timing jitter of solitons using synchronous amplitude modulators [142]. Since the frame rate is much lower than the symbol rate, this technique is not too hard to implement. Alternatively, the periodic time lenses could be free running without synchronizing them to the OFDM frames. Let the timing shifts between the OFDM frame and the driving voltage of the phase modulators at the transmitter and receiver be t_1 and t_2. The parameters t_1 and t_2 can be estimated using digital signal processing at the receiver.

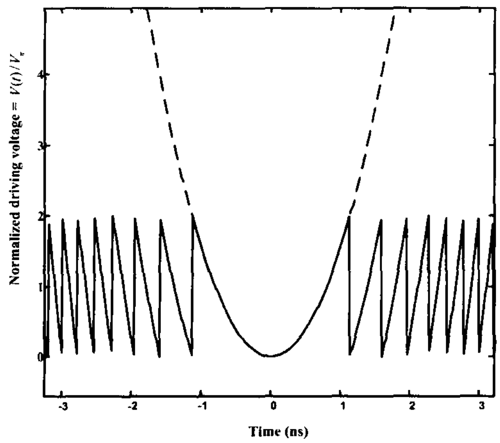

Figure 6.4: The driving voltage varying as time for the phase modulator in a time-lens-based system.

6.3 Simulation and Results

B.W. of OFDM signal ($= f_s$)	Space of sub-chs.
20 GHz	19.53 MHz
No. of sub-chs.	No. of frames
1024	64
Cyclic prefix	Cyclic suffix
1/8 T_{FT}	N/A
No. of PRBS	$S_1(= \beta_2^F F)$
2^{17}	0.407 ns^2

Table 6.1: OFDM parameters. PRBS= Pseudo-random bit sequence.

To compare the performance of the optical OFDM using time lenses with the conventional OFDM using FFT, the bit error rate (BER) is calculated at the receiver as a function of the launch power. Fiber nonlinearity and amplified spontaneous emission (ASE) noise are both taken into account. The simulation parameters are given in Table 6.1 for OFDM setup and Table 6.2 for the transmission link setup, respectively. The data rate is 40 Gb/s, and we use 4-QAM format as the message data. The OFDM bandwidth, f_s is 20 GHz. The number of sub-channels is 1024 and the space between sub-channels, is 19.53 MHz. 64 OFDM symbols are simulated such that the total number of bits is 2^{17}. A De Bruijin sequence of length 2^{17} is used in the Monte-Carlo simulation. The accumulated second-order dispersion in the time-lens-based system is 0.407 ns^2. The bandwidth of optical filter used in our simulation is 10 GHz. The cyclic prefix for optical OFDM using time lenses can be realized using delay lines and couplers for each OFDM frame.

Date rate	Modu. format	Trans. distance
40 Gb/s	4-QAM	2400 km
Fiber loss	Noise figure	Fiber disp.
0.2 dB/km	5 dB	17 ps/(km·nm)
Fiber nonlinear coefficient	Amp. spans	B.W. of opt. filter
1.1099 km^{-1} W^{-1}	30	10 GHz

Table 6.2: Transmission link parameters.

First, the amplitudes of $m_I(t)$ and $m_Q(t)$ are carefully chosen such that they operate in the linear region of MZM. We choose P_m (as defined in Eq. (6.8)) to be 0.12 mW. The disadvantage of choosing such low values is that the significant laser power is lost after introducing MZMs. Fig. 6.5 shows the BER as a function of launch power, P_{in} (as defined in Eq. (6.9)), at P_m = 0.12 mW. The launch power to the fiber-optic link can be varied by changing the laser power P_c (as defined in Eq. (6.7)). The broken lines with squares and diamonds show the back-to-back BER for the case of FFT-based and time-lens-based OFDM, respectively. Back-to-back BER is calculated by introducing a noise source that is equivalent to the cascade of all in-line amplifiers. The solid line with crosses stands for the conventional coherent OFDM using FFT and the circles stand for the coherent OFDM using time lenses, respectively. It is found that both of these two schemes of coherent OFDM systems have almost the same performance. This is because the nature of both conventional OFDM based on FFT and optical OFDM using time

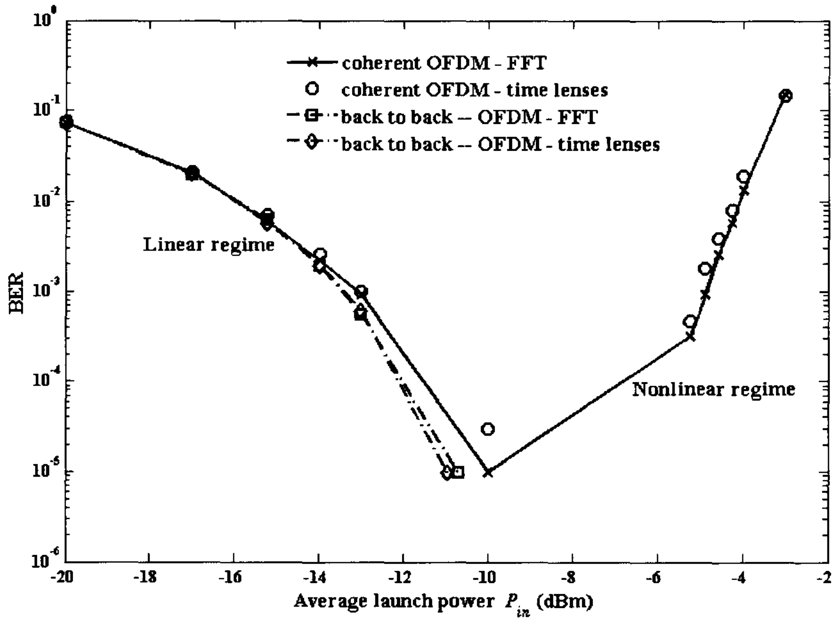

Figure 6.5: BER v.s. launch power for coherent OFDM at 0.12 mW.

lenses is essentially same and the only difference is that for the conventional OFDM, the IFT/FT is implemented in electrical domain but for the optical OFDM, that is done in the optical domain using Fourier transforming property of time lenses. However, the advantage of optical OFDM is that all the signal processing needed to obtain OFDM signal can be accomplished in the optical domain. This implies that intrinsically higher available bandwidth in optical domain can be utilized and thereby, high speed digital signal processing (DSP) to implement FFT/IFFT can be eliminated. From Fig. 6.5, it is can be seen that when the launch power is small, BER decreases as the launch power increases. This is the linear regime as shown on the left-hand side of Fig. 6.5. When the launch power becomes large, the fiber nonlinearity dominates over the ASE noise, such that the BER increases with the launch power. This is the nonlinear regime as depicted on the right-hand side of Fig. 6.5.

Fig. 6.6 (a) shows the normalized in-phase component of input $m(t)$ of the first 32 bits in the first OFDM frame for a coherent optical OFDM system using time lenses. The solid and dotted lines in Fig. 6.6 (b) show the normalized output current after the coherent detector, but before the time-reversing circuit at the average optical launch power of -13 dBm and -4 dBm, respectively. The significant nonlinear impairment can be seen for the case of $P_{in} = -4$ dBm , while for the case of $P_{in} = -13$ dBm, the effect of fiber nonlinearity is negligible. Note that the output bit sequence shown in Fig. 6.6 (b) is time-reversed within a frame. Fig. 6.7 (a) and 6.7 (b) show the spectra of FFT-based and time-lens-based OFDM. As can be seen, they are identical and therefore, the coherent OFDM using time lenses has the same spectral efficiency as the OFDM using FFTs.

The above simulation is done under the assumption that MZM is working as a linear modulator. However, when the power of driving message signal launched to MZM increases, this assumption would not hold any more. Next, we study the impact of MZM nonlinearity as well as fiber nonlinearity on the coherent OFDM system based on FFT and time lenses. First, to investigate the nonlinear effect induced by MZM alone, the fiber nonlinearity is turned off and the ASE noise is adjusted to generate the OSNR required

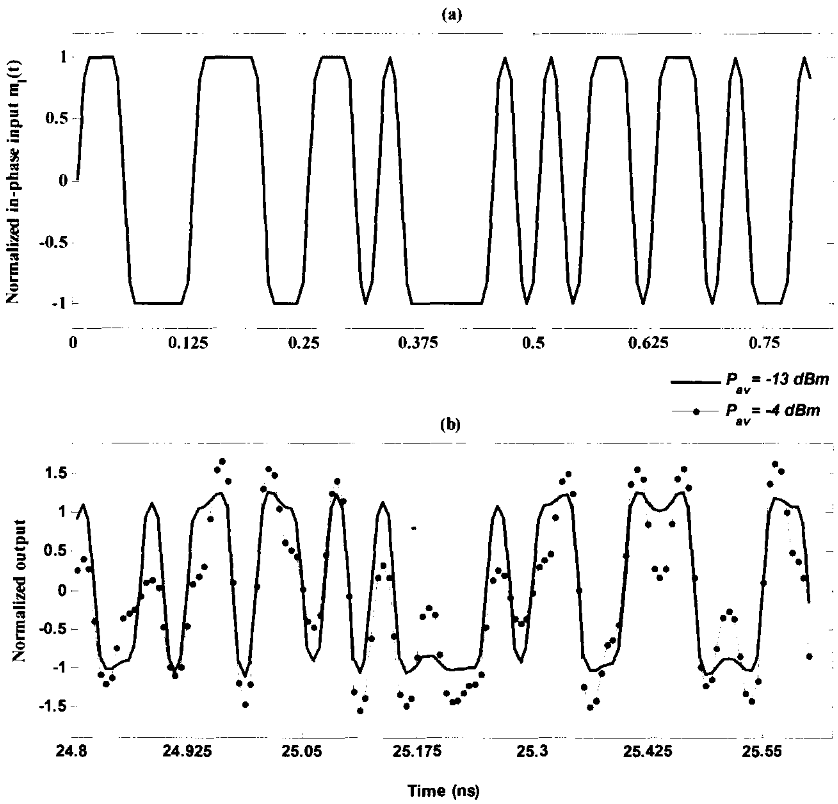

Figure 6.6: (a) Normalized in-phase input $m_I(t)$, and (b) the corresponding output of the coherent detector.

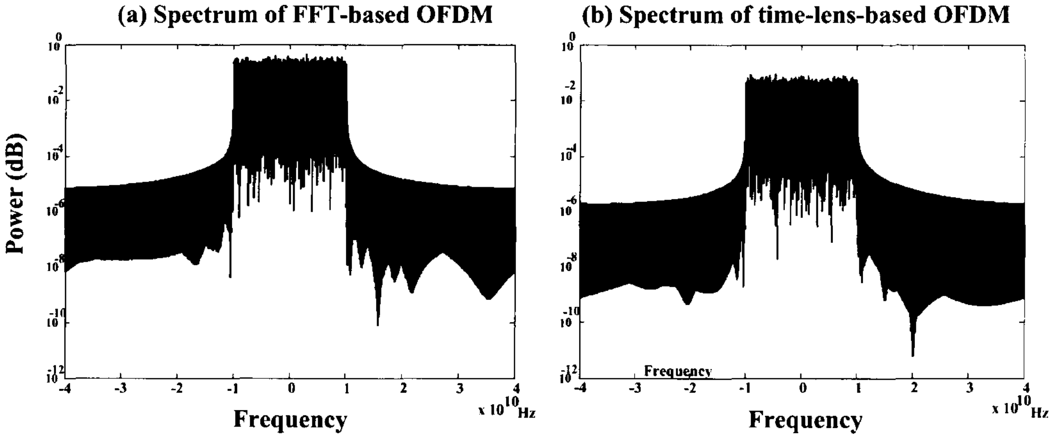

Figure 6.7: (a) Spectrum of the FFT-based OFDM signal, and (b) spectrum of the time-lens-based OFDM signal.

to obtain the BER of 2×10^{-3}.

Fig. 6.8 shows the required OSNR at BER of 2×10^{-3} varying as the average power of the driving message signal. Fig. 6.8 (a) shows the MZM nonlinear effect on coherent OFDM systems without fiber nonlinearity. In Fig. 6.8 (b), the fiber nonlinearity is taken into account and the power launched to the transmission fiber is at -10 dBm. In both cases, it is shown that the required OSNR at BER of 2×10^{-3} for coherent optical OFDM based on FFT increases drastically when $P_m > 200$ mW, whereas for the coherent optical OFDM using time lenses, the required OSNR at BER of 2×10^{-3} does not change significantly. For the coherent OFDM using FFT, the MZM is placed between IFFT block at the transmitter and FFT block at the receiver, so MZM nonlinearity destroys the orthogonality of sub-channels of OFDM signal, which leads to the significant impairment on the coherent OFDM using FFT. In contrast, for the coherent OFDM using time lenses, MZM is placed before IFT, so that the OFDM signal can be demodulated correctly after passing through FT. Therefore, the MZM nonlinearity only has minor impairment on the coherent OFDM using time lenses as can be seen in Fig. 6.8. When the fiber nonlinearity is present (Fig. 6.8 (b)), the required OSNR at BER of 2×10^{-3} increases by $1 \sim 2$ dB

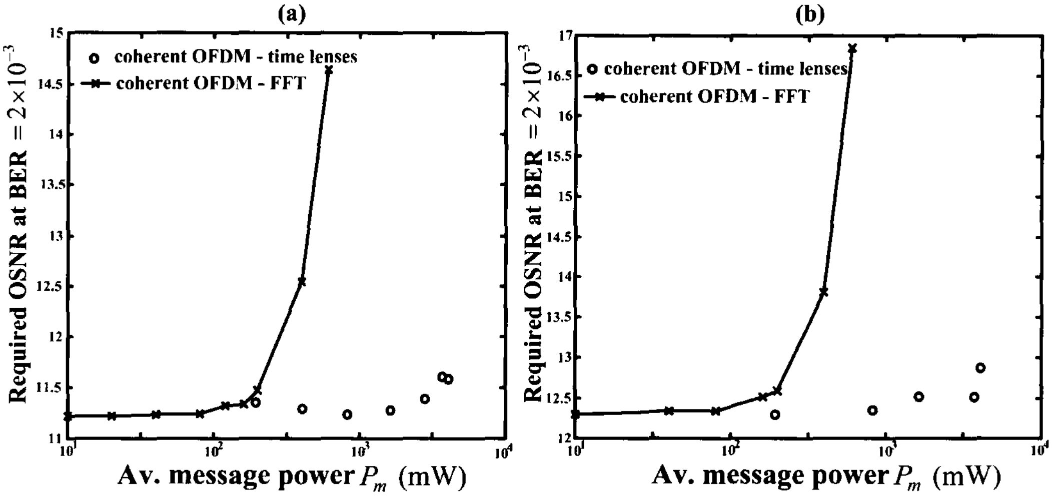

Figure 6.8: Nonlinear impairments induced by MZM for coherent OFDM. (a) $\gamma = 0$, (b) $\gamma = 1.1099$ km^{-1} W^{-1} , $P_{in} = -10$ dBm.

for both coherent OFDM schemes, compared to that shown in Fig. 6.8 (a). This implies that the fiber nonlinearity further worsens the system performance along with the MZM nonlinearity. Fig. 6.9 shows the BER as a function of the launch power, P_{in} , when a larger average power of electrical driving message signal, P_m is chosen. The parameters used for Fig. 6.9 are same as that of Fig. 6.5 except that $P_m = 0.12$ mW in Fig. 6.5 and $P_m = 500$ mW in Fig. 6.9. In Fig. 6.5, we found that the performance of the OFDM based on FFT is almost same as that based on time lenses. In contrast, when P_m is large, OFDM based on time lenses has a superior performance as can be seen from Fig. 6.9.

6.4 Conclusions

A coherent optical OFDM scheme utilizing time lenses for implementing Fourier transforms both at the transmitter and at the receiver is analyzed. Impact of MZM nonlinearity as well as the fiber nonlinearity on the performance of the optical OFDM system is studied. The results are compared with the optical OFDM using FFTs. It is found that

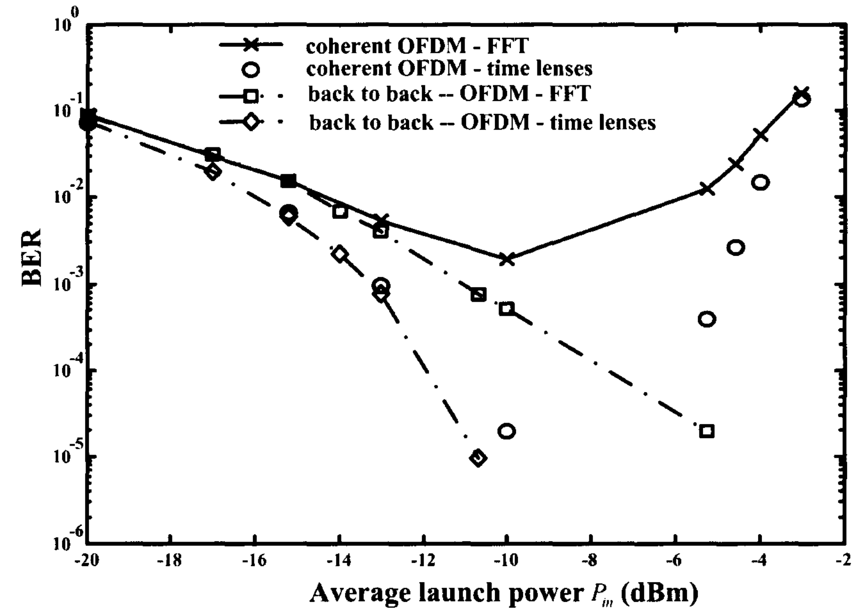

Figure 6.9: BER v.s. launch power for coherent OFDM at $P_m = 500$ mW.

when the driving voltage of the MZM is large, MZM nonlinearity destroys orthogonality of sub-channels of OFDM signal for coherent OFDM using FFT, and therefore degrades its performance significantly, whereas for the coherent OFDM using time lenses, MZM nonlinearity only has minor impairment because the Fourier transform block is introduced after the MZM. When the MZM operates in the linear regime, almost same performance is obtained for both schemes. In addition, the setup of time-lens-based Fourier transformer is discussed and a novel scheme to obtain the quadratic phase chirp without requiring the quadratic driving voltage is proposed. Important advantages of time-lens–based OFDM are that (i) FT can be done in optical domain almost instantaneously, whereas the FFT in digital domain is slow and requires significant computational efforts, (ii) optical domain Fourier transform has a large bandwidth ($\sim$ THz) and therefore, FT/IFT can be performed at a large system rate.

Chapter 7

Investigation and Comparison of Digital Back-Propagation Schemes for OFDM and Single-Carrier Fiber-Optic Transmission Systems

7.1 Introduction

Digital backward propagation (BP) schemes have drawn significant research interest recently because of their ability to undo fiber linear and nonlinear impairments [81], [87], [89]-[91], [143, 144]. Orthogonal frequency-division multiplexing (OFDM) is believed to suffer from fiber nonlinearity because of the large peak-to-average power ratio (PAPR). Digital BP could compensate for fiber nonlinear effects to some extent and therefore, it is important to compare the single-carrier (SC) and OFDM systems in a coherent system that utilizes digital BP. In this chapter, we investigate two types of digital BP schemes for SC and OFDM systems based on 16 quadrature amplitude modulation (QAM). The first scheme is the perfect BP with very small step size. This scheme provides the highest performance improvement. However, in this case, computational cost is quite large because of small step size. The second scheme is the one that uses the step size equal to the amplifier spacing (AS-BP). This scheme is computationally cheaper, but the performance improvement is moderate. We compare the performance of SC and OFDM systems using these BP schemes. For SC systems, we consider two types of pulses – Nyquist pulses with rectangular spectrum and the standard raised-cosine NRZ pulses. Our results show that OFDM has almost the same performance as SC-Nyquist and they both outperform SC-NRZ, when either of digital BP schemes is used.

In principle, digital BP scheme could undo the deterministic (bit-pattern dependent) nonlinear impairments, but it cannot compensate for stochastic nonlinear impairments such as nonlinear phase noise. In-line optical amplifiers change the amplitude of the optical field envelope randomly and fiber nonlinear effects such as self-phase modulation (SPM) convert the amplitude fluctuations to phase fluctuations which is known as nonlinear phase noise. The impact of nonlinear phase noise was first studied in Ref. [145] for dispersion-free fiber-optic systems. Refs. [146] and [147] have found that the fiber dispersion lowers the impact of nonlinear phase noise. When the digital BP scheme is used, deterministic nonlinear impairments such as SPM, XPM and FWM can be suppressed and therefore, stochastic nonlinear impairments such as nonlinear phase noise could become dominant. For constant intensity formats such as quadrature phase-shift keying (QPSK), amplitude noise does not lead to penalty. However, for systems based on QAM, amplitude noise becomes important because of several amplitude levels. In this chapter, we investigate the impact of nonlinear amplitude noise on OFDM and SC systems. The phase fluctuations caused by ASE and SPM (or cross-phase modulation (XPM)) translates into amplitude fluctuations because of fiber dispersion leading to nonlinear amplitude noise. Our numerical simulation results show that the standard deviations of nonlinear phase and amplitude noise are lower for OFDM and SC-Nyquist systems as compared to SC-NRZ systems, which explains the reason for performance advantage of OFDM/SC-Nyquist system over SC-NRZ system when the BP is used.

This chapter is organized as follows. In Section 7.2, we review the background on backward propagation, including Nonlinear Schrödinger Equation, symmetric split-step Fourier method (S-SSFM), and also define two types of BP schemes. In Section 7.3, we compare the performances of the OFDM, SC-NRZ and SC-Nyquist. The impact of electrical filter bandwidth and the impact of nonlinear phase/amplitude noise in OFDM/SC systems with BP are also investigated.

7.2 Theoretical Background on Backward Propagation (BP)

The signal propagation along a fiber is governed by nonlinear Schrödinger equation (NLSE) [33],

$$\frac{\partial u}{\partial z} = \left[\hat{D} + \hat{N}\right] u, \tag{7.1}$$

where $\hat{D}$ denotes the linear operator given by

$$\hat{D} = -i\frac{\beta_2(z)}{2}\frac{\partial^2}{\partial t^2} + \frac{\beta_3(z)}{6}\frac{\partial^3}{\partial t^3} - \frac{\alpha(z)}{2}, \tag{7.2}$$

and $\hat{N}$ denotes the nonlinear operator given by

$$\hat{N} = i\gamma(z)|u|^2, \tag{7.3}$$

$u(t, z)$ is the electrical field envelope of the signal, $\beta_2(z)$, $\beta_3(z)$, $\alpha(z)$ and $\gamma(z)$ are the profiles of second-order, third-order fiber dispersion coefficients, loss/gain and nonlinear coefficient, respectively. Fiber loss is fully compensated after each span by EDFAs. Eq. (7.1) can be numerically solved using split-step Fourier method (SSFM). The solution of Eq. (7.1) is given by

$$u(t, L) = Mu(t, 0), \tag{7.4}$$

where

$$M = \exp\left\{\int_0^L \left[D(z) + N(z)\right] dz\right\}. \tag{7.5}$$

Here, L is the total transmission distance. The distortions caused by dispersion and nonlinearity, can be undone by means of digital signal processing (DSP). Suppose we multiply Eq. (7.4) by M^{-1}, we obtain

$$u(t,0) = M^{-1}u(t,L). \tag{7.6}$$

Since $\exp(x)\exp(-x) = 1$ for any operator x, it follows that

$$M^{-1} = \exp\left\{-\int_0^L [D(z) + N(z)]\,dz\right\}, \tag{7.7}$$

which is equivalent to solving the following partial differential equation

$$\frac{\partial u}{\partial z} = -\left[\hat{D} + \hat{N}\right]u, \tag{7.8}$$

with the initial condition $u(t, L)$. Since Eq. (7.8) can be obtained by reversing the spatial variable z in Eq. (7.1), this technique is referred to as backward propagation (BP) [81], [87], [89]-[91], [143, 144]. In comparison with the mid-span phase conjugation technique, in which the third-order dispersion can not be canceled [81], [148]-[150], BP has the advantage that it can be used to compensate for any higher order dispersion. BP can be implemented digitally, either at transmitter/receiver or jointly at both, by numerically solving Eq. (7.8) using DSP. In this work, we focus on the receiver-based backward propagation compensation.

To solve the NLSE, the S-SSFM is used which is shown in Fig. 7.1. In Fig. 7.1, the length of each fiber span is divided into M small segments of step size, h. Smaller h gives better performance, but leads to more extensive calculation efforts. At the receiver, after the coherent detection, the received signal with complex field envelope passes through a digital BP compensator implemented using DSP. An ideal BP compensator is shown in Fig. 7.2. In this work, we will discuss two types of BP. For type I, the BP has step size equal to amplifier spacing, called AS-BP, and for type II, very small step size (same step size as that used in forward propagation) is used in BP. We call this perfect BP. In this chapter, the NLSE is solved using the non-iterative symmetric SSFM, and its

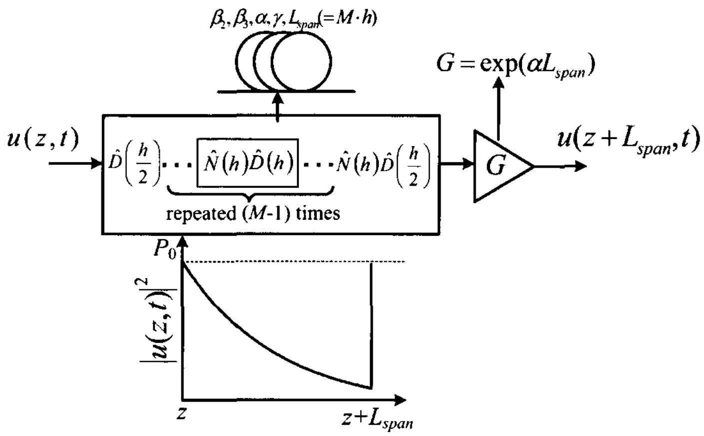

Figure 7.1: Symmetric split-step Fourier method (SSFM) used to simulate the signal forward propagation through the transmission fiber.

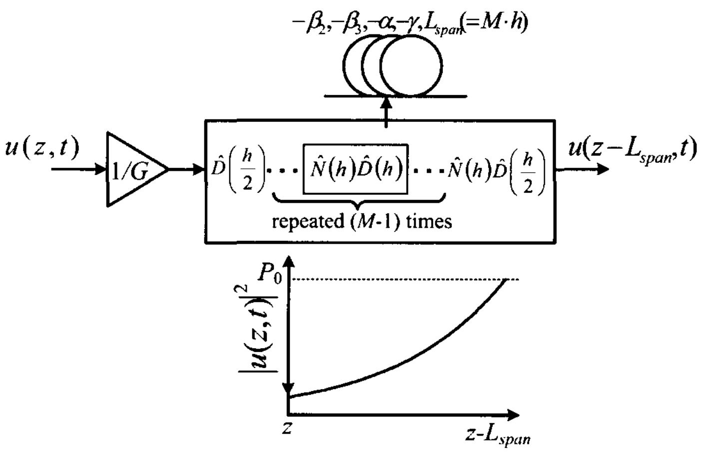

Figure 7.2: An ideal BP compensator for a single span.

corresponding forward propagation mathematical expression for one fiber span is given by [33],

$$u(z+h,t) = \exp\left(\frac{h}{2}\hat{D}\right)\exp\left(\int_{z}^{z+h}\hat{N}(\tau)d\tau\right)\exp\left(\frac{h}{2}\hat{D}\right)u(z,t). \tag{7.9}$$

Note that, at the end of each span, the gain, $G = \exp(\alpha L_{span})$ is applied, and L_{span} is the fiber span length between amplifiers. The mathematical expression of backward propagation therefore can be written as

$$u[L-(z+h),t] = \exp\left(-\frac{h}{2}\hat{D}\right)\exp\left(\int_{L-z}^{L-(z+h)}\hat{N}(\tau)d\tau\right)\exp\left(-\frac{h}{2}\hat{D}\right)u(L-z,t), \tag{7.10}$$

where L is the total transmission distance. One of the disadvantages of the ideal BP is that computational complexity increases significantly as h decreases. In Ref. [143], it is proposed to use asymmetric split-step Fourier scheme with step size equal to amplifier spacing (AS-BP) and with a variable parameter to optimize the BER. The AS-BP can be realized as [89], [143],

$$u_1(z,t) = u(L-z,t)\exp\left(-i\eta\gamma\left|u(L-z,t)\right|^2 L_{\text{eff}}\right), \tag{7.11}$$

$$\widetilde{u}[L-(z+L_{\text{span}}),\omega] = \widetilde{u}_1(z,\omega)\exp\left[-i\left(\frac{\beta_2}{2}\omega^2+\frac{\beta_3}{6}\omega^3\right)L_{\text{span}}\right], \tag{7.12}$$

where

$$L_{\text{eff}} = \frac{1-\exp(-\alpha_0 L_{\text{span}})}{\alpha_0}, \tag{7.13}$$

α_0 is the fiber loss coefficient, $\widetilde{u}_1(z,\omega)$ is the Fourier transform of $u_1(z,t)$, and η is the variable parameter to be optimized. In the case of AS-BP, the computational complexity increases linearly with the number of spans.

7.3 Results and Discussion

We have simulated a N span fiber-optic transmission system without inline pre- and post-dispersion compensation in optical domain. Table 7.1 shows the system parameters used in our simulation. These parameters are used throughout the chapter unless otherwise specified. For perfect BP, very small step size is chosen so that nonlinear phase does not exceed 0.005 rad. A pseudo-random bit sequence (PRBS) of length 2^{21} is used in the simulation. The bit rate is 100 Gb/s and the corresponding symbol rate for 16-QAM is 25 Gbaud. We assume that the coherent receiver is ideal and mainly focus on the impairments caused by dispersion and nonlinearity. Digital backward propagation (BP) provides equalization for both linear and nonlinear impairments and therefore, no other equalizer is used.

In this chapter, we compare three types of modulation/multiplexing schemes. The first scheme is OFDM system with 1024 sub-carriers. Each sub-carrier is modulated by 16-QAM data. The second scheme is the single-carrier (SC) modulated by 16-NRZ-QAM. The third scheme is the SC modulated by 16-QAM that uses the Nyquist pulse so that the bandwidth of the OFDM and this SC system is roughly same. The electrical filter bandwidths shown in Table 7.1 are so chosen as to optimize the performance.

<table>
<tr><td>Bit rate</td><td>Modulation format</td><td>Amplifier spacing</td><td>Noise figure</td></tr>
<tr><td>100 Gb/s</td><td>16-QAM</td><td>80 km</td><td>5 dB</td></tr>
<tr><td>β_2</td><td>β_3</td><td>γ</td><td>α_0</td></tr>
<tr><td>-21.7 ps^2/km</td><td>0.125 ps^3/km</td><td>1.1099 $W^{-1}km^{-1}$</td><td>0.2 dB/km</td></tr>
<tr><td rowspan="2">OFDM</td><td>No. of sub-channels</td><td>FFT-points</td><td>Electrical filter bw</td></tr>
<tr><td>1024</td><td>4×1024</td><td>13.75 GHz</td></tr>
<tr><td rowspan="3">SC</td><td>Pulse shape</td><td>Roll-off factor</td><td>Electrical filter bw</td></tr>
<tr><td>NRZ (raised cosine)</td><td>0.8</td><td>20 GHz</td></tr>
<tr><td>Nyquist pulse (sinc)</td><td>N/A</td><td>13.75 GHz</td></tr>
</table>

Table 7.1: System parameters used in simulation.

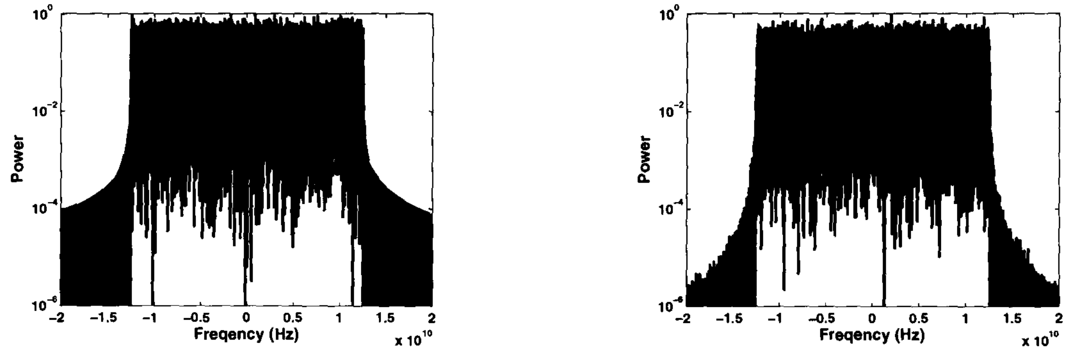

(a) Spectrum of OFDM signal. (b) Spectrum of SC-Nyquist signal.

Figure 7.3: Normalized spectra of OFDM and SC-Nyquist signals.

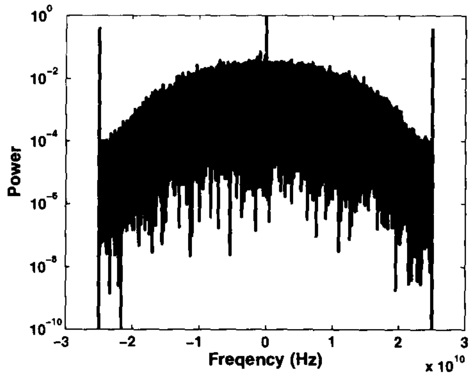

Figure 7.4: Normalized spectrum of SC-NRZ signal.

7.3.1 Comparison of system performance for OFDM, SC-NRZ and SC-Nyquist

Figs. 7.3(a), 7.3(b) and 7.4 show the spectra of OFDM, SC-Nyquist and SC-NRZ signals, respectively. The spectral power is normalized. We can see from Figs. 7.3(a), 7.3(b) that the bandwidth and shape of the spectra of OFDM and SC-Nyquist are almost same. The one-sided bandwidth is around 12.5 GHz for both OFDM and SC-Nyquist. For the SC-NRZ, however, the bandwidth reaches about 20 GHz as shown in Fig. 7.4.

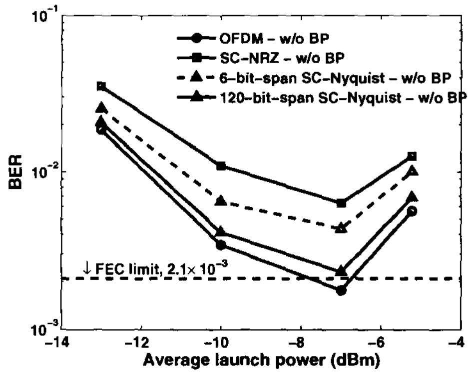

Figure 7.5: BER v.s. average launch power in the case without BP. Transmission distance= 13×80 km.

Fig. 7.5 shows the BER v.s. the average launch power for OFDM and single-carrier (SC) systems without BP, at the transmission distance of 13×80 km. The curve with circles shows that the OFDM system can go as far as 13 fiber spans at BER of 2.1×10^{-3}, and has a superior performance over SC-NRZ systems (the curve with squares). The solid and dashed curves with triangles denote the SC-Nyquist system, for which the *sinc* function, used to generate the Nyquist pulses, has a spanning of 120 bit slots (solid), and 6 bit slots (dashed), respectively. It can be seen that the longer the single Nyquist pulse spans, the better performance is achieved. This is because the bandwidth of the SC-Nyquist system approximates ideal Nyquist bandwidth when the duration of *sinc* function increases. However, it would be difficult to implement the long duration Nyquist pulses in practical high-speed transmission systems. From Fig. 7.5, we see that SC-Nyquist is much better than SC-NRZ when the 120-bit-span *sinc* function is used, and has almost the same performance compared to OFDM. It is mainly because the SC-Nyquist has narrower signal bandwidth compared to that of SC-NRZ, and therefore less ASE noise is introduced for SC-Nyquist.

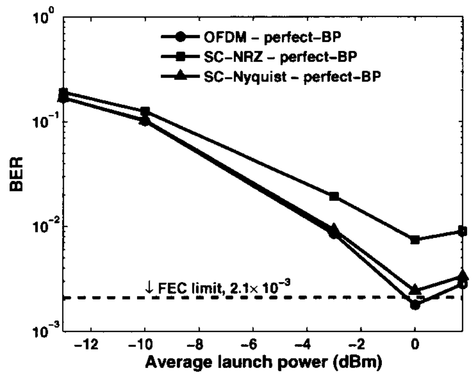

Figure 7.6: BER v.s. average launch power in the case of perfect-BP. Transmission distance= 82 × 80 km. 120 bit-span Nyquist pulses are used for SC-Nyquist.

Fig. 7.6 shows the BER v.s. average launch power for both OFDM and SC systems with perfect-BP, at the transmission distance of 82×80 km. From Fig. 7.6, we see that the OFDM and SC-Nyquist systems (the curves with circles and triangles) using perfect-BP have the performance advantage over the SC-NRZ with perfect-BP. There is a five-fold increase in system reach as compared to that without BP for OFDM/SC-Nyquist. The slightly better performance of OFDM over SC-Nyquist is shown when the launch power increases, which results from the truncation of the Nyquist pulses leading to broadened spectrum. In the nonlinear regime, the signal spectrum is further broadened due to fiber nonlinearity, and therefore the out-band signal components are strengthened. Before the digital BP, the electrical filter with bandwidth shown in Table 7.1 is applied to remove the out-band signal, which leads to larger distortion for SC-Nyquist than for OFDM when the perfect-BP is used.

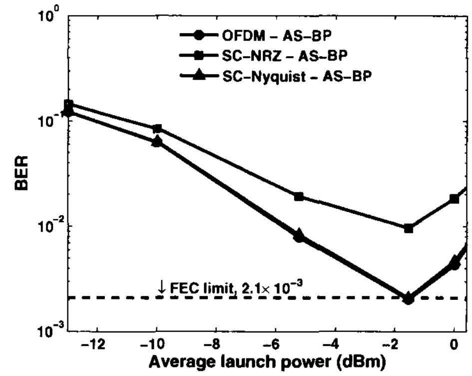

Figure 7.7: BER v.s. average launch power in the case of AS-BP. Transmission distance= 52×80 km.

Fig. 7.7 shows BER as a function of average launch power in the case of BP with step size of amplifier spacing (AS-BP), at the transmission distance of 52×80km. The OFDM and SC-Nyquist (the curves with circles and triangles) have almost the same performance when AS-BP is used. The parameter η (given in Eq. (7.11)) is optimized for each scheme and is found to be in the range of 1.0-1.3. The system reach for OFDM/SC-Nyquist with AS-BP can be increased by 3 times of that without BP. It can also be seen from Figs. 7.5, 7.6 and 7.7 that the optimum launch power is increased from -7 dBm in the case without BP, to -1.5 dBm in the case of AS-BP, and finally to 0 dBm in the case of perfect-BP. The advantages of 5.5 dB and 7 dB in launch power are achieved for AS-BP and perfect-BP, respectively.

Figs. 7.8(a) and 7.8(b) show the optimum BER varying as a function of number of transmission fiber spans for the cases of perfect-BP and AS-BP, respectively. It can be seen that OFDM has achieved the maximum system reach in both cases, then SC-Nyquist, the worst is SC-NRZ.

In the above studies, we have shown that OFDM/SC-Nyquist has better performance as compared to SC-NRZ when digital BP is used. To understand the performance advantage of OFDM over SC, we investigate the impact of the electrical filter bandwidth and

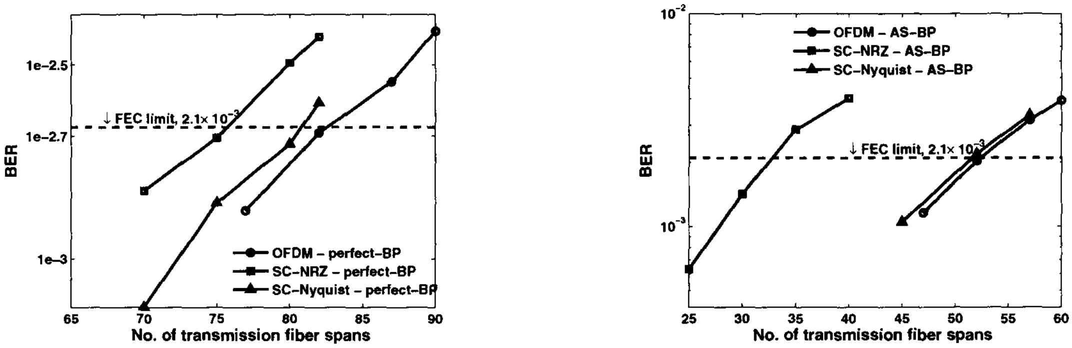

(a) Perfect-BP. (b) AS-BP.

Figure 7.8: Optimum BER v.s. no. of transmission fiber spans.

the impact of nonlinear phase/amplitude noise on OFDM/SC systems using BP in the following work.

7.3.2 Impact of the electrical filter bandwidth on OFDM/SC systems with BP

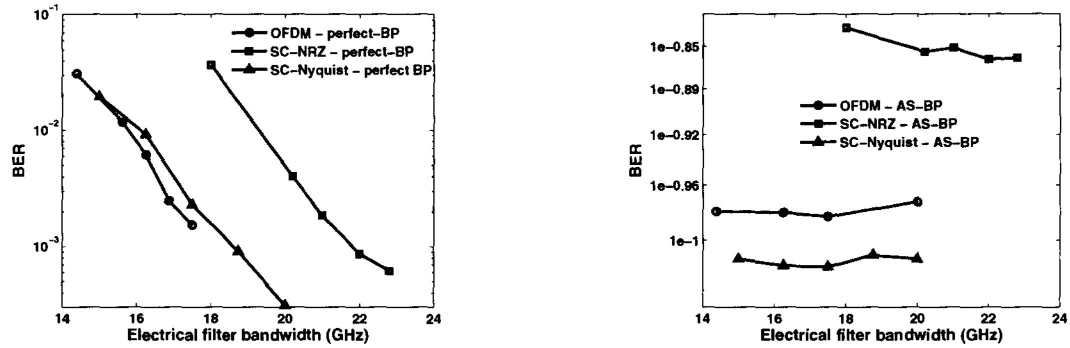

(a) Perfect BP. Average launch power= 4.77 dBm. The transmission distance is 60×80 km.

(b) AS BP. Average launch power= 4.77 dBm. The transmission distance is 33 × 80 km.

Figure 7.9: BER v.s. electrical filter bandwidth for perfect-BP and AS-BP.

In the absence of fiber nonlinearity, as the electrical filter bandwidth increases beyond the symbol rate, the performance degrades due to increased ASE power within the filter bandwidth. However, in the presence of nonlinearity and BP, it is desirable to have the large electrical filter bandwidth. To see the impact of electrical filter bandwidth on the nonlinear transmission system with BP, we find the BER of OFDM/SC with perfect-BP and AS-BP by changing the electrical filter bandwidth. We have chosen relatively large launch power so that the system operates in the nonlinear regime. Fig. 7.9(a) shows BER v.s. electrical filter bandwidth in the case of perfect-BP. It can be seen that the system performance improves as the electrical filter bandwidth increases for OFDM/SC with perfect BP. This is because the fiber nonlinearity broadens the signal spectrum and out-of-band signal components are truncated after passing through the narrow electrical filter. In other words, four wave mixing (FWM) sidebands generated by the forward propagation in fibers is removed by the ideal digital backward propagation if the electrical filter bandwidth is very large. However, if the electrical filter bandwidth is small ($\leq$ symbol rate), FWM sidebands generated by the fiber are cut off, but the digital backward propagation generates new FWM sidebands which are reflected at the computational edge (in frequency domain) and appear at the other edge leading to in-band cross-talk. From a practical standpoint, it would be challenging to increase the filter bandwidth due to the unavailability of high speed Analog-to-Digital (A/D) convertors. Fig. 7.9(b) shows BER v.s. electrical filter bandwidth for OFDM/SC with AS-BP. It can be seen that in the case of AS-BP, the fiber nonlinearity is not fully compensated, and therefore the increasing of electrical filter bandwidth gives a less benefit for the performance improvement for OFDM/SC with AS-BP.

7.3.3 Impact of nonlinear phase/amplitude noise with BP for OFDM, SC-NRZ and SC-Nyquist

When BP is used in OFDM/SC systems, the nonlinear effects are suppressed to some extent, as shown in the above work. However, the stochastic nonlinear impairments such as nonlinear phase/amplitude noise cannot be compensated using BP, and therefore it could become dominant impairment in OFDM/SC systems with BP. The amount of nonlinear phase/amplitude noise is measured by calculating the standard deviations of the phase and amplitude of received data symbols.

The received symbol for SC systems can be written as

$$s_r(i) = A_i \exp(j\theta_i), \tag{7.14}$$

where A_i and θ_i are the amplitude and phase of the sampled 16-QAM symbol at the i-th sampling time iT_s, where T_s is the symbol interval. The total samples used to calculate the variances of phase and amplitude in our simulation are 2^{19}. The phase and amplitude variances are calculated as follows:

$$\mathrm{var}(\theta) =< \theta^2 > - < \theta >^2, \tag{7.15}$$

and

$$\mathrm{var}(A) =< A^2 > - < A >^2, \tag{7.16}$$

and therefore, the corresponding standard deviation of phase and the normalized standard deviation of amplitude are given by

$$\sigma_\theta = \sqrt{\mathrm{var}(\theta)}, \tag{7.17}$$

$$\sigma_A = \sqrt{\mathrm{var}(A)}/ < A >, \tag{7.18}$$

where $< \cdot >$ stands for mean value. For OFDM systems, the complex information symbols are obtained after the fast Fourier transform (FFT) in digital domain. Then, the standard deviations of phase and amplitude are calculated following the same procedures given in Eqs. (7.15)- (7.18).

To investigate the impact of nonlinear phase/amplitude noise, we first turn off the ASE of in-line amplifiers and do the noise loading after the BP such that the SNR before the decision is same as that in the case of in-line amplifiers with ASE. We call this "lumped ASE" and in this case, nonlinear interaction between signal and ASE is absent. In Figs. 7.10(a) and 7.10(b), the dashed lines show the case of lumped ASE with perfect-

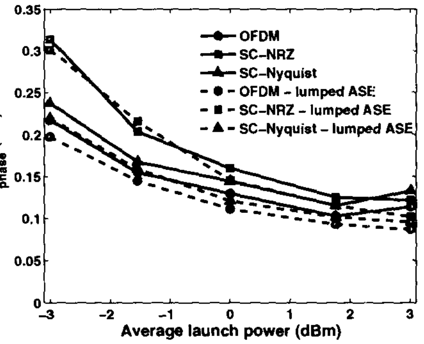

(a) The standard deviation of phase noise.

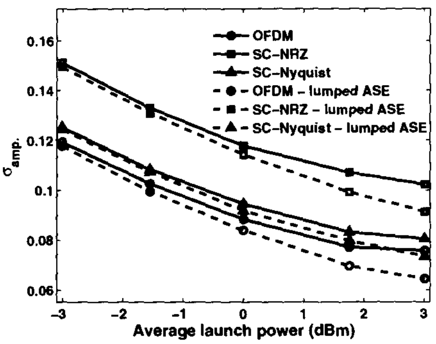

(b) The normalized standard deviation of amplitude noise.

Figure 7.10: The standard deviations of phase/amplitude noise v.s. average launch power for perfect-BP. The transmission distance is 60×80 km.

BP. The solid lines correspond to the case of in-line amplifiers with ASE. The difference between these curves is a measure of nonlinear phase/amplitude noise. From Figs. 7.10(a) and 7.10(b), we see that the nonlinear phase/amplitude noise causes almost the same amount of effects on OFDM, SC-Nyquist, and SC-NRZ when perfect-BP is used. The solid lines in Fig. 7.10(a) show that the phase deviation decreases initially as a function of launch power (linear regime) and then starts increasing because of nonlinear phase noise and uncompensated deterministic nonlinear effects (intra-channel XPM (IXPM), intra-channel FWM (IFWM)) due to finite bandwidth of filters. The dashed lines show the phase deviation due to linear phase noise and uncompensated IXPM and IFWM effects. The larger phase deviation of SC-NRZ results mainly from its inherently wider signal bandwidth as compared to OFDM and SC-Nyquist. In Fig. 7.10(b), the standard deviation of amplitude noise decreases as the launch power increases for the case of lumped ASE which indicates that the amplitude fluctuations due to IXPM and IFWM become quite small at large launch powers with perfect BP. However, in real systems (solid lines), σ_{amp} starts increasing at large launch powers indicating that nonlinear amplitude noise due to ASE-nonlinearity coupling becomes important. Nonlinear amplitude/phase noise set an upper limit on the optimum launch power.

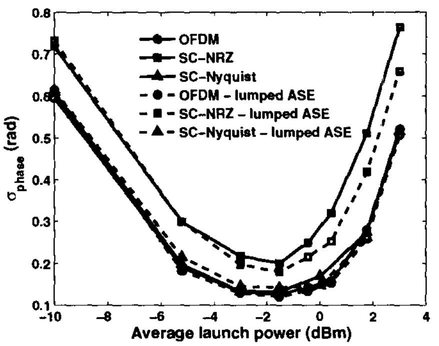

(a) The standard deviation of phase noise.

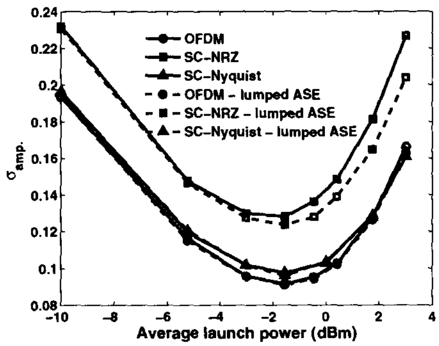

(b) The normalized standard deviation of amplitude noise.

Figure 7.11: The standard deviations of phase/amplitude noise v.s. average launch power for AS-BP. The transmission distance is 33×80 km.

Fig. 7.11(a) and 7.11(b) show standard deviations of phase and amplitude noise v.s. the average power for AS-BP at the transmission distance of 33×80 km. The solid lines stand for the case of distributed ASE, and the dashed lines show the lumped ASE simulations for OFDM/SC systems with AS-BP. The trends in Figs. 7.11(a) and 7.11(b) are similar to those in Figs. 7.10(a) and 7.10(b). From Figs. 7.11(a) and 7.11(b), we see that for OFDM and SC-Nyquist systems with AS-BP, the nonlinear phase/amplitude noise leads to negligible impact. However, it causes significant impairment for the SC-NRZ system as the large difference of standard deviation of phase/amplitude noise can be seen in Figs. 7.11(a) and 7.11(b). The main difference between perfect BP and AS-BP is that at large launch powers, the standard deviations of amplitude and phase noise increase with launch power for the case of AS-BP (Figs. 7.11) whereas it decreases or remains constant at large launch powers for the case of perfect BP (Figs. 7.10). This is because AS-BP does not fully compensate for SPM, IXPM and IFWM.

7.4 Conclusion

We have investigated the digital backward propagation (BP) scheme for OFDM and single-carrier systems. The performance comparison has been made among OFDM, SC-Nyquist, and SC-NRZ using amplifier spacing BP (AS-BP)/perfect-BP. The results show that OFDM with BP has maximum system reach as compared to SC-Nyquist and SC-NRZ with BP. When AS-BP is used, the maximum transmission distances are 52×80 km, 51×80 km and 32×80 km for OFDM, SC-Nyquist and SC-NRZ, respectively. When the perfect BP is used, the corresponding numbers are 82×80 km, 80×80 km and 76×80 km, respectively. The impact of electrical filter bandwidth has been investigated. The performance of OFDM/SC systems using perfect-BP improves as the electrical filter bandwidth increases. For the first time to our knowledge, the impact of nonlinear amplitude noise in OFDM/SC systems with BP is investigated. It is found that OFDM/SC-Nyquist with BP has less amount of nonlinear phase/amplitude noise as compared to the SC-NRZ with BP due to the narrower electrical filter bandwidth.

Chapter 8

Conclusions and Future Plans

This thesis is focused on the studies of various limiting factors in the designs of a long-haul fiber-optic communication system, and the implementations of the corresponding approaches used to mitigate the resulting impairments. The analytical expressions for the conditional PDFs and variances of bit '1' and bit '0' in a dispersion-managed coherent fiber-optic system based on BPSK are derived. The good agreement between the analytical calculations and numerical simulations are achieved. The conditional PDF given bit '1' or '0' becomes asymmetric when IFWM is dominant, while it becomes almost symmetric when ASE noise increases. The optimum system parameters are found by analytically calculating the variance of IFWM, and a lot of computation efforts can be saved compared to numerical simulations. It is found that the optimum dispersion compensation ratio approaches 0.5 as the average dispersion of the dispersion-managed transmission fiber becomes large.

Next, various configurations of a 4-f time-lens system is studied. The direct inverse Fourier transform has been realized by properly choosing the signs and amount of dispersion and phase shift parameter. The 2-f subsystem T2 of the 4-f system is chosen to be anti-symmetric with respect to the 2-f subsystem T1; that is, $\beta_2^{(2)} = -\beta_2^{(1)}$ and $C_2 = -C_1$ such that T2 provides the exact inverse Fourier transform, which makes the output bit sequence not time-reversed. Two of the possible applications using the time-lens–based optical signal processing scheme are also discussed. One is a tunable wavelength division demultiplexer. The temporal filter in this example is an amplitude modulator. The driving voltage to the amplitude modulator can be dynamically changed to select the desirable channel, which make it suitable for the application of dynamic channel dropping in an optical network. The other application is a higher-order fiber dispersion compensator, in which the temporal filter is a phase modulator that generates a summation of several independent phase shifts, each of which corresponds to the amount of the that caused by the certain order of fiber dispersion, but with opposite signs. This dispersion compensation technique can flexibly compensate for any order of fiber dispersion by simply changing the driving voltage to the phase modulator. One of the most important advantages of the time-lens-based temporal filtering technique is that temporal filter can be dynamically altered by changing the input voltage to the amplitude/phase modulator leading to the potential applications for dynamic switching and multiplexing in optical networks.

A direct-detection optical orthogonal frequency-division multiplexing (DD-O-OFDM) system is realized using time lenses. The first 2-f subsystem (T1) carries out inverse Fourier transform and the second 2-f subsystem (T2) demodulates the OFDM signal by implementing Fourier transform. The output of T2 is the original input signal of T1 multiplied by a phase factor due to fiber dispersive effects. In direct detection, the photodiode removes the dispersive effects and just recovers the power of the input signal. It is shown that the third- and higher-order dispersive effects can be considerably reduced using time-lens-based DD-O-OFDM. Results also show that the time-lens-based DD-O-OFDM can tolerate the fiber nonlinearity to some extent.

A time-lens-based coherent optical OFDM (CO-O-OFDM) scheme is proposed. The impact of MZM nonlinearity and the fiber nonlinearity is studied. The conventional CO-O-OFDM using fast Fourier transform (FFT) is compared with the time-lens-based CO-O-OFDM. It is found that the time-lens-based CO-O-OFDM has much better tolerance to MZM-induced nonlinear effects than the FFT-based CO-O-OFDM. In addition, a periodical driving voltage has been proposed to set up the time lens to avoid directly using the quadratically increasing driving voltage. The time-lens-based CO-O-OFDM also have some advantages. Fist, the Fourier transform (FT) is done in the optical domain and the processing speed only depends on the propagation speed of light in the time-lens-bases system, whereas state-of-the-art FFT in DSP is still slow and needs much more computational efforts. Second, the optical domain FT has inherently large bandwidth and as a result, allows the system operating at a large information rate.

Lastly, the digital backward propagation (DBP) schemes for OFDM and single-carrier systems are studied. The performance comparison has been made among OFDM, SC-Nyquist, and SC-NRZ in the cases of without DBP, with amplifier spacing DBP (AS-BP) and with perfect-BP. Results show that OFDM and SC-Nyquist perform better as compared to SC-NRZ when DBP is used. It is found that five/three fold increase in system reach can be obtained for OFDM systems if perfect/AS -BP is used. The impact of electrical filter bandwidth has also been studied. The performance of OFDM/SC systems using perfect-BP initially improves as the electrical filter bandwidth increases. The impact of nonlinear phase/amplitude noise on OFDM/SC systems with BP is investigated. It is found that the nonlinear phase/amplitude noise has less impact on OFDM/SC-Nyquist than on SC-NRZ when DBP is used due to the narrower electrical filter bandwidth.

The digital backward propagation (DBP) has been shown an effective equalization scheme for OFDM systems. But the performance is limited by the nonlinear phase/amplitude noise. It has been demonstrated recently that all-optical regeneration technology can suppress the amplitude distortion and therefore mitigate the nonlinear phase noise. It will be interesting to investigate a fiber-optic communication system with all-optical regenerators inserted and the BP at the receiver. To better understand the impact of nonlinear amplitude/phase noise on OFDM, the mathematical analysis of nonlinear phase/amplitude noise will be carried out. Also, the system capacity of an optical OFDM system can be further enhanced using multi-mode fibers, which will be investigated in the future research work.

The research outcomes obtained in the thesis mainly result from the computer-aided simulations. Therefore, to better verify the simulation results, much more efforts in experimental investigations will be made in the future work.

Appendix A

Time-Lens–Based FT and IFT

A.1

The output signal at the end of 2-f subsystem T1 is given by

$$\begin{aligned} u(t,2f_1) &= \frac{1}{2\pi}\int_{-\infty}^{+\infty}\tilde{U}\left(\omega,f_{1+}\right)\times \\ &\quad \exp\left(\frac{i}{2}\beta_{22}^{(1)}f_1\omega^2-i\omega t\right)d\omega, \end{aligned} \tag{A.1}$$

where

$$\tilde{U}\left(\omega,f_{1+}\right) = \frac{1}{2\pi}\int_{-\infty}^{\infty}\tilde{U}\left(\omega-\Omega,f_{1-}\right)\tilde{H}_1(\Omega)d\Omega. \tag{A.2}$$

Substituting Eq. (A.2) into Eq. (A.1), we obtain

$$\begin{aligned} u(t,2f_1) &= \left(\frac{1}{2\pi}\right)^2\int_{-\infty}^{+\infty}\int_{-\infty}^{\infty}\tilde{U}\left(\omega-\Omega,f_{1-}\right)\tilde{H}_1(\Omega)\times \\ &\quad \exp\left(\frac{i}{2}\beta_{22}^{(1)}f_1\omega^2-i\omega t\right)d\Omega d\omega. \end{aligned} \tag{A.3}$$

From Eqs. (4.7) and (4.6), we have

$$\tilde{U}\left(\omega,f_{1-}\right)=\tilde{U}(\omega,0)\exp\left(\frac{i}{2}\beta_{21}^{(1)}f_1\omega^2\right) \tag{A.4}$$

and

$$H_1(\omega)=\sqrt{i\pi/C_1}\exp\left(-i\frac{\omega^2}{4C_1}\right). \tag{A.5}$$

Let $\omega' = \omega - \Omega$ in Eq. (A.3). Inserting Eqs. (A.4) and (A.5) into Eq. (A.3) and rearranging terms, we obtain

$$\begin{aligned} u(t, 2f_1) &= \left(\frac{1}{2\pi}\right)^2 \sqrt{\frac{i\pi}{C_1}} \int_{-\infty}^{\infty} \phi(\omega')\tilde{U}(\omega', 0) \times \\ &\quad \exp\left(\frac{i}{2}\beta_{21}^{(1)} f_1 \omega'^2\right) \times \\ &\quad \exp\left(\frac{i}{2}\beta_{22}^{(1)} f_1 \omega'^2 - i\omega' t\right) d\omega', \end{aligned} \tag{A.6}$$

where

$$\begin{aligned} \phi(\omega') &= \int_{-\infty}^{+\infty} \exp\left(\frac{i}{2}\beta_{22}^{(1)} f_1 \Omega^2 - i\frac{\Omega^2}{4C_1}\right) \times \\ &\quad \exp\left(i\beta_{22}^{(1)} f_1 \omega' \Omega - i\Omega t\right) \, d\Omega. \end{aligned} \tag{A.7}$$

The Ω^2 terms appearing in the argument of the exponent in Eq. (A.7) are eliminated if we select the chirp coefficient C_1, dispersion $\beta_{22}^{(1)}$, and the fiber length f_1 are related by

$$C_1 = \frac{1}{2\beta_{22}^{(1)} f_1}. \tag{A.8}$$

Hence, Eq. (A.7) becomes

$$\begin{aligned} \phi(\omega') &= \int_{-\infty}^{+\infty} \exp\left(i\beta_{22}^{(1)} f_1 \omega' \Omega - i\Omega t\right) d\Omega \\ &= 2\pi\delta\left(t - \beta_{22}^{(1)} f_1 \omega'\right), \end{aligned} \tag{A.9}$$

where $\delta(\cdot)$ is a delta function. Inserting Eq. (A.9) into Eq. (A.6), we finally obtain

$$\begin{aligned} u(t, 2f_1) &= \frac{\sqrt{i\pi/C_1}}{2\pi \left|\beta_{22}^{(1)} f_1\right|} \tilde{U}\left(\frac{t}{\beta_{22}^{(1)} f_1}, 0\right) \times \\ &\quad \exp\left[-it^2 \left(\frac{1}{\beta_{22}^{(1)} f_1} - \frac{\left(\beta_{21}^{(1)} + \beta_{22}^{(1)}\right)}{2\left(\beta_{22}^{(1)}\right)^2 f_1}\right)\right]. \end{aligned} \tag{A.10}$$

A.2

If $\beta_{21}^{(2)} = \beta_{22}^{(2)}$ in T2, following the same derivation as in Appendix A, we obtain

$$u(t, 2f_1 + 2f_2) = \frac{\sqrt{i\pi/C_2}}{2\pi\left|\beta_{22}^{(2)} f_2\right|}\, \tilde{U}\left(\frac{t}{\beta_{22}^{(2)} f_2}, 2f_1\right) \tag{A.11}$$

where

$$\tilde{U}\left(\frac{t}{\beta_{22}^{(2)} f_2}, 2f_1\right) = \mathcal{F}\left\{u(t, 2f_1)\right\}\Big|_{\omega=t/\beta_{22}^{(2)} f_2}. \tag{A.12}$$

From Eqs. (4.14) and (4.15), we have

$$u(t, 2f_1) = \frac{\sqrt{i\pi/C_1}}{2\pi\left|\beta_{22}^{(1)} f_1\right|}\, \tilde{U}\left(\frac{t}{\beta_{22}^{(1)} f_1}, 0\right) \tag{A.13}$$

and

$$\mathcal{F}\left\{\tilde{U}\left(\frac{t}{\beta_{22}^{(1)} f_1}, 0\right)\right\} = \left(2\pi\left|\beta_{22}^{(1)} f_1\right|\right) \times u\left(-\beta_{22}^{(1)} f_1 \omega, 0\right). \tag{A.14}$$

With the help of Eq. (A.13) and Eq. (A.14) and noting that

$$1/C_1 = 2\beta_{22}^{(1)} f_1 \tag{A.15}$$

$$1/C_2 = 2\beta_{22}^{(2)} f_2, \tag{A.16}$$

we obtain

$$u(t, 2f_1 + 2f_2) = \frac{i\sqrt{\beta_{22}^{(1)} f_1 \beta_{22}^{(2)} f_2}}{\left|\beta_{22}^{(1)} f_1\right|} \times u\left(-\frac{\beta_{22}^{(1)} f_1}{\beta_{22}^{(2)} f_2} t, 0\right). \tag{A.17}$$

Ignoring the trivial constant in Eq. (A.17), we finally obtain

$$u(t, 2f_1 + 2f_2) = u\left(-\frac{\beta_{22}^{(1)} f_1}{\beta_{22}^{(2)} f_2} t, 0\right). \tag{A.18}$$

A.3

For **Case 2**, from Eq. (4.23), we have

$$u(t, 2f_1) = \frac{\sqrt{i\pi/C_1}}{2\pi\left|\beta_{22}^{(1)} f_1\right|}\, \tilde{U}\left(\frac{t}{\beta_{22}^{(1)} f_1}, 0\right) \exp\left(-i\frac{t^2}{\beta_{22}^{(1)} f_1}\right). \tag{A.19}$$

The Fourier transform of Eq. (4.23) is given by

$$\mathcal{F}\left\{u(t, 2f_1)\right\} = \tilde{U}\left(\omega, 2f_1\right). \tag{A.20}$$

After propagating in the first single-mode fiber of T2, we obtain

$$\tilde{U}\left(\omega, 2f_1 + f_{2-}\right) = \tilde{U}\left(\omega, 2f_1\right) \exp\left(\frac{i}{2}\beta_{21}^{(2)} f_2 \omega^2\right), \tag{A.21}$$

where $\tilde{U}\left(\omega, 2f_1 + f_{2-}\right)$ is the Fourier transform of the signal right before the time lens 2. Noting that

$$\tilde{U}\left(\omega, 2f_1\right) = \tilde{U}\left(\omega, f_{1+}\right) \exp\left(\frac{i}{2}\beta_{22}^{(1)} f_1 \omega^2\right), \tag{A.22}$$

substituting Eq. (A.22) into Eq. (A.21) and choosing $\beta_{21}^{(2)} f_2 = -\beta_{22}^{(1)} f_1$, we obtain

$$\tilde{U}\left(\omega, 2f_1 + f_{2-}\right) = \tilde{U}\left(\omega, f_{1+}\right), \tag{A.23}$$

which leads to

$$u\left(t, 2f_1 + f_{2-}\right) = u\left(t, f_{1+}\right). \tag{A.24}$$

After the time lens 2, we obtain

$$u\left(t, 2f_1 + f_{2+}\right) = u\left(t, 2f_1 + f_{2-}\right) \exp\left(iC_2 t^2\right). \tag{A.25}$$

The first time lens introduces a quadratic phase factor

$$u\left(t, f_{1+}\right) = u\left(t, f_{1-}\right) \exp\left(iC_1 t^2\right). \tag{A.26}$$

If $C_2 = -C_1$, inserting Eq. (A.24) and Eq. (A.26) into Eq. (A.25), we obtain

$$u\left(t, 2f_1 + f_{2+}\right) = u\left(t, f_{1-}\right). \tag{A.27}$$

From Eq. (A.27), we have

$$\tilde{U}(\omega, 2f_1 + f_{2+}) = \tilde{U}(\omega, f_{1-}). \tag{A.28}$$

After propagating in the second single-mode fiber of T2, we obtain

$$\tilde{U}(\omega, 2f_1 + 2f_2) = \tilde{U}(\omega, 2f_1 + f_{2+}) \exp\left(\frac{i}{2}\beta_{22}^{(2)} f_2 \omega^2\right). \tag{A.29}$$

Also note that

$$\tilde{U}(\omega, f_{1-}) = \tilde{U}(\omega, 0) \exp\left(\frac{i}{2}\beta_{21}^{(1)} f_1 \omega^2\right). \tag{A.30}$$

Substituting Eq. (A.28) and Eq. (A.30) to Eq. (A.29) and choosing $\beta_{22}^{(2)} f_2 = -\beta_{21}^{(1)} f_1$, we obtain

$$\tilde{U}(\omega, 2f_1 + 2f_2) = \tilde{U}(\omega, 0) \tag{A.31}$$

and

$$u(t, 2f_1 + 2f_2) = u(t, 0), \tag{A.32}$$

where $u(t, 2f_1 + 2f_2)$ is the output signal of T2 and $u(t, 0)$ is the input signal of T1. In summary, for the **Case 2**, if we choose

$$\beta_{21}^{(2)} f_2 = -\beta_{22}^{(1)} f_1, \tag{A.33}$$

$$C_2 = -C_1, \tag{A.34}$$

$$\beta_{22}^{(2)} f_2 = -\beta_{21}^{(1)} f_1, \tag{A.35}$$

then at the end of the 4-f time-lens system, we can exactly replicate the input signal without time reversal.

Bibliography

[1] G. P. Agrawal, *Fiber-Optic Communication Systems*, 2nd Ed., John Wiley & Sons, Inc., New York (1997).

[2] T. H. Maiman, "Stimulated optical radiation in ruby," *Nature* **187**, 493 (1960).

[3] T. Miya, Y. Terunuma, T. Hosaka, and T . Miyoshita, "Ultimate low-loss single-mode fibre at 1.55 μm," *Electron. Lett.* **15**, 106 (1979).

[4] L.G. Cohen, C. Lin, and W. G. French, "Tailoring zero chromatic dispersion into the 1.5-1.6 μm low-loss spectral region of single-mode fibres," *Electron. Lett.* **15**, 334 (1979).

[5] R. Wyatt and W. J. Devlin, "10 kHz linewidth 1.5 μm InGaAsP external cavity laser with 55 nm tuning range," *Electron. Lett.* **19**, 110 (1983).

[6] T. Mukai and Y. Yamamoto, "Optical direct amplification for fibre ransmission," *Rev. Electr. Commun. Lab.* **3**, 340 (1983).

[7] K. C. Byron, "Simultaneous amplification and pulse compression in a single-mode optical fibre," *Electron. Lett.* **22**, 1275 (1986).

[8] H. J. Shaw and M. Digonnet, "Fiber optic amplifier," U.S. patent No. 4674830, filed Nov. 25, 1983, issued Jun. 23, 1987.

[9] R. J. Mears, L. Reekie, I. M. Jauncey, and D. N. Payne, "Low-noise erbium-doped fibre amplifier operating at 1.54 μm," *Electron. Lett.* **23**, 1026 (1987).

[10] E. Desurvire, J. Simpson, and P. C. Becker, "High-gain erbium-doped traveling-wave fiber amplifier," *Opt. Lett.* **12**, 888 (1987).

[11] O. E. Delange, "Wideband optical communication systems: Part II-Frequency division multiplexing," *Proc. IEEE* **58**, 1683 (1970).

[12] W. J. Tomlinson and C. Lin, "Optical wavelength-division multiplexer for the 1-1.4 μm spectral region," *Electron. Lett.* **14**, 345 (1978).

[13] H. Ishio, J. Minowa, and K. Nosu, "Review and status of wavelength-division-multiplexing technology and its application," *J. Lightwave Technol.* **2**, 448 (1984).

[14] T . Okoshi, "Feasibility study of frequency-division multiplexing optical fiber communication systems using optical heterodyne or homodyne schemes," Pap. Tech. Group, IECE Japan, OQE78-139, Feb. 27, (1979).

[15] Y. Yamamoto, "Study on optical digital modulation-demodulation systems," Pap. Tech. Group, IECE Japan, CS79-144 (1979).

[16] T. Okoshi and K. Kikuchi, "Frequency stabilization of semiconductor lasers for heterodyne-type optical communication schemes," *Electron. Lett.* **16**, 179 (1980).

[17] F. Favre and D. LeGuen, "High frequency stability of laser diode for heterodyne communication systems," *Electron. Lett.* **16**, 709 (1980).

[18] S. Saito, Y. Yamamoto, and T. Kimura, "Optical heterodyne detection of directly frequency modulated semiconductor lasesrig - nals," *Electron. Lett.* **16**, 826 (1980).

[19] Y. Yamamoto, "Receiver performance evaluation of various digital optical modulation-demodulation systems in the 0.5-IO-pm-wavelength region," *IEEE J. Quantum Electron.* **QE-16**, 1251 (1980).

[20] Y. Yamamoto and T. Kimura, "Coherent optical fiber transmission systems," *IEEE J. Quantum Electron.* **QE-17**, 919 (1981).

[21] E. E. Basch and T. G. Brown, "Introduction to coherent optical fiber transmission," *IEEE Commun. Mag.* **23**, 23 (1985).

[22] J. Salz, "Modulation and detection for coherent lightwave communication," *IEEE Commun. Mag.* **24**(6), 38 (1986).

[23] T. Okoshi, "Recent advances in coherent optical fiber communication systems," *J. Lightwave Technol.* **5**, 44 (1987).

[24] T. Kimura, "Coherent optical fiber transmission," *J. Lightwave Technol.* **5**, 414 (1987).

[25] T. Okoshi and K. Kikuchi, *Coherent optical fiber communications*, Kluwer Adademic Publishers (1988).

[26] R. A. Linke and A. H. Gnauck, "High-capacity coherent lightwave systems," *J. Lightwave Technol.* **6**, 1750 (1988).

[27] R. Wyatt and W. J. Devlin, "10 kHz linewidth 1.5 μm InGaAsP external cavity laser with 55 nm tuning range," *Electron. Lett.* **19**, 110 (1983).

[28] S. Tsukamoto, D. Ly-Gagnon, K. Katoh, and K. Kikuchi, "Coherent Demodulation of 40-Gbit/s Polarization-Multiplexed QPSK Signals with 16-GHz Spacing after 200-km Transmission," *OFC*, PDP29 (2005).

[29] K. Kikuchi, "History of coherent optical communication and challenges for the future," Digest of the IEEE/LEOS Summer Topical Meetings, pp. 107-108, 21-23 July 2008.

[30] E. Ip, A. P. T. Lau, D. J. F. Barros, and J. M. Kahn, "Coherent detection in optical fiber systems," *Opt. Express* **16**, 753 (2008).

[31] E. Ip and J. M. Kahn, "Fiber impairment compensation using coherent detection and digital signal processing," *J. Lightwave Technol.* **28**, 502 (2010).

[32] M. Born and E. Wolf, *Principles of Optics*, 7th Ed., Prentice Hall, London (1993).

[33] G. P. Agrawal, *Nonlinear fiber optics*, 3rd Ed., Chapt. 2, Academic Press, San Diego (2001).

[34] T. Koch and R. Alferness,"Dispersion compensation by active predistorted signal synthesis," *J. Lightwave Technol.* **3**, 800 (1985).

[35] R.I. Killey, P.M. Watts, V. Mikhailov, M. Glick, and P. Bayvel, "Electronic dispersion compensation by signal predistortion using digital processing and a dual-drive Mach-Zehnder Modulator," *IEEE Photon. Technol.* **17**, 714 (2005).

[36] D. McGhan, C. Laperle, A. Savehenko, C. Li; G. Mak, and M. O'Sullivan, "5120 km RZ-DPSK transmission over G652 fiber at 10 Gb/s with no optical dispersion compensation," Technical Digest of OFC/NFOEC, Paper PDP27, Anaheim, CA (2005).

[37] J. McNicol, M. O'Sullivan, K. Roberts, A. Comeau, D. McGhan, and L. Strawczynski, "Electrical domain compensation of optical dispersion," Technical Digest of OFC/NFOEC, Paper OThJ3, Anaheim, CA (2005).

[38] B. L. Kasper, J. C. Campbell, J. P. Talman, A. H. Gnauck, J. E. Bowers, and W. S. Holden, "An APD/FET optical receiver operating at 8 Gbit/s," *J. Lightwave Technol.* **LT-5**, 344 (1987).

[39] B. Widrow, "Adaptive filters," in *Aspects of Network and System Theory*, R. E. Kalman and N. De Claris, Eds. New York: Holt, Rinehart, Winston, 563 (1970).

[40] R. W. Lucky, "Automatic equalization for digital communications," *B.S.T.J.* **44**, 547 (1965).

[41] J. G. Proakis, *Digital Communications*, McGraw-Hill, New York (1983).

[42] A. Gersho and T. L. Lim, "Adaptive cancellation of intersymbol interference for data transmission," *B.S.T.J.* **60**, 1997 (1981).

[43] J. H. Winters and R. D. Gitlin, "Electrical signal processing techniques in long-haul fiber-optic systems," *IEEE Trans. Commun.* **38**, 1439 (1990).

[44] J. G. Proakis, *Digital Communications*, 4th Ed., McGraw-Hill, Boston (2001).

[45] A.J. Weiss, "On the performance of electrical equalization in optical fiber transmission systems," *IEEE Photon. Technol. Lett.* **15**, 1225 (2003).

[46] H. F. Haunstein, S. G. Wolfgang, A. Dittrich, K. Sticht, and R. Urbansky, "Principles for electronic equalization of polarization-mode dispersion," *J. Lightwave Technol.* **22**, 1169 (2004).

[47] O. E. Agazzi, D. E. Crivelli, and H. S. Carrer, "Maximum likelihood sequence estimation in the presence of chromatic and polarization mode dispersion in intensity modulation/direct detection optical channels," in *Proc. IEEE Int. Conf. Communications (ICC)*, 2787 (2004).

[48] O. E. Agazzi, M. R. Hueda, H. S. Carrer, and D. E. Crivelli, "Maximum-likelihood sequence estimation in dispersive optical channels," *J. Lightwave Technol.* **23**, 749 (2005).

[49] D. Sadot, G. Katz, and U. Mahlab, "Advanced trends in electrical dispersion compensation in optical communications OOK systems," Int. Conf. on Transparent Optical Networks, **1**, 123 (2006).

[50] N. Benvenuto, G. Cherubini, *Algorithms for Communications Systems and their Applications*, John Wiley & Sons (2002).

[51] B. Spinnler, F. N. Hauske, and M. Kuschnerov, "Adaptive equalizer complexity in coherent optical receivers," in Proc. of ECOC 2008, paper We.2.E.4. (2008).

[52] B. Widrow, S. Stearns, *Adaptive Signal Processing*, Prentice-Hall Signal Processing Series (1985).

[53] D. N. Godard, "Self-Recovering Equalization and Carrier Tracking in Two-Dimensional Data Communication Systems", IEEE Trans. on Commun. **COM-28**, 1867 (1980).

[54] M. Kuschnerov, F. N. Hauske, K. Piyawanno, B. Spinnler, E. D. Schmidt, A. Napoli, and B. Lankl, "Adaptive chromatic dispersion equalization for non-dispersion managed coherent systems," in Proc. of OFC 2009, paper OMT1 (2009).

[55] C. Lin, H. Kogelnik, and L. G. Cohen, "Optical-pulse equalization of low-dispersion transmission in single-mode fibers in the 1.3C1.7 μm spectral region," *Opt. Lett.* **5**, 476 (1980).

[56] L. J. Cimini. Jr., L. J. Greenstein, A. A. M. Saleh, "Optical equalization to combat the effects of laser chirp and fiber dispersion," *J. Lightwave Technol.* **8**, 649 (1990).

[57] G. P. Agrawal, *Applications of Nonlinear fiber Optics*, Academic Press, San Diego, CA (2001).

[58] D. K. W. Lam, B. K. Garside, and K. O. Hill, "Dispersion cancellation using optical-fiber filters," *Opt. Lett.* **7**, 291 (1982).

[59] B. H. Kolner, "Generalization of the concepts of focal length and f-number to space and time," *J. Opt. Soc. Am. A* **11**(12), 3229 (1994).

[60] A. Papoulis, "Pulse compression, fiber communications, and diffraction: a unified approach," *J. Opt. Soc. Am. A* **11**, 3 (1994).

[61] J. Van Howe and C. Xu, "Ultrafast optical signal processing based upon space-time dualities," *J. Lightwave Technol.*" **24**, 2649 (2006).

[62] A. W. Lohmann and D. Mendlovic, "Temporal filtering with time lenses," *Appl. Opt.* **31**, 6212 (1992).

[63] D. Yang, S. Kumar, and H. Wang, "Temporal filtering for optical communication systems," *Opt. Commun.* **281**, 238 (2008).

[64] S. Kumar and D. Yang, "Optical implementation of orthogonal frequency-division multiplexing using time lenses," *Opt. Lett.* **33**, 2002 (2008).

[65] R. W. Chang, "Synthesis of band-limited orthogonal signals for multi-channel data transmission," *Bell System Technical Journal* **46**, 1775 (1966).

[66] R. W. Chang, "Orthogonal frequency multplex data transmission system," U.S. patent No. 34884555, filed Nov. 14, 1966, issued Jan. 6, 1970.

[67] S. B. Weinstein and P. M. Ebert, "Data transmission by frequency-division multiplexing using the discrete fourier transform," *IEEE Trans. Commun. Technol.* **19**, 628 (1971).

[68] Q. Pan and R. J. Green, "Bit-error-rate performance of lightwave hybrid AM/OFDM systems with comparison with AM/QAM systems in the presence of clipping impulse noise," *IEEE Photon. Technol. Lett.* **8**, 278 (1996).

[69] B. J. Dixon, R. D. Pollard, and S. Iezekiel, "Orthogonal frequency-division multiplexing in wireless communication systems with multimode fiber feeds," *IEEE Trans. Microwave Theory and Techniq.* **49**, 1404 (2001).

[70] W. Shieh and C. Athaudage, "Coherent optical orthogonal frequency division multiplexing," *Electron. Lett.* **42**, 587 (2006).

[71] A. J. Lowery, L. Du, and J. Armstrong, "Orthogonal frequency division multiplexing for adaptive dispersion compensation in long haul WDM systems," *Opti. Fiber Commun. Conf. (OFC)*, paper PDP 39, Anaheim, CA (2006).

[72] I. Djordjevic and B. Vasic, "Orthogonal frequency division multiplexing for high-speed optical transmission," *Opt. Express* **14**, 3767 (2006).

[73] S. L. Jansen, I. Morita and H. Tanaka, "16 × 52.5-Gb/s, 50-GHz spaced, POLMUX-CO-OFDM transmission over 4,160 km of SSMF enabled by MIMO processing KDDI R&D Laboratories," in *European Conference on Optical Communications (ECOC)*, Paper PD1.3, Berlin, Germany (2007).

[74] S. L. Jansen, I. Morita, and H. Tanaka, "10 × 121.9-Gb/s PDM-OFDM Transmission with 2-b/s/Hz Spectral Efficiency over 1,000 km of SSMF," *OFC/NFOEC*, San Diego, paper PDP2 (2008).

[75] C. Sethumadhavan, X. Liu, E. Burrows, and L. Buhl, "Hybrid 107-Gb/s Polarization-multiplexed DQPSK and 42.7-Gb/s DQPSK transmission at 1.4- bits/s/Hz spectral efficiency over 1280 km of SSMF and 4 bandwidth-managed ROADMs," in *European Conference on Optical Communication (ECOC)*, Paper PD 1.9, Berlin, Germany (2007).

[76] Y. Ma, W. Shieh, and Q. Yang, "Bandwidth-efficient 21.4 Gb/s coherent optical 2 × 2 MIMO OFDM transmission," in *Optical Fiber Communication Conference and Exposition and The National Fiber Optic Engineers Conference*, OSA Technical Digest (CD) (Optical Society of America, 2008), paper JWA59 (2008).

[77] W. Shieh, Q. Yang, and Y. Ma, "107 Gb/s coherent optical OFDM transmission over 1000-km SSMF fiber using orthogonal band multiplexing," *Opt. Express* **16**, 6378 (2008).

[78] A. J. Lowery, "Improving sensitivity and spectral efficiency in direct-detection optical ofdm systems," OFC/NFOEC, paper OMM4 (2008).

[79] B. J. C. Schmidt, Z. Zan, L. B. Du, and A. J. Lowery, "100 Gbit/s transmission using single-band direct-detection optical OFDM," OSA/OFC/NFOEC, paper PDPC3 (2009).

[80] K. Lee, C. T. D. Thai, and J. K. Rhee, "All optical discrete Fourier transform processor for 100 Gbps OFDM transmission," *Opt. Express* **16**, 4023 (2008).

[81] W. Shieh, H. Bao, and Y. Tang, "Coherent optical OFDM: theory and design," *Opt. Express* **16**, 841 (2008).

[82] W. Shieh and I. Djordjevic, *OFDM for Optical Communications*, Chapt. 3, Amsterdam ; Boston : Elsevier : Academic Press (2010).

[83] A. Hasegawa and F. Tappert, "Transmission of stationary nonlinear optical pulses in dispersive dielectric fibers. I. Anomalous dispersion," *Appl. Phys. Lett.* **23**, 142 (1973).

[84] I. Shake, H. Takara, K. Mori, S. Kawanishi, and Y. Yamabayashi, "Influence of inter-bit four-wave mixing in optical TDM transmission," *Electron. Lett.* **34**, 1600 (1998).

[85] P. V. Mamyshev and N. A. Mamysheva, "Pulse-overlapped dispersionmanaged data transmission and intrachannel four-wave mixing," *Opt. Lett.* **24**, 1454 (1999).

[86] R. J. Essiambre, B. Mikkelsen, and G. Raybon, "Intra-channel crossphase modulation and four-wave mixing in high-speed TDM systems," *Electron. Lett.* **35**, 1576 (1999).

[87] X. Li, X. Chen, G. Goldfarb, E. Mateo, I. Kim, F. Yaman, and G. Li, "Electronic post-compensation of WDM transmission impairments using coherent detection and digital signal processing," *Opt. Express* **16**, 880 (2008).

[88] E. Ip and J. M. Kahn, "Compensation of dispersion and nonlinear effects using digital backpropagation," *J. of Lightwave Technol.* **26**, 3416 (2008).

[89] E. Ip and J. M. Kahn, "Nonlinear impairment compensation using backpropagation," in Optical Fibre, New Developments, In-Tech., Vienna, Austria (Invited Chapter) (2010).

[90] E. Mateo, L. Zhu, and G. Li, "Impact of XPM and FWM on the digital implementation of impairment compensation for WDM transmission using backward propagation," *Opt. Express* **16**, 16124 (2008).

[91] G. Goldfarb and G. Li, "Efficient backward-propagation using waveletbased filtering for fiber backwardpropagation," *Opt. Express* **17**, 8815 (2009).

[92] E. M. Ip and J. M. Kahn, "Fiber Impairment Compensation Using Coherent Detection and Digital Signal Processing," *J. Lightwave Technol.* **28**, 502 (2010).

[93] T. Yu, E. A. Golovochenko, A. N. Pilipetskii and C. R. Menyuk, "Dispersion managed soliton interaction in optical fibers," *Opt. Lett.* **22**, 793 (1997).

[94] M. Matsumoto, "Analysis of interaction between stretched pulses propagating in dispersion-managed fibers," *IEEE Photon. Technol. Lett.*, vol. 10, pp. 373-375, Mar. 1998.

[95] S. Kumar, M. Wald, F. Lederer, and A. Hasegawa, "Soliton interaction in strongly dispersion managed optical fibers," *Opt. Lett.*, vol. 23, pp. 1019-1021, 1998.

[96] I. Shake, H. Takara, K. Mori, S. Kawanishi, and Y. Yamabayashi, "Influence of interbit four-wave mixing in optical TDM transmission," *Electron. Lett.*, vol. 34, no. 16, pp. 1600-1601, 1998.

[97] P. V. Mamyshev and N. A. Mamysheva, "Pulse-overlapped dispersion-managed data transmission and intrachannel four-wave mixing," *Opt. Lett.*, vol. 24, pp. 1454-1456, Nov. 1, 1999.

[98] R. J. Essiambre, B. Mikkelsen, and G. Raybon, "Intra-channel crossphase modulation and four-wave mixing in high-speed TDM systems," *Electron. Lett.*, vol. 35, no. 19, pp. 1576-1578, 1999.

[99] A. Mecozzi, C. B. Clausen, and M. Shtaif, "Analysis of intrachannel nonlinear effects in highly dispersed optical pulse transmission," *IEEE Photon. Technol. Lett.*, vol. 12, no. 4, pp. 292-294, Apr. 2000.

[100] A. Mecozzi, C. B. Clausen, and M. Shtaif, "System impact of intrachannel nonlinear effects in highly dispersed optical pulse transmission," *IEEE Photon. Technol. Lett.*, vol. 12, pp. 1633-1635, Dec. 2000.

[101] A. Mecozzi, C. B. Clausen, M. Shtaif, S. Park, and A. H. Gnauck, "Cancellation of timing and amplitude jitter in symmetric links using highly dispersed pulses," *IEEE Photon. Technol. Lett.*, vol. 13, pp. 445-447, May 2001.

[102] S. Kumar, "Intrachannel four-wave mixing in dispersion managed RZ systems," *IEEE Photon.s Technol. Lett.*, vol. 13, pp. 800-802, Aug. 2001.

[103] M. J. Ablowitz and T. Hirooka, "Resonant intrachannel pulse intraction in dispersion-managed transmission systems," I*EEE J. Sel. Topics Quantum Electron.*, vol. 8, no. 3, pp. 603-614, May/Jun. 2002.

[104] S. Kumar, J. C. Mauro, S. Raghavan and D. Q. Chowdhury, "Intrachannel nonlinear penalties in dispersion-managed trasmission systems," *IEEE J. Sel. Topics Quantum Electron.*, vol. 8, no. 8, pp. 626-631, May/June 2002.

[105] R. J. Essiambre, G. Raybon and B. Mikkelsen, *Chapt. 6 in Optical Fiber Telecommunications IV B Systems and Impairments*, San Diego: Academic Press, 2002.

[106] S. Kumar and D. Yang, "Second-order theory for self-phase modulation and cross-phase modulation in optical fibers," *J. Lightw. Tech.*, vol. 23, no. 6, pp. 2073-2080, June 2005.

[107] A. P. T. Lau, S. Rabbani and J. M. Kahn, "On the statistics of intrachannel four-wave mixing in phase-modulated optical communication systems," *J. Lightw. Tech.*, vol. 26, no. 14, pp. 2128-2135, July 2008.

[108] J. P. Gordon and L. F. Mollenauer, "Phase noise in photonic communications systems using linear amplifiers," *Opt. Lett.*, vol. 15, no. 23, pp. 1351-1353, 1990.

[109] B. H. Kolner and M. Nazarathy, "Temporal imaging with a time lens," *Opt. Lett.* **14**, 630 (1989).

[110] N. K. Berger, B.Levit, S. Atkins, and B. Fischer, "Time-lens-based spectral analysis of optical pulses by electrooptic phase modulation," *Electron. Lett.* **36**, 1644 (2000).

[111] J. Azana and M. A. Muriel, "Real-time optical spectrum analysis based on the time-space duality in chirped fiber gratings," *IEEE J. Quantum Electron.* **36**, 517 (2000).

[112] J. W. Goodman, *Introduction to Fourier Optics*, 2nd Ed., McGraw-Hill, San Francisco (1996).

[113] Won-Jin Choi, A. E. Bond, K. Jongwoo Kim, J. Zhang, R. Jambunathan, H. Foulk, S. O'Brien, J. Van Norman, D. Vandegrift, C. Wanamaker, J. Shakespeare, and H. Cao, "Low insertion loss and low dispersion penalty InGaAsP quantum-well high-speed electroabsorption modulator for 40-Gb/s very-short-reach, long-reach, and long-haul applications," *J. Lightwave Technol.* **20**, 2052 (2002).

[114] H. Fukano, T. Yamanaka, M. Tamura, and Y. Kondo, "Very-low-driving-voltage electroabsorption modulators operating at 40 Gb/s," *J. Lightwave Technol.* **24**, 2219 (2006).

[115] S. Kumar, "Compensation of third-order dispersion using time reversal in optical transmission systems," *Opt. Lett.* **32**, 346 (2007).

[116] V. Srikant, "Broadband dispersion and dispersion slope compensation in high bit rate and ultra long haul systems," *Optical Fiber Communication Conference (OFC)*, OSA Technical Digest Series Optical Society of America, Anaheim, California, paper TuH1 (2001).

[117] P. K. Kondratko, A. Leven, Young-Kai Chen, J. Lin, Ut-Va Koc, Kun-Yii Tu, and J. Lee, "12.5-GHz optically sampled interference-based photonic arbitrary waveform generator," *IEEE Phon. Tech. Lett.* **17**, 2727 (2005).

[118] M. Nakazawa, E. Yamada, H. Kubota, and K. Suzuki, "104 Gbit/s soliton data transmission over one million kilometres," *Electron. Lett.* **27**, 1270 (1991).

[119] A. J. Lowery, and J. Armstrong, "10 Gb/s multimode fiber link using power efficient orthogonal frequency division multiplexing," *Opt. Express* **13**, 10003 (2005).

[120] I. B. Djordjevic, and B. Vasic, "Orthogonal frequency division multiplexing for high speed optical transmission," *Opt. Express* **14**, 3767 (2006).

[121] T. Jannson, "Real time Fourier transformation in dispersive optical fibers," *Opt. Express* **8**, 232 (1983).

[122] A. J. Lowery, L. B. Du and J. Armstrong, "Performance of optical OFDM in ultralong-haul WDM lightwave systems," *J. Lightwave Technol.* **25**, 131 (2007).

[123] S. L. Jansen, I. Morita, T. C. Schenk, D. van den Borne, and H. Tanaka, "Optical OFDM–a candidate for future long-haul optical transmission systems," in *Optical Fiber Communication Conference and Exposition and The National Fiber Optic Engineers Conference*, OSA Technical Digest (CD) (Optical Society of America, 2008), paper OMU3.

[124] D. Yang and S. Kumar, "Realization of optical OFDM using time lenses and its comparison with conventional OFDM for fiber-optic systems," in *Proc. of* 35^{th} *European Conference on Optical Communication (ECOC)* , Vienna (2009).

[125] T. Hirooka and M. Nakazawa, "Optical adaptive equalization of high-speed signals using time-domain optical Fourier transformation," *J. Lightwave Technol.* **24**, 2530 (2006).

[126] J. Conradi, *Bandwidth-Efficient Modulation Formats for Digital Fiber Transmission Systems*, Chapt. 16, Academic Press (2002).

[127] A. J. Lowery, "Fiber nonlinearity mitigation in optical links that use OFDM for dispersion compensation," *IEEE Photon. Technol. Lett.* **19**, 1556 (2007).

[128] L. B. Du and A. J. Lowery, "Fiber nonlinearity compensation for co-OFDM systems with periodic dispersion maps," in *Optical Fiber Communication Conference*, OSA Technical Digest (CD) (Optical Society of America, 2009), paper OTuO1.

[129] W. Shieh, X. Yi, Y. Ma, and Y. Tang, "Theoretical and experimental study on PMD-supported transmission using polarization diversity in coherent optical OFDM systems," *Opt. Express* **15**, 9936 (2007).

[130] A. J. Lowery, "Fiber nonlinearity pre- and post-compensation for long-haul optical links using OFDM," *Opt. Express* **15**, 12965 (2007).

[131] A. J. Lowery, S. Wang and M. Premaratne, "Calculation of power limit due to fiber nonlinearity in optical OFDM systems," *Opt. Express* **15**, 13282 (2007).

[132] M. Nazarathy, J. Khurgin, R. Weidenfeld, Y. Meiman, P. Cho, R. Noe, I. Shpantzer, and V. Karagodsky, "Phased-array cancellation of nonlinear FWM in coherent OFDM dispersive multi-span links," *Opt. Express* **16**, 15777 (2008).

[133] S. L. Jansen, I. Morita, K. Forozesh, S. Randel, D. Van den Borne and H. Tanaka, "Optical OFDM, a hype or is it for real?," in *Proc. of European Conference on Optical Communication (ECOC)* pp. 49-52, Brussels (2008).

[134] B. S. Krongold, Y. Tang and W. Shieh, "Fiber nonlinearity mitigation by PAPR reduction in coherent optical OFDM system via active constellation extension," in *Proc. of European Conference on Optical Communication (ECOC)* pp. 157-158, Brussels 2008).

[135] S. Hellerbrand, B. Goebel, and N. Hanik, "Trellis shaping for reduction of the peak-to-average power ratio in coherent optical OFDM systems," in *Optical Fiber Communication Conference*, OSA Technical Digest (CD) (Optical Society of America, 2009), paper JThA48.

[136] L. Du and A. J. Lowery, "Improving nonlinearity precompensation in direct-detection optical OFDM communications systems," in *Proc. of European Conference on Optical Communication (ECOC)* pp. 147-148, Brussels (2008).

[137] Y. Benlachtar, G. Gavioli, V. Mikhailov and R. I. Killey, "Experimental investigation of SPM in long-haul direct-detection OFDM systems," *Opt. Express* **16**, 15477 (2008).

[138] Y. Tang, W. Shieh, X. Yi, R. Evans, "Optimum design for RF-to-optical up-converter in coherent optical OFDM systems," *IEEE Photon. Technol. Lett.* **19**, 483 (2007).

[139] Y. Tang, K. P. Ho, and W. Shieh, "Coherent optical OFDM transmitter design employing predistortion," *IEEE Photon. Technol. Lett.* **20**, 954 (2008).

[140] J. Leibrich, A. Ali and W. Rosenkranz, "OFDM transceiver design for optimizing sensitivity and long-haul performance," *IEEE/LEOS Summer Topical Meetings*, pp. 249-250 (2008).

[141] A. Ali, J. Leibrich, and W. Rosenkranz, "Spectral efficiency and receiver sensitivity in direct detection optical-OFDM," in *Optical Fiber Communication Conference*, OSA Technical Digest (CD) (Optical Society of America, 2009), paper OMT7.

[142] H. Kubota and M. Nakazawa, "Soliton transmission control in time and frequency domains, " *IEEE J. Quantum Electron.* **29**, 2189 (1993).

[143] E. Ip and J. M. Kahn, "Compensation of Dispersion and Nonlinear Effects using Digital Backpropagation," J. of Lightwave Technol. **26**, 3416 (2008).

[144] E. M. Ip and J. M. Kahn, "Fiber Impairment Compensation Using Coherent Detection and Digital Signal Processing," *J. Lightwave Technol.* **28**, 502 (2010).

[145] J. P. Gordon and L. F. Mollenauer, "Phase noise in photonic communications systems using linear amplifiers," *Opt. Lett.* **15**, 1351 (1990).

[146] A. G. Green, P. P. Mitra, and L. G. L. Wegener, "Effect of chromatic dispersion on nonlinear phase noise," *Opt. Lett.* **28**, 2455 (2003).

[147] S. Kumar, "Effect of dispersion on nonlinear phase noise in optical transmission systems," *Opt. Lett.* **30**, 3278 (2005).

[148] S. Watanabe and M. Shirasaki, "Exact compensation for both chromatic dispersion and Kerr effect in a transmission fiber using optical phase conjugation," *J. Lightwave Technol.* **14**, 243 (1996).

[149] S. L. Jansen, D. van den Borne, C. C. Monsalve, S. Spalter, P. M. Krummrich, G. D. Khoe, and H. de Waardt, "Reduction of Gordon-Mollenauer phase noise by midlink spectral inversion," *IEEE Photon. Technol. Lett.* **17**, 923 (2005).

[150] S. Kumar and L. Liu, "Reduction of nonlinear phase noise using optical phase conjugation in quasi-linear optical transmission systems," *Opt. Express* **15**, 2166 (2007).